Cytotoxic mechanism of membrane targeting photosensitizer-incorporated HVJ-E in prostate cancer

膜を標的とした光感受性薬剤含有 **HVJ-E** の
前立腺がんにおける細胞傷害機構

Medical Beam Physics Laboratory (Awazu Lab.)
Graduate School of Frontier Biosciences, Osaka University
4th year of 5-year PhD program 32A14008
Mizuho INAI

Main research advisor:	**Prof. Kunio AWAZU** **(Medical Beam Physics Laboratory)**
Co-research advisors:	**Prof. Toru NAKANO** **(Laboratory of Stem Cell Pathology)** **Prof. Masaru ISHII** **(Department of Immunology and Cell Biology)** **Prof. Yasushi INOUE** **(Nano Biophotonics Group)**

Abstract

Development of prostate specific antigen screening has resulted in dramatic reduction in overall prostate cancer mortality. Survival improvement of advanced-stage cancer patients, however, is still limited and the establishment of effective modality is eagerly awaited. To tackle this problem, photodynamic therapy (PDT), which is based on light absorption and photochemistry, has emerged as a potential treatment that results in malignant prostatic tissue eradication. PDT has the advantage of high selectivity, yet its limited treatment depth hinders this method to become an integral part of clinical practice. Thus, more potent agents that allow induction of multiple cell death pathways are needed to enhance treatment outcome.

In the previous study, a novel photosensitizer named porphyrus envelope (PE) was established by inserting lipidated protoporphyrin IX (PpIX lipid) into the replication-deficient viral particle, hemagglutinating virus of Japan envelope (HVJ-E). The drug-release mechanism and its efficacy over conventional photosensitizer 5-aminolevulinic acid (5-ALA) have already been confirmed. This study focuses on uncovering cellular localization of PE and characterizing its ability to induce multiple anti-tumor effects *in vitro* to investigate the effectiveness of PE-mediated PDT against malignant prostate cancer.

Localization and cellular uptake of PE in cells were confirmed via confocal laser scanning microscope and a cell-based fluorescent assay. Furthermore, the effect of direct cytotoxic effect induced by PE was confirmed through analyzing wound-healing ability and colony-forming activity of prostate cancer cells. The effect of PE-mediated PDT was investigated by observing generated reactive oxygen species (ROS) and induced cell death pathway. The combination index (CI) was also calculated to confirm the synergistic activity of HVJ-E and PE-mediated PDT. The results have shown how PE rapidly localizes to the cell membrane after 10 min incubation while ensuring selective uptake of a photosensitizing agent in cancer cells. Direct cytotoxicity induced by PE largely inhibited wound healing and colony-forming activity in all conditions. Furthermore, time-dependent increase in ROS production was observed, and induction of both apoptotic and necrotic cell death pathways was confirmed. PE-mediated PDT was most effective in 5 h sample, which exhibited high fluorescence intensity for ROS. Besides, it is notable that

treatment with PE-mediated PDT could result in more rapid cell death than HVJ-E or PpIX lipid alone, suggesting the enhanced therapeutic outcome of PE-mediated PDT. The synergistic activity of HVJ-E and PE-mediated PDT was confirmed with CI of < 1.

To summarize, these results demonstrate the high therapeutic efficacy of PE-mediated PDT with rapid drug delivery to cell membrane and induction of cell death via multiple pathways. Synergistic effect of HVJ-E and photodynamic reactions represents a promising treatment for advanced and metastatic prostate cancer.

Table of Contents

1. Introduction 1
1.1 Prostate cancer in cancers 1
1.2 Treatment options for advanced prostate cancer 1
1.3 Photodynamic therapy (PDT) as an alternative treatment 3
1.3.1 Photodynamic therapy for prostate cancer 3
1.3.2 Basic photochemistry 3
1.3.3 PDT-mediated cell death 4
1.4 Drawbacks of current PDT method for prostate cancer 6
1.5 Novel photosensitizer that induces multiple death pathways 6
1.5.1 Photosensitizer that localize in cell membrane 6
1.5.2 Novel photosensitizer delivery system for PDT 7
1.5.3 Novel photosensitizer that combines HVJ-E with PpIX lipid: porphyrus envelope (PE) 9
1.6 Aim of this study 9
1.7 Outline of this dissertation 10
References 11

2. Photosensitizer delivery by PE 15
2.1 Materials and Methods 16
2.1.1 Cell line and culture 16
2.1.2 Photosensitizers 16
2.1.3 Confocal Microscopy 16
2.1.4 Fluorescence assay for uptake of PpIX 17
2.1.5 Statistical analysis 17
2.2 Experimental results 18
2.2.1 Membrane-targeting delivery of PE 18
2.2.2 Uptake of PE-inserted PpIX lipid in prostate cancer 19
2.3 Discussion 21
2.4 Summary 21
References 22

3. Direct cytotoxic effect induced by PE 24
3.1 Materials and Methods 25
3.1.1 Cell line and culture 25
3.1.2 Photosensitizers 25
3.1.3 Direct cytotoxic effect of PE 25
3.1.4 Wound healing ability of PE 26
3.1.5 Colony forming ability of PE 26
3.1.6 Statistical analysis 27
3.2 Experimental results 28
3.2.1 Level of PE-induced direct cytotoxic effect in PC-3 cells 28
3.2.2 Level of PE-induced direct cytotoxic effect in PC-3 cells after laser irradiation 31
3.2.3 Inhibition of wound healing activity in PC-3 cells 33
3.2.4 Inhibition of colony forming activity in PC-3 cells 36
3.3 Discussion 38

3.4 Summary **39**
References **40**

4. Therapeutic efficacy of PE-mediated PDT 42
4.1 Materials and Methods **45**
4.1.1 Cell line and culture 45
4.1.2 Photosensitizers 45
4.1.3 ROS production 45
4.1.4 Cell death pathway 46
4.1.5 PDT experiment 47
4.1.6 Synergistic effect 49
4.1.7 Statistical analysis 49
4.2 Experimental results **50**
4.2.1 Intracellular ROS/Superoxide generation in PC-3 cells 50
4.2.2 Mode of cell death induced in PC-3 cells 53
4.2.3 Therapeutic efficacy of PE-mediated PDT 55
4.2.4 Synergy quantification of PE-mediated PDT 57
4.3 Discussion **62**
4.4 Summary **65**
References **66**

5. Efficacy of PE-mediated PDT towards different cell lines 69
5.1 Materials and Methods **70**
5.1.1 Cell line and culture 70
5.1.2 Photosensitizers 70
5.1.3 Fluorescence assay for uptake of PpIX 70
5.1.4 Direct cytotoxic effect of PE 71
5.1.5 PDT experiment 71
5.1.6 Statistical analysis 72
5.2 Experimental results **73**
5.2.1 Cellular uptake of PpIX lipid in different cell lines 73
5.2.2 Effect of PE-induced direct cytotoxicity in different cell lines 75
5.2.3 Effect of PE-mediated PDT in different cell lines 78
5.3 Discussion **80**
5.4 Summary **81**
References **82**

6. Efficacy of PE-mediated PDT in 3D tumor spheroid model 83
6.1 Materials and Methods **85**
6.1.1 Cell line and culture 85
6.1.2 Photosensitizers 85
6.1.3 Number of PC-3 cells in spheroid system 85
6.1.4 Fluorescence assay for uptake of PpIX 86
6.1.5 Direct cytotoxic effect of PE 86
6.1.6 PDT experiment 86
6.1.7 Statistical analysis 87
6.2 Experimental results **88**
6.2.1 Comparison of PC-3 cell numbers in 2D and 3D spheroid model 88
6.2.2 Uptake of PE-inserted PpIX lipid in PC-3 spheroids 90

6.2.3 Effect of PE-induced direct cytotoxicity towards PC-3 spheroids 92
6.2.4 Effect of PE-mediated PDT towards PC-3 spheroids 95
6.3 Discussion 97
6.4 Summary 101
References 102
7. Conclusion 104

List of Figures

Figure 1-1 Schematic representation of PDT cancer killing effect 5
Figure 1-2 Preparation scheme of porphyrus envelope (PE)..... 9
Figure 2-1 Chemical structure of PpIX lipid..... 15
Figure 2-2 PpIX lipid localization in PC-3 cells 18
Figure 2-3 Uptake of photosensitizers in PC-3 cells..... 20
Figure 3-1 Ultrastructural analysis of PE 24
Figure 3-2 Direct cytotoxic effect induced in PC-3 cells 29
Figure 3-3 Morphological change in PC-3 cells after treatment 30
Figure 3-4 Morphological change in PC-3 cells treated with light exposed PE..... 31
Figure 3-5 Cell survival rate after treating PC-3 cells with light irradiated PE 32
Figure 3-6 Wound healing ability of treated PC-3 cells 34
Figure 3-7 Wound surface area of PC-3 cells after PDT treatment..... 35
Figure 3-8 Colony formation in PC-3 cells after treatment..... 36
Figure 3-9 Relative fluorescence units of colony forming PC-3 cells 37
Figure 4-1 Optical setup of the laser diode used in this experiment 47
Figure 4-2 Profile of ROS/superoxide in PC-3 cells after treatment..... 51
Figure 4-3 ROS/superoxide signal intensity in PC-3 cells..... 52
Figure 4-4 Mode of cell death induced in PC-3 cells before and after PDT 54
Figure 4-5 Therapeutic efficacy of PE-mediated PDT..... 56
Figure 4-6 Logarithmic median effect plots for PC-3 cells..... 58
Figure 4-7 Logarithmic combination index plot for PC-3 cells 60
Figure 4-8 Cytotoxic pathway induced via HVJ-E and PE-mediated PDT 63
Figure 5-1 Cancer selective uptake of PpIX lipid via PE..... 74
Figure 5-2 Direct cytotoxic effect in PNT2 cells and DU145 cells..... 76
Figure 5-3 Morphological change in cells after PE treatment..... 77
Figure 5-4 Effect of PE-mediated PDT in PNT2 cells and DU145 cells 79
Figure 6-1 Number of PC-3 cells in spheroid system 89
Figure 6-2 Uptake of PpIX lipid in PC-3 spheroids..... 91
Figure 6-3 Morphological changes in PC-3 spheroids after treatment..... 93
Figure 6-4 Effect of direct cytotoxicity in PC-3 spheroids 94
Figure 6-5 Therapeutic efficacy of PDT in PC-3 spheroids..... 96

List of Tables

Table 4-1 Synergy assignment criteria for CI values 49
Table 4-2 Parameters for cytotoxicity induced in PC-3 cells 59
Table 4-3 CI values of PE and PE-PDT in combination 61
Table 6-1 PpIX lipid fluorescence in a single cell 97
Table 6-2 Cell death induced by PE-mediated direct cytotoxic effect 98
Table 6-3 Cell death induced by PE-mediated PDT 100

1. Introduction

1.1 Prostate cancer in cancers

The prostate is one of the four major cancer sites in men. At present, 1 in 5 men is expected to be diagnosed with this disease and 1 in 39 accounts for the death [1], [2]. Advancement in screening methods like prostate-specific antigen screening has contributed to the overall decline in prostate cancer mortality, yet survival improvement is not confirmed in advanced stage patients [3], [4]. Previous studies have shown that almost all prostate cancer will eventually grow into the metastatic castration-resistant state, the point at which all of the first-line therapies become ineffective [4], [5]. At this stage, the average overall survival rate becomes 1.5 years [6].

Prostate cancer is known to be reliant on androgen signaling, a characteristic which is also maintained in the castration-resistant state. In advanced stage cancer, genes responsible for androgenic hormone signaling gets upregulated, and the number of androgen receptors increases. The local production of androgens and androgen receptor activation is also observed due to the enhancement of 5α-reductase activity and elevated level of testosterone [7], [8]. These activities make prostate cancers hypersensitive to androgen; thus, the amount of androgen required for tumor growth in metastatic castration-resistant prostate cancer is much less than the amount for average condition [8]–[11]. Furthermore, a drug that acts androgen antagonist, such as flutamide, can transform into agonist after several weeks of treatment, further enabling the tumor progression [12], [13].

1.2 Treatment options for advanced prostate cancer

Treatment options for prostate cancer vary depending on the stage of this disease. Usage of systemic treatment is common in advanced prostate cancer since the surgical method, and radiation therapy are not very useful at this stage. Androgen deprivation therapy (ADT) is the first-line therapy for castration-naïve advanced prostate cancer and is effective in controlling tumor cell growth [5]. Its drastic cancer-killing effect, however, is limited to initial treatment [14].

Development of castrate resistance is often observed 2 years after ADT initiation and this change is terminal [15], [16]. Once the tumor obtains androgen-independent characteristic, typical survival in patients drops down to < 18 months, and 5-year survival rate becomes less than 29% [16]–[18]. In fact, 85% of patients with castration-resistant prostate cancer have metastases, with 65–75% experiencing bone metastases which severely reduce their quality of life [16], [19]. First-line chemotherapeutic drug docetaxel is added to the treatment scheme when the patients start to show the signs of metastases; however, the usage of this therapeutic is only effective until cancer gains resistance to it. Novel systemic agents, such as cabazitaxel and abiraterone, are said to increase the survival rate, but so far, the overall survival rate is only extended for 4 months [18].

Sipuleucel-T is a first immunotherapeutic drug for hormone-refractory prostate cancer that utilizes white blood cells to destroy cancer cells [5], [20]. Many believe immunotherapy holds the key to overcome cancer in advanced stages; however, limited level of T cell infiltration in prostate cancer restricts the therapeutic outcome, and it is only effective in slowing down the progression rate [21]. Although current immunotherapy allows for the extension of overall survival to 25 months, it is still very costly with no effective treatment available once this method is confirmed to be ineffective [17], [19]. Thus, the importance of combination therapy has been addressed for more effective treatment against metastatic castration-resistant prostate cancer [22].

Furthermore, since treatment population for prostate cancer is elderly, the treatment itself should not be too aggressive [23]. With the current method, long-term hormone therapy results in the loss of bone minerals, causing the inevitable destruction of bone structure [24]. Palliative medicine is often performed, yet it is not curative. Also, application of chemotherapeutics frequently results in severe side-effects that disable the continuation of these drugs [15], [16]. Sipuleucel-T is one of the few treatment methods that does not exhibit severe side-effects; however, flu-like symptoms are inevitable, with 65% of patients reporting the adverse effect [25].

1.3 Photodynamic therapy (PDT) as an alternative treatment

Photodynamic therapy (PDT) is a therapeutic modality that is being used in various oncologic sites, such as esophagus, skin, brain, and bladder. This method has been recognized as an attractive alternative for metastatic disease, as it allows cancer-selective treatment without inducing cumulative toxicity after repeated treatment [26]–[28]. In PDT for urological tumors, the prostate is considered as the main target for primary and salvage treatment [29].

1.3.1 Photodynamic therapy for prostate cancer

First PDT for prostate cancer was performed in 1990 by Windahl *et al.* using first generation photosensitizer, polyporphyryn, who reported the reduction in PSA level after treatment [30]. Since then, extensive research has been ongoing to establish effective PDT strategy for both primary and metastatic prostate cancer. In fact, studies using second generation photosensitizer, mesotetra (hydroxyphenyl) chlorin (mTHPC) and 5-aminolevulunic acid, succeeded in reducing prostate tumor volume and the serum PSA level to 30–50% while preserving normal prostate [31]–[33].

In addition, the light delivery for prostate PDT exhibits technical feasibilities, as it can be done through interstitial PDT, which mimicks the procedure for prostate biopsies and brachytherapy. The guidance of transrectal ultrasound and a perineal template can simply be applied in prostate PDT to place the optical fibers, which are inserted within the plastic needles, to the desired place [33]. Since salvage treatment does not exist after conventional therapeutic modalities, these promising results and its feasible procedure together make PDT an attractive alternative as a minimally invasive therapy [34]. Furthermore, since PDT has unique cancer killing scheme of using ROS to induce various cell death pathways, it can eliminate the induction of cross resistance that appeared problematic in conventional therapeutic modalities [35].

1.3.2 Basic photochemistry

During PDT, prostate cancer tissues are irradiated with light after the period required for sufficient accumulation of light-sensitive drug called photosensitizer (PS). Since light used for PDT matches the photon absorption spectrum of the drug, ground singlet state PS is converted to the excited singlet state. The excited singlet state PS then relaxes to triplet state PS which undergoes one of the following two reactions to create reactive

oxygen species (ROS): 1) electron transfer reaction that results in the formation of superoxide anion $O_2^{\bullet-}$, hydrogen peroxide H_2O_2, and hydroxyl radical •OH (Type 1) or 2) energy transfer that generates singlet oxygen $^1O_2$ (Type 2) [27], [29], [31], [36]. Type II reaction is considered to be the primary reaction induced via PDT and the produced $^1O_2$ can result in the formation of secondary ROS [37], [38].

1.3.3 PDT-mediated cell death

Resulting $O_2^{\bullet-}$, H_2O_2,•OH and $^1O_2$ together induce oxidative stress in cells which leads to 1) direct cancer cell killing, 2) vasculature shutdown, and 3) anti-tumor immunity response (Figure 1-1) [36].

Direct cancer cell killing

Primary $^1O_2$ produced in cells via PDT has a short half-life of < 4 μs; therefore, its effect at the spatial level is limited to approximately 157 nm [38]. The half-life of $O_2^{\bullet-}$ and •OH is also < 4 μs, with H_2O_2 being the most stable ROS with the half-life of 1 min [39]. Thus, the degree of photodamage is limited to a local or proximal area of destruction [27]. To date, the full range of PS has been analyzed for their precise localization in cells, and the type of induced cell death. PS can localize in cellular organelles, such as lysosomes, mitochondria, Golgi apparatus, endoplasmic reticulum (ER), and cell membrane [40]. The previous study has reported that apoptotic pathway is often induced by PS that exhibits lysosomal, mitochondrial, or ER localization, whereas PS that accumulates in cell membrane has been reported to induce necrotic pathway [27], [41].

Apoptosis resulting from mitochondrial damage has been reported to be the dominant cell death pathway induced after PDT [26], [36], [41]. Light irradiation will cause mitochondrial-membrane damage that results in the release of cytochrome c to the cytosol. The cytosolic release of cytochrome c will induce the formation of the multiprotein complex that contains cytochrome c, Apaf-1, and caspase-9, which is known as apoptosome. Apoptosome formation will generate procaspases that enhance protein cleavage and DNA fragmentation, resulting in apoptotic cell death [41].

Vasculature shutdown

In addition, PDT can induce hypoxia in treated tumor area which causes nutrient deprivation [35], [41]. Since tumor-induced angiogenesis is required for tumor growth and migration, the significant reduction of tumor blood flow will inhibit the tumor cell

growth. Therefore, $O_2^{\bullet-}$, H_2O_2,•OH, and $^1O_2$ produced after PDT that reacts with cancer vasculature can act to kill the cancer cells.

Anti-tumor immunity response

The conventional therapies, such as surgery and radiotherapy, are known to be immunosuppressive. On the other hand, PDT induces acute stress response in the tumor tissues that acts to upregulate the immune response [28], [42]. In fact, PDT is a highly effective inducer of danger signaling, such as damage-associated molecular patterns and chemokines, which are detected by innate immune cells, including neutrophils and macrophages [28], [35]. PDT-treated cells can also act as inflammatory mediators that will recruit dendritic cell (DC)-activated $CD8^+$ T cells required for cancer cell killing [35]. Previous researchers have reported how the absence in $CD8^+$ T cells activation and infiltration in cancer cells results in the significant reduction of PDT effect, suggesting how adaptive immunity plays a crucial role in PDT effect [43]–[45].

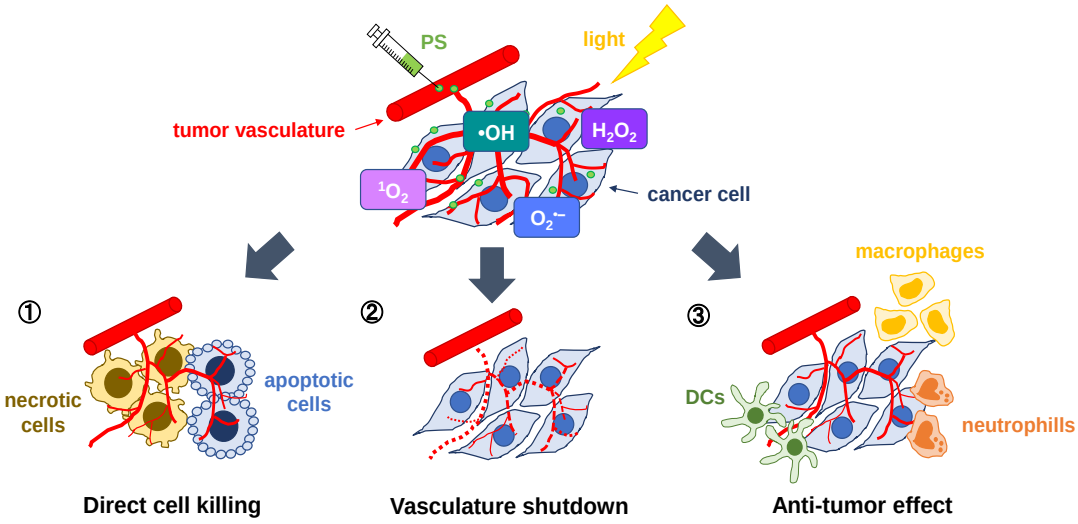

Figure 1-1 Schematic representation of PDT cancer killing effect
Photosensitzer (PS) will absorb the light and will produce reactive oxygen species (ROS) including superoxide anion $O_2^{\bullet-}$, hydrogen peroxide H_2O_2, and hydroxyl radical •OH, and singlet oxygen ($^1O_2$) after several reactions. Produced $O_2^{\bullet-}$, H_2O_2, •OH, and $^1O_2$ both induce 1) direct cancer cell killing, 2) vasculature shutdown, and 3) anti-tumor immunity effect in tumor.

1.4 Drawbacks of current PDT method for prostate cancer

As mentioned above, prostate PDT can be performed via relatively feasible method, and is believed to bring promising therapeutic outcome upon clinical application. However, PDT is still not a curative modality for large and disseminated tumors [36]. Thus, enhancement in induced toxicity is urgently recquired to ensure a comprehensive treatment of the entire gland to make prostate PDT a clinically relevant method [35]. Intense research is currently being carried out to combine anti-tumor reagents and PDT to allow for more enhanced anti-tumor immunity to cure widely spread tumors.

In addition, prostate cancer is usually seen as multifocal, where accumulated PS and treatment outcome appear heterogeneous, which results in PS being distributed throughout the normal tissues [29], [40], [41]. Thus, cancer selectivity and cellular localization must be carefully chosen for better therapeutic outcome. Novel PDT methods which ensures short drug-light interval that achieves user-friendly treatment with cost efficiency is also eagerly awaited [27].

1.5 Novel photosensitizer that induces multiple death pathways

In this study, cell membrane-localizing PS that induces various cell death pathways is established to acquire and enhance cancer selectivity and treatment efficacy for prostate PDT.

1.5.1 Photosensitizer that localize in cell membrane

PS that localizes in cell membrane is rarely found in the field of PDT; however, the photodynamic reaction caused by cell membrane-associated PS is known to be 10-fold higher than those observed in other cellular organelles-targeting drugs [27], [28]. Thus, cell membrane was selected as the main target for novel prostate PDT.

The cell death pathway induced in PS that localizes in cell membrane is necrotic which results in the loss of membrane integrity and the spillage of intracellular components [26]. Robust inflammatory reaction will result from the rupture of cell membrane, initiating the immune cell recruitment and antigen presentation [28]. In addition, enhanced level of lethal damage to proximal cells are observed in necrotic cells [26]. This effect by itself and the damage to adhesive molecules localized in cell membrane can both reduce adhesive activity of cancer cells, inhibiting the metastatic

potential of this disease [26], [40]. Furthermore, necrotic cells can induce the production of heat-shock protein (Hsp) 70. In fact, 15–25% of total cellular Hsp70 has been confirmed to be exposed to the cell surface right after the treatment [42]. Since inflammation and antigen-presenting cell activation can be induced through this phenomenon, immune response in tumor can be enhanced through the expression of extracellular HSP70 [28], [35].

1.5.2 Novel photosensitizer delivery system for PDT

Membrane-targeting delivery of PS can be achieved by utilizing site-specific vehicles. Several studies have already been performed using nanocarriers and monoclonal antibodies to allow for higher therapeutic efficacy [41]. This study focuses on the use of replication-deficient hemagglutinating virus of Japan (HVJ; Sendai virus) particle (HVJ-envelope; HVJ-E) to specifically deliver PS in cell membrane of recurrent prostate cancers.

Cancer selective delivery via HVJ-E

HVJ-E consists of two viral glycoproteins, hemagglutinin-neuraminidase (HN) and fusion (F) proteins, which are responsible for inducing membrane fusion at host plasma membrane [46]. The previous study has confirmed that HVJ-E can easily be created by ultraviolet (UV) irradiation [46]. In addition, HN proteins in HVJ-E exhibits strong affinity towards gangliosides GD1a and SPG that are highly expressed on castration-resistant prostate cancer cells [46], [47]. The expression of these receptors are significantly reduced in normal prostate epithelium; therefore, selective delivery can be achieved by this drug delivering moiety [46], [47].

Direct cytotoxic effect of HVJ-E

HVJ-E is known to induce cancer cell-selective apoptosis and necroptosis. Previous study using castration-resistant prostate cancer cell lines PC-3 and DU145 has revealed how a signalling pathway involving retinoic acid-inducible gene-I (RIG-I) and mitochondrial antiviral signalling protein (MAVS) enhances the expression level of apoptosis inducers, phorbol-12-myristate-13-acetate-induced protein 1 (Noxa) and tumor necrosis factor-related apoptosis-inducing ligand (TRAIL) [46], [48]–[50]. It has also been revealed that HVJ-E-fused cells exhibit cell division cessation and enter apoptotic

reaction [47]. Furthermore, ROS formation resulting from elevated Ca^{2+} causes necroptosis in cancer cells [46], [51], [52].

Anti-tumor immune response in HVJ-E-treated cells

Infiltration of natural killer (NK) cells, dendritic cells (DCs), $CD4^+$ T cells, and $CD8^+$ T cells in malignant tissue is confirmed after HVJ-E treatment [53]–[55]. In HVJ-E-treated tumors, local secretion of interferon (INF)-inducible chemokine CXCL10 recruits NK cells and activates them via INF-α, β at relatively early stage of 12–24 h [54]. In addition, activated RIG-I via HVJ-E treatment can mediate the production of intracellular adhesion molecule-1 (ICAM-1) in prostate cancer cells [56]. Since ICAM-1 strongly binds with lymphocyte function-associated antigen 1 (LFA-1) expressed on CTL and NK cells, immune cells sensitivity towards cancer cells is enhanced [56]. Furthermore, HVJ-E is known to induce Toll-like receptor independent DCs maturation via NFκB activation [53]. Matured DCs will then upregulate $CD4^+$ T cells by INF-γ, enhancing the production of $CD8^+$ T cells [53]. Although regulatory T cells (Treg) normally inhibits the activity of $CD8^+$ T cells in cancer cells, HVJ-E treatment can rescue $CD8^+$ T cells from the suppressive phenotype. Upon injection of HVJ-E, carbohydrate on F-glycoprotein in HVJ-E is recognized by DCs which induces the production of interleukin (IL)-6 [57]. This IL-6 has been reported to inhibit the activity of Treg and enhance cancer killing ability of $CD8^+$ T cells [53]. IL-6 is an inflammatory factor; however, Treg suppression by IL-6 is thought to be safe, as inflammatory response nor tissue damage is observed in mice [53].

Clinical trial using HVJ-E in prostate cancer

Fujita *et al.* performed phase I/II clinical trial to analyze the therapeutic efficacy of HVJ-E in castration-resistant prostate cancer patients. This study reported the reduced expression of PSA after low-dose HVJ-E-treatment [58]. High-dose HVJ-E-treatment is now being performed to testify the safety and immunogenic property of this modality.

These characteristics make HVJ-E a potential drug carrier that exhibits innate and adaptive immunities against metastatic and recurrent prostate cancer cells. Thus,

combination of HVJ-E and PDT has a high potential of exhibiting synergistic therapeutic effect.

1.5.3 Novel photosensitizer that combines HVJ-E with PpIX lipid: porphyrus envelope (PE)

To utilize HVJ-E as a photosensitizer carrier while fully exploiting unique characteristics of HVJ-E, damage to the HVJ-E structure had to be avoided to prevent the leakage of viral RNA fragments that trigger anti-tumor activity. Thus, as we have previously reported, lipidated form of PpIX (PpIX lipid), which mainly utilizes type II photodynamic processes, was chosen to create a novel photosensitizer, porphyrus envelope (PE; Figure 1-2) [59], [60].

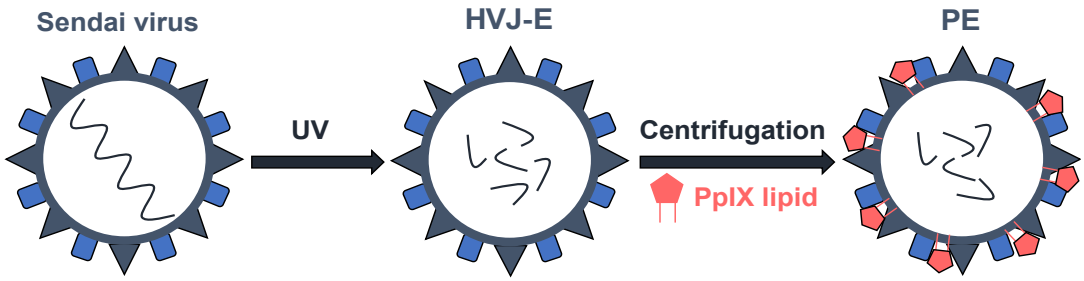

Figure 1-2 Preparation scheme of porphyrus envelope (PE)
Ultraviolet (UV)-irradiated Sendai virus particles, hemagglutinating virus of Japan envelope (HVJ-E), was used in this study. Lipidated protoporphyrin IX (PpIX lipid) was inserted in HVJ-E membrane via centrifugation to create a novel photosensitizer named porphyrus envelope (PE).

1.6 Aim of this study

This study aims to establish a PDT regimen that induces multiple cell death pathways for novel prostate cancer therapy. Previous study has already confirmed PDT efficacy of PE-mediated PDT over 5-aminolevulinic acids-mediated PDT; however, its localization in cells and its ability to induce direct cytotoxicity and selective PDT remains to be uncovered. Thus, membrane-targeting delivering potential and its therapeutic efficacy against recurrent prostate cancer were analyzed using normal prostate epithelia PNT2 and castration-resistant human prostate cancer cell line PC-3 and DU145.

1.7 Outline of this dissertation

PE mediated drug delivery and its efficacy will be discussed in Chapter 2. Direct cytotoxic effect induced by PE will then be addressed in Chapter 3. PDT efficacy of PE-mediated PDT and its ability to induce synergistic efficacy at different incubation period will be testified in Chapter 4. In addition, therapeutic efficacy of PE-mediated PDT towards prostate cancer cell line, DU145, and normal prostate epithelia, PNT2, will be confirmed to see the therapeutic selectivity and cancer killing efficacy in Chapter 5. Furthermore, therapeutic outcome of PE-mediated PDT using biologically mimicking 3D model will be analyzed in Chapter 6. Summary of all the work will be provided in Chapter 7.

References

[1] R. L. Siegel, K. D. Miller, and A. Jemal, "Cancer statistics, 2016," *CA. Cancer J. Clin.*, vol. 66, no. 1, pp. 7–30, 2016.

[2] A. C. Society, "Key Statistics for Prostate Cancer," 2017. [Online]. Available: https://www.cancer.org/cancer/prostate-cancer/about/key-statistics.html. [Accessed: 13-Nov-2017].

[3] J. N. Wu, K. M. Fish, C. P. Evans, R. W. Devere White, and M. A. Dallera, "No improvement noted in overall or cause-specific survival for men presenting with metastatic prostate cancer over a 20-year period," *Cancer*, vol. 120, no. 6, pp. 818–823, 2014.

[4] E. S. Antonarakis *et al.*, "AR-V7 and Resistance to Enzalutamide and Abiraterone in Prostate Cancer," *N. Engl. J. Med.*, vol. 371, no. 11, pp. 1028–1038, 2014.

[5] "NNCN guidelines for patients: prostate cancer," *National Comprehensive Cancer*, 2016. [Online]. Available: https://www.nccn.org/patients/guidelines/prostate/files/assets/basic-html/page-1.html#. [Accessed: 13-Nov-2017].

[6] T. Karantanos, C. P. Evans, B. Tombal, T. C. Thompson, R. Montironi, and W. B. Isaacs, "Understanding the mechanisms of androgen deprivation resistance in prostate cancer at the molecular level," *Eur. Urol.*, vol. 67, no. 3, pp. 470–479, 2015.

[7] K. J. Pienta and D. Bradley, "Mechanisms underlying the development of androgen-independent prostate cancer," *Clinical Cancer Research*, vol. 12, no. 6. pp. 1665–1671, 2006.

[8] R. B. Montgomery *et al.*, "Maintenance of intratumoral androgens in metastatic prostate cancer: A mechanism for castration-resistant tumor growth," *Cancer Res.*, vol. 68, no. 11, pp. 4447–4454, 2008.

[9] L. Graham and M. T. Schweizer, "Targeting persistent androgen receptor signaling in castration-resistant prostate cancer," *Medical Oncology*, vol. 33, no. 5. 2016.

[10] J. Holzbeierlein *et al.*, "Gene Expression Analysis of Human Prostate Carcinoma during Hormonal Therapy Identifies Androgen-Responsive Genes and Mechanisms of Therapy Resistance," *Am. J. Pathol.*, vol. 164, no. 1, pp. 217–227, 2004.

[11] C. D. Chen *et al.*, "Molecular determinants of resistance to antiandrogen therapy," *Nat. Med.*, vol. 10, no. 1, pp. 33–39, 2004.

[12] M. Hara, Takahito; Miyazaki, Jun-ichi; Araki, Hideo; Yamaoka, Masuo; Kanzaki, Naoyuki; Kusaka, Masami; Miyamoto, "Novel mutations of androgen receptor: a possible mechanism of bicalutamide withdrawal syndrome," *Cancer Res.*, vol. 63, pp. 149–153, 2003.

[13] M. E. Taplin *et al.*, "Selection for androgen receptor mutations in prostate cancers treated with androgen antagonist," *Cancer Res.*, vol. 59, no. 11, pp. 2511–2515, 1999.

[14] W. P. Harris, E. A. Mostaghel, P. S. Nelson, and B. Montgomery, "Androgen deprivation therapy: progress in understanding mechanisms of resistance and optimizing androgen depletion," *Nat. Clin. Pract. Urol.*, vol. 6, no. 2, pp. 76–85, 2009.

[15] A. S. Merseburger, A. Alcaraz, and C. A. von Klot, "Androgen deprivation therapy

as backbone therapy in the management of prostate cancer," *OncoTargets and Therapy*. pp. 7263–7274, 2016.
[16] S. Oudard, "Progress in emerging therapies for advanced prostate cancer," *Cancer Treatment Reviews*. pp. 275–289, 2013.
[17] T. A. West, B. E. Kiely, and M. R. Stockler, "Estimating scenarios for survival time in men starting systemic therapies for castration-resistant prostate cancer: A systematic review of randomised trials," *Eur. J. Cancer*, vol. 50, no. 11, pp. 1916–1924, 2014.
[18] B. S. Seal, C. V. Asche, K. Puto, and P. D. Allen, "Efficacy, patient-reported outcomes (PROs), and tolerability of the changing therapeutic landscape in patients with metastatic prostate cancer (MPC): A systematic literature review," *Value Heal.*, vol. 16, pp. 872–890, 2013.
[19] P. J. Toren and M. E. Gleave, "Evolving landscape and novel treatments in metastatic castrate-resistant prostate cancer," *Asian J. Androl.*, vol. 15, pp. 342–349, 2013.
[20] A. Enock and U. Ndefo, "Sipuleucel-T (Provenge) Injection The First Immunotherapy Agent (Vaccine) For Hormone-Refractory Prostate Cance," *Drug Forecast*, vol. 36, no. 4, pp. 197–202, 2011.
[21] M. Bilusic, R. A. Madan, and J. L. Gulley, "Immunotherapy of Prostate Cancer: Facts and Hopes," *Clin. Cancer Res.*, vol. 23, no. 22, pp. 1–7, 2017.
[22] G. Bryant, L. Wang, and D. J. Mulholland, "Overcoming oncogenic mediated tumor immunity in prostate cancer," *International Journal of Molecular Sciences*, vol. 18, no. 7. 2017.
[23] H. I. Scher *et al.*, "Design and end points of clinical trials for patients with progressive prostate cancer and castrate levels of testosterone: Recommendations of the Prostate Cancer Clinical Trials Working Group," *Journal of Clinical Oncology*. pp. 1148–1159, 2008.
[24] Y. Kakehi, M. Sugimoto, and R. Taoka, "Evidenced-based clinical practice guideline for prostate cancer (summary: Japanese Urological Association, 2016 edition)," *International Journal of Urology*. pp. 648–666, 2017.
[25] S. Gupta, E. Carballido, and M. Fishman, "Sipuleucel-T for therapy of asymptomatic or minimally symptomatic, castrate-refractory prostate cancer: An update and perspective among other treatments," *Onco. Targets. Ther.*, vol. 4, pp. 79–96, 2011.
[26] A. P. Castano, T. N. Demidova, and M. R. Hamblin, "Mechanisms in photodynamic therapy: part two—cellular signaling, cell metabolism and modes of cell death," *Photodiagnosis Photodyn Ther*, vol. 2, no. 1, pp. 1–23, 2005.
[27] A. P. Castano, T. N. Demidova, and M. R. Hamblin, "Mechanisms in photodynamic therapy: Part one - Photosensitizers, photochemistry and cellular localization," *Photodiagnosis and Photodynamic Therapy*. pp. 279–293, 2004.
[28] T. Kushibiki, T. Hirasawa, S. Okawa, and M. Ishihara, "Responses of Cancer Cells Induced by Photodynamic Therapy," *J. Healthc. Eng.*, vol. 4, no. 1, pp. 87–108, 2013.
[29] G. Bozzini *et al.*, "Photodynamic therapy in urology: What can we do now and where are we heading?," *Photodiagnosis and Photodynamic Therapy*. pp. 261–273, 2012.
[30] T. Windahl, S. O. Andersson, and L. Lofgren, "Photodynamic therapy of localised

prostatic cancer," *The Lancet*, vol. 336, no. 8723. p. 1139, 1990.
[31] T. Gheewala, T. Skwor, and G. Munirathinam, "Photosensitizers in prostate cancer therapy," *Oncotarget*, vol. 8, no. 18, pp. 30524–30538, 2017.
[32] S. H. Selman, D. Albrecht, R. W. Keck, P. Brennan, and S. Kondo, "Studies of tin ethyl etiopurpurin photodynamic therapy of the canine prostate.," *J. Urol.*, vol. 165, no. 5, pp. 1795–801, 2001.
[33] C. M. Moore, D. Pendse, and M. Emberton, "Photodynamic therapy for prostate cancer—a review of current status and future promise," *Nat. Clin. Pract. Urol.*, vol. 6, no. 1, pp. 18–30, 2009.
[34] J. H. Pinthus, A. Bogaards, R. Weersink, B. C. Wilson, and J. Trachtenberg, "Photodynamic therapy for urological malignancies: Past to current approaches," *Journal of Urology*. pp. 1201–1207, 2006.
[35] P. Agostinis *et al.*, "Photodynamic therapy of cancer: An update," *CA. Cancer J. Clin.*, vol. 61, no. 4, pp. 250–281, 2011.
[36] D. Nowis, M. Makowski, T. Stokłosa, M. Legat, T. Issat, and J. Gołąb, "Direct tumor damage mechanisms of photodynamic therapy," *Acta Biochimica Polonica*. pp. 339–352, 2005.
[37] K. D. Sattler, "Handbook of Nanophysics. 6. Nanoelectronics and Nanophotonics," *Handb. Nanophysics*, vol. 6, p. 779, 2010.
[38] M. R. Hamblin and P. Mroz, *Advances in Photodynamic Therapy: Basic, Translational, and Clinical*. 2008.
[39] Z. Zhou, J. Song, L. Nie, and X. Chen, "Reactive oxygen species generating systems meeting challenges of photodynamic cancer therapy," *Chem. Soc. Rev.*, vol. 45, pp. 6597–6626, 2016.
[40] C. A. Robertson, D. H. Evans, and H. Abrahamse, "Photodynamic therapy (PDT): A short review on cellular mechanisms and cancer research applications for PDT," *J. Photochem. Photobiol. B Biol.*, vol. 96, pp. 1–8, 2009.
[41] T. A. Debele, S. Peng, and H. C. Tsai, "Drug carrier for photodynamic cancer therapy," *International Journal of Molecular Sciences*, vol. 16, no. 9. pp. 22094–22136, 2015.
[42] A. P. Castano, P. Mroz, and M. R. Hamblin, "Photodynamic therapy and anti-tumour immunity," *Nat. Rev. Cancer*, vol. 6, no. 7, pp. 535–545, 2006.
[43] M. Korbelik and I. Cecic, "Contribution of myeloid and lymphoid host cells to the curative outcome of mouse sarcoma treatment by photodynamic therapy," *Cancer Lett.*, vol. 137, no. 1, pp. 91–98, 1999.
[44] E. S. Abdel-Hady *et al.*, "Immunological and viral factors associated with the response of vulval intraepithelial neoplasia to photodynamic therapy," *Cancer Res.*, vol. 61, no. 1, pp. 192–196, 2001.
[45] E. Kabingu, L. Vaughan, B. Owczarczak, K. D. Ramsey, and S. O. Gollnick, "CD8+ T cell-mediated control of distant tumours following local photodynamic therapy is independent of CD4+ T cells and dependent on natural killer cells," *Br. J. Cancer*, vol. 96, no. 12, pp. 1839–1848, 2007.
[46] K. Saga and Y. Kaneda, "Oncolytic Sendai virus-based virotherapy for cancer: recent advances," *Oncolytic Virotherapy*, vol. 4, pp. 141–147, 2015.
[47] Y. Kawaguchi, Y. Miyamoto, T. Inoue, and Y. Kaneda, "Efficient eradication of hormone-resistant human prostate cancers by inactivated Sendai virus particle," *Int. J. Cancer*, vol. 124, pp. 2478–2487, 2009.

[48] T. Matsushima-Miyagi *et al.*, "TRAIL and Noxa are selectively upregulated in prostate cancer cells downstream of the RIG-I/MAVS signaling pathway by nonreplicating Sendai virus particles," *Clin. Cancer Res.*, vol. 18, no. 22, pp. 6271–6283, 2012.

[49] C. Ploner, R. Kofler, and A. Villunger, "Noxa: At the tip of the balance between life and death," *Oncogene*. pp. 84–92, 2008.

[50] P. A. Holoch and T. S. Griffith, "TNF-related apoptosis-inducing ligand (TRAIL): A new path to anti-cancer therapies," *Eur. J. Pharmacol.*, vol. 625, pp. 63–72, 2009.

[51] M. B. Hallett, P. Fuchst, and A. K. Campbell, "Sendai virus causes a rise in intracellular free Ca2+ before cell fusion," *Biochem. J*, vol. 206, pp. 671–674, 1982.

[52] P. Vandenabeele, L. Galluzzi, T. Vanden Berghe, and G. Kroemer, "Molecular mechanisms of necroptosis: An ordered cellular explosion," *Nature Reviews Molecular Cell Biology*. pp. 700–714, 2010.

[53] M. Kurooka and Y. Kaneda, "Inactivated Sendai virus particles eradicate tumors by inducing immune responses through blocking regulatory T cells," *Cancer Res.*, vol. 67, no. 1, pp. 227–236, 2007.

[54] A. Fujihara, M. Kurooka, T. Miki, and Y. Kaneda, "Intratumoral injection of inactivated Sendai virus particles elicits strong antitumor activity by enhancing local CXCL10 expression and systemic NK cell activation," *Cancer Immunol. Immunother.*, vol. 57, pp. 73–84, 2008.

[55] C. Y. Chang, J. A. Tai, S. Li, T. Nishikawa, and Y. Kaneda, "Virus-stimulated neutrophils in the tumor microenvironment enhance T cell-mediated anti-tumor immunity," *Oncotarget*, vol. 7, no. 27, pp. 42195–42207, 2016.

[56] S. Li, T. Nishikawa, and Y. Kaneda, "Inactivated Sendai virus particle upregulates cancer cell expression of intercellular adhesion molecule-1 and enhances natural killer cell sensitivity on cancer cells," *Cancer Sci.*, vol. 108, no. 12, pp. 2333–2341, 2017.

[57] H. Suzuki, M. Kurooka, Y. Hiroaki, Y. Fujiyoshi, and Y. Kaneda, "Sendai virus F glycoprotein induces IL-6 production in dendritic cells in a fusion-independent manner," *FEBS Lett.*, vol. 582, no. 9, pp. 1325–1329, 2008.

[58] K. Fujita *et al.*, "Phase I/II clinical trial to assess safety and efficacy of intratumoral and subcutaneous injection of HVJ-E in castration-resistant prostate cancer patients," *Cancer Gene Ther.*, vol. 24, pp. 277–281, 2017.

[59] M. Yamauchi *et al.*, "A novel photodynamic therapy for drug-resistant prostate cancer cells using porphyrus envelope as a novel photosensitizer," *Photodiagnosis Photodyn. Ther.*, vol. 11, no. 1, pp. 48–54, 2014.

[60] S. Tachikawa, M. E. El-Zaria, R. Inomata, S. Sato, and H. Nakamura, "Synthesis of protoporphyrin-lipids and biological evaluation of micelles and liposomes," *Bioorganic Med. Chem.*, vol. 22, no. 17, pp. 4745–4751, 2014.

2. Photosensitizer delivery by PE

Necrotic cells after PDT can intensify the inflammatory response and enhance the anti-tumor immune activity in cancer cells [1]–[3]. Membrane-localizing PS has been reported to be the efficient necrosis inducer; however, PS that allows explicit targeting of cell membrane is rarely found in current PDT modality [2], [4]. In this study, HVJ-E was utilized to enhance and improve the accumulation efficacy of photosensitizer in the cell membrane. As has been discussed in *Section 1.5.2*, HVJ-E can induce membrane fusion at host cell membrane via HN proteins and F proteins [5]. Fusion activity induced by HVJ-E can occur at short incubation period as 10 s that this drug delivering vehicle may be able to shorten the drug-light interval [6], [7].

PpIX lipid used in this study has been reported to share the similar lipid structure as HVJ-E; therefore, PS insertion in HVJ-E membrane can easily be achieved via centrifugation (Figure 2-1) [8]–[10]. Since HVJ-E mediates membrane fusion at host cell surface, direct delivery of inserted PpIX lipid in cancer cell membrane should be achieved. In this chapter, localization of PE-inserted PpIX lipid was analyzed by confocal laser scanning microscopy. In addition, drug delivering efficacy of PE was addressed by determining the uptake of PpIX lipid in PC-3 cells.

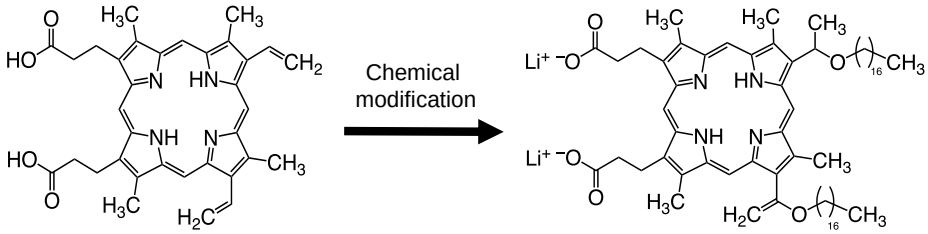

Figure 2-1 Chemical structure of PpIX lipid

Protoporphyrin IX (PpIX) was modified with alkyl group (C17) and lithium salt to provide with amphiphilic property.

2.1 Materials and Methods

2.1.1 Cell line and culture

10% fetal bovine serum (FBS, S1820, Biowest, France) and 100 units/mL penicillin-streptomycin (P4458, Sigma-Aldrich, USA) were added to Dulbecco's modified Eagle's medium (D-MEM, D6046, Sigma-Aldrich, USA) to create complete D-MEM. Androgen-independent human prostate cancer cell line PC-3 was cultured in complete D-MEM at 37°C with humidity in 5% CO_2 atmosphere. For cell seeding, cells were harvested after reaching 80% confluence. All studies were conducted using stable lines.

2.1.2 Photosensitizers

Preparation of PE was done as follows: First, 5 mM PpIX lipid was diluted with Dulbecco's phosphate buffered saline (D-PBS, D8537, Sigma-Aldrich, USA) to 10.5 μM solution. HVJ-E was then prepared as previously reported and was separated to 2500 hemagglutination units (HAU; 1 HAU corresponds to 10^6–10^7 HVJ-E particles) each [8], [11]. This HVJ-E was suspended in 10.5 μM PpIX lipid solution with a final volume of 1 mL [11]. Then, PE was prepared by inserting PpIX lipid into HVJ-E via centrifugation (20,000 × g, 4°C, 10 min) [8]. Finally, the supernatant was removed after centrifugation and the pellet of PE was suspended in 835 μL of complete D-MEM. The ratio of PpIX lipid to HVJ-E in PE was 3.5 pmol/HAU.

In addition, 5-aminolevulinic acid hydrochloride (5-ALA, A7793, Sigma-Aldrich, USA) was dissolved in complete D-MEM to create 1 mM 5-ALA solution and 5 mM PpIX lipid was diluted with complete D-MEM to 10.5 μM. Suspensions of HVJ-E was prepared at concentrations of 1000 HAU/500 μL and 150 HAU/50 μL by suspending it in complete D-MEM. 5-ALA was stored at –20°C and an aqueous solution of 5 mM PpIX lipid was stored at 4°C [10]. All reagents were prepared prior to each experiment.

2.1.3 Confocal Microscopy

Confocal laser scanning microscope was used to observe the red fluorescence of PpIX lipid in PC-3 cells (EclipseTi equipped with A1R/A1, Nikon, Japan). In this experiment, cell chamber slides (Nunc® Lab-Tek® II, Thermo Fisher Scientific, USA) were used to seed the cells. PC-3 cells with a density of 3.0×10^4 cells/chamber were cultured at 37°C

in 5% CO_2 for 24 h to let the cells adhere to the well bottom. Then, cells were treated for 10 min, 1 h, 3 h, or 5 h in PE suspension (1000 HAU/500 μL) at 37°C in 5% CO_2. Following the incubation, cells were washed twice with D-PBS at room temperature. To indicate the cellular localization of PpIX lipid in PC-3 cells, lipophilic fluorescent dye PKH67 (MINI67-1KT, Sigma-Aldrich, USA) was used to label the cell membrane, and Hoechst® 33342 (2′-[4-ethoxyphenyl]-5-[4-methyl-1-piperazinyl]-2,5′-bi-1*H*-benzimidazole) solution (R37605, Thermo Fisher Scientific, USA) was used to visualize the cell nuclei. The excitation wavelengths were set to 403 nm for PpIX lipid and Hoechst® 33342, and 488 nm for PKH67. Detection wavelength ranges were 662–737 nm for PpIX lipid, 500–550 nm for PKH67, and 425–475 nm for Hoechst® 33342. The laser power was adjusted to exclude the autofluorescence from the cells.

2.1.4 Fluorescence assay for uptake of PpIX

Relative cellular uptake of PpIX lipid delivered by PE was measured using a cell-based fluorescent assay. A black 96-well cell culture plate with a clear bottom (Falcon® 353219, BD, USA) was used in this experiment. PC-3 cells with a density of 5.0×10^3 cells/well were incubated at 37°C in 5% CO^2 condition for 24 h. The following day, cells were exposed to 50 μL of complete D-MEM, 5-ALA solution, PpIX lipid solution, HVJ-E suspension, or PE suspension for 10 min, 30 min, 1 h, 2h, 3 h, 4 h or 5 h. To observe the cellular uptake of photosensitive agents in cells, cells were washed with D-PBS once, and were lysed in D-PBS containing 0.1% sodium dodecyl sulphate (31606-75, Nacalai Tesque, Japan). Fluorescence intensity of PpIX was measured right after this process using a fluorescence microplate reader (SpectraMAX Gemini, Molecular Devices, USA) at an excitation wavelength of 401 nm and an emission wavelength of 625 nm.

2.1.5 Statistical analysis

All results are expressed as the means ± standard deviation (SD) for six cases ($n = 6$). A two-tailed unpaired Student's *t*-test was performed between two sample groups, and a probability value of $*P < 0.01$ was considered statistically significant.

2.2 Experimental results

2.2.1 Membrane-targeting delivery of PE

The localization of PpIX lipid in PC-3 cells at respective immersion time was observed using confocal laser scanning microscope. The accumulation of PpIX lipid delivered with PE was observed alongside the cell membrane, confirming the site-specific delivering ability of PE (Figure 2-2). Intracellular uptake of PpIX lipid was observed after 5 h incubation; however, membrane-specific localization of PpIX lipid was evident in all samples treated with PE. Enlarged multinucleated cell called syncytia was confirmed in 5 h sample, indicating the cell-to-cell fusion.

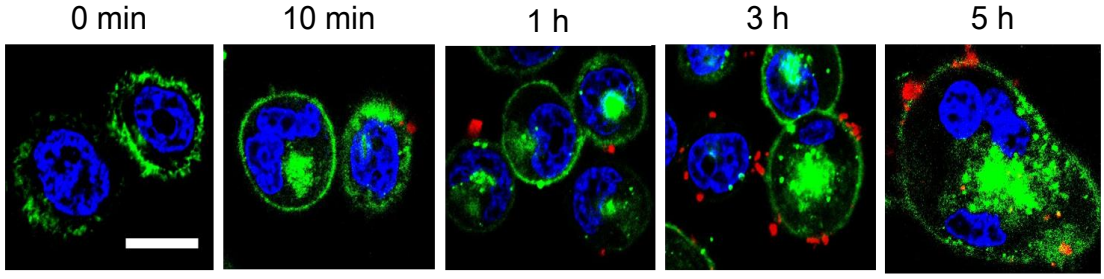

Figure 2-2 PpIX lipid localization in PC-3 cells

Confocal images of live PC-3 cells after incubating with PE for 0 min–5 h at a concentration of 1000 HAU/500 μL. PpIX lipid (red), PKH67-labeled cell membrane (green), and Hoechst®33342-labeled nucleus (blue) are shown. PE successfully delivered PpIX lipid to cell membrane at all time periods. Multinucleated syncytia formation was also observed in 5 h sample (nucleus indicated by white arrowheads). Scale bar indicates 20 μm.

2.2.2 Uptake of PE-inserted PpIX lipid in prostate cancer

Cellular uptake of PpIX lipid delivered by PE was compared with the amount of intracellular PpIX or PpIX lipid after induction with 1 mM 5-ALA or administration of exogenous PpIX lipid (Figure 2-3). Fluorescence intensity was not recognizable in cells treated with either D-MEM or HVJ-E suspension; however, cells treated with photosensitizers exhibited significant uptake of PpIX or PpIX lipid. Accumulation of 5-ALA-induced PpIX in PC-3 cells demonstrated the highest PpIX fluorescence intensity after 3 h incubation period, yet this intensity was approximately 30-fold lower than that of fluorescence intensity for PpIX lipid delivered with PE. Exogenous PpIX lipid and PE administration both resulted in high cellular uptake of photosensitizer. However, stronger fluorescence was observed in cells treated with PE with significant difference. In fact, fluorescence was approximately 1.2–2-fold higher in PE-treated cells. These results together suggest that PE allows rapid and efficient delivery to cell membrane.

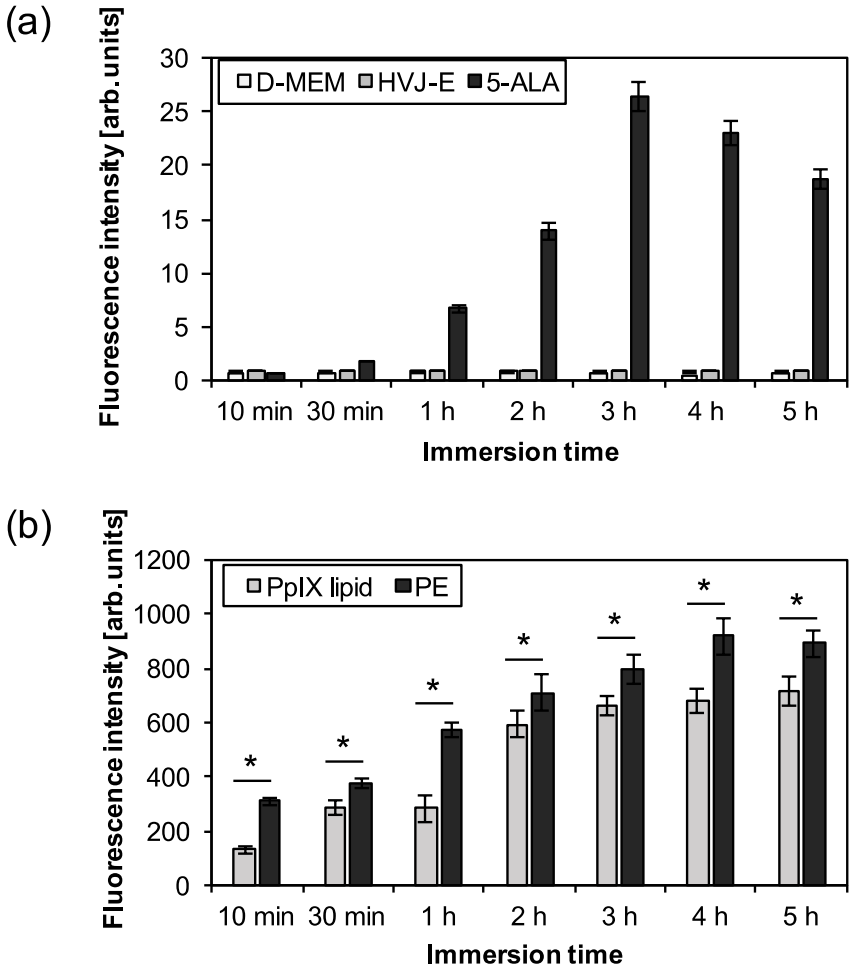

Figure 2-3 Uptake of photosensitizers in PC-3 cells

Fluorescence intensities of accumulated PpIX or PpIX lipid in PC-3 cells. Cells were incubated with (a) complete D-MEM, HVJ-E, or 5-ALA, and (b) PpIX lipid or PE. Samples treated with 5-ALA exhibited highest fluorescence intensity after 3 h incubation period. Both PpIX lipid and PE resulted in much higher photosensitizer uptake, yet PE treatment was confirmed to be significantly effective in delivering PpIX lipid to cancer site than PpIX lipid alone ($n = 6$; $^*P < 0.01$).

2.3 Discussion

Previous studies have shown how selective delivery of PS into the plasma membrane result in the loss of membrane integrity and spillage of cytosolic constituents, resulting in necrotic cell death [2]–[4]. As has been displayed by the data shown in Figure 2-2, fusion activity of PE could directly distribute PS in host cell membrane after 10 min immersion time. Thus, it is highly likely that necrosis is induced by PS delivery via PE. Necrotic death is known to exhibit rapid cell disruption and enhanced inflammatory reactions that potentiates cytokine production; therefore, PE should act as an immune inducer in the treatment scheme, enhancing the therapeutic outcome [3], [12], [13].

Furthermore, photosensitizer accumulation via PE was confirmed to be more effective than PpIX produced via 5-ALA biosynthesis and exogenous PpIX lipid administration (Figure 2-3). Although 5-ALA is known as a highly selective reagent with reduced cell toxicity, 5-ALA itself is not a photosensitive component and requires more than 2 h to be biologically synthesized into light-sensitive PpIX [14]–[16]. Sequential change of fluorescence intensity observed after PE administration indicated how fusion capability of PE readily allows rapid administration of PpIX lipid in PC-3 cells. Rapid and efficient delivery of PpIX lipid by PE may shorten the drug-light interval, while ensuring high PDT outcome.

Hemagglutinin-neuraminidase (HN) glycoproteins distributed on the bilayer of HVJ-E has been noted to exhibit affinity towards glycosphingolipids that contain sialic acids, named GD1a and SPG [5], [17]. The number of these receptors is approximately 2.6-fold higher in PC-3 cells than that in normal prostate epithelia; thus, PE-mediated PDT should allow for highly selective treatment [17].

2.4 Summary

PE could deliver PpIX lipid to cancer plasma membrane at all immersion times. PS localization in plasma membrane can induce acute inflammation due to necrosis; therefore, PE should trigger similar cell death pathway. In addition, significant uptake of PpIX lipid in PC-3 cells was observed 10 min after PE administration. Conventional photosensitizer 5-ALA requires more than 2 h to be efficiently accumulated in PC-3 cells. Thus, drug-light interval may be shorted by utilizing PE as a PS carrier.

References

[1] T. Kushibiki, T. Hirasawa, S. Okawa, and M. Ishihara, "Responses of Cancer Cells Induced by Photodynamic Therapy," *J. Healthc. Eng.*, vol. 4, no. 1, pp. 87–108, 2013.

[2] A. P. Castano, T. N. Demidova, and M. R. Hamblin, "Mechanisms in photodynamic therapy: Part one - Photosensitizers, photochemistry and cellular localization," *Photodiagnosis and Photodynamic Therapy*. pp. 279–293, 2004.

[3] A. P. Castano, T. N. Demidova, and M. R. Hamblin, "Mechanisms in photodynamic therapy: part two—cellular signaling, cell metabolism and modes of cell death," *Photodiagnosis Photodyn Ther*, vol. 2, no. 1, pp. 1–23, 2005.

[4] T. A. Debele, S. Peng, and H. C. Tsai, "Drug carrier for photodynamic cancer therapy," *International Journal of Molecular Sciences*, vol. 16, no. 9. pp. 22094–22136, 2015.

[5] K. Saga and Y. Kaneda, "Oncolytic Sendai virus-based virotherapy for cancer: recent advances," *Oncolytic Virotherapy*, vol. 4, pp. 141–147, 2015.

[6] M. Inai, M. Yamauchi, N. Honda, H. Hazama, S. Tachikawa, H. Nakamura, T. Nishida, H. Yasuda, Y. Kaneda, and K. Awazu, "Hemagglutinating virus of Japan envelope (HVJ-E) allows targeted and efficient delivery of photosensitizer for photodynamic therapy against advanced prostate cancer," in *Optical Molecular Probes, Imaging and Drug Delivery, OMP 2015*, 2015.

[7] Y. Kaneda, T. Nakajima, T. Nishikawa, S. Yamamoto, H. Ikegami, N. Suzuki, H. Nakamura, R. Morishita, and H. Kotani, "Hemagglutinating Virus of Japan (HVJ) Envelope Vector as a Versatile Gene Delivery System," *Mol. Ther.*, vol. 6, no. 2, pp. 219–226, 2002.

[8] M. Yamauchi, N. Honda, H. Hazama, S. Tachikawa, H. Nakamura, Y. Kaneda, and K. Awazu, "A novel photodynamic therapy for drug-resistant prostate cancer cells using porphyrus envelope as a novel photosensitizer," *Photodiagnosis Photodyn. Ther.*, vol. 11, no. 1, pp. 48–54, 2014.

[9] M. Yamauchi, N. Honda, H. Hazama, S. Tachikawa, H. Nakamura, Y. Kaneda, and K. Awazu, "Effective photodynamic therapy in drug-resistant prostate cancer cells utilizing a non-viral anti-tumor vector (a secondary publication)," *Laser Ther.*, vol. 25, no. 1, pp. 55–62, 2016.

[10] S. Tachikawa, M. E. El-Zaria, R. Inomata, S. Sato, and H. Nakamura, "Synthesis of protoporphyrin-lipids and biological evaluation of micelles and liposomes," *Bioorganic Med. Chem.*, vol. 22, no. 17, pp. 4745–4751, 2014.

[11] M. Inai, N. Honda, H. Hazama, S. Akter, S. Fuse, H. Nakamura, T. Nishikawa, Y. Kaneda, and K. Awazu, "Photodynamic therapy using a cytotoxic photosensitizer porphyrus envelope that targets the cell membrane," *Photodiagnosis Photodyn. Ther.*, vol. 20, pp. 238–245, 2017.

[12] A. P. Castano, P. Mroz, and M. R. Hamblin, "Photodynamic therapy and anti-tumour immunity," *Nat. Rev. Cancer*, vol. 6, no. 7, pp. 535–545, 2006.

[13] C. A. Robertson, D. H. Evans, and H. Abrahamse, "Photodynamic therapy (PDT): A short review on cellular mechanisms and cancer research applications for PDT," *J. Photochem. Photobiol. B Biol.*, vol. 96, pp. 1–8, 2009.

[14] M. Wachowska, A. Muchowicz, M. Firczuk, M. Gabrysiak, M. Winiarska, M. Wańczyk, K. Bojarczuk, and J. Golab, "Aminolevulinic acid (ala) as a prodrug in

photodynamic therapy of cancer," *Molecules,* vol. 16, no. 5, pp. 4140–4164, 2011.

[15] R. Chen, Z. Huang, G. Chen, Y. Li, X. Chen, J. Chen, and H. Zeng, "Kinetics and subcellular localization of 5-ALA-induced PpIX in DHL cells via two-photon excitation fluorescence microscopy," *Int. J. Oncol.*, vol. 32, no. 4, pp. 861–867, 2008.

[16] J. Kloek, W. Akkermans, and G. M. J. B. van Henegouwen, "Derivatives of 5-aminolevulinic acid for photodynamic therapy: Enzymatic conversion into protoporphyrin," *Photochem. Photobiol.*, vol. 67, no. 1, pp. 150–154, 1998.

[17] Y. Kawaguchi, Y. Miyamoto, T. Inoue, and Y. Kaneda, "Efficient eradication of hormone-resistant human prostate cancers by inactivated Sendai virus particle," *Int. J. Cancer*, vol. 124, pp. 2478–2487, 2009.

3. Direct cytotoxic effect induced by PE

Previous study using ultra-high voltage electron microscopy revealed that PE was approximately 200 nm in diameter with protrusions observed at the surface (Figure 3-1). These properties are similar to those observed in HVJ or HVJ-E alone; therefore, it is highly likely that PE maintains the oncolytic potential that is unique to these particles [1]–[3].

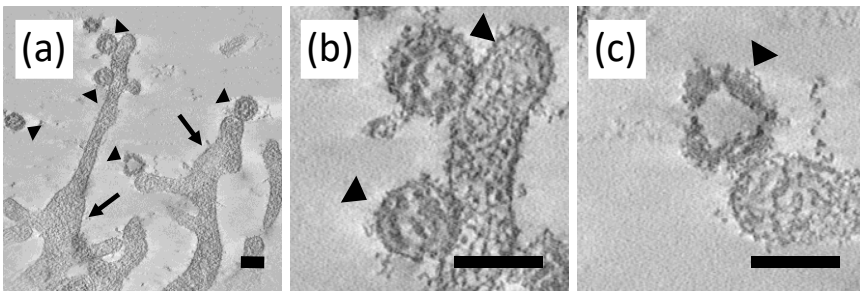

Figure 3-1 Ultrastructural analysis of PE

Ultrastructural analysis of porphyrus envelope after 10 min incubation. Scale bars indicate 200 nm. (a) Tomographic image of a 0.7-μm-thick-section indicated that porphyrus envelope (arrowhead) was approximately 200 nm in diameter. Most of the porphyrus envelope were making contact with microvilli of PC-3 cells (arrow); (b,c) Enlarged images of porphyrus envelope revealed tubule-like protrusions at the surface of each particles.

As has been discussed in *Section 1.5.2*, HVJ-E is known to induce cancer-selective apoptosis and necroptosis [4]–[10]. Thus, similar cell death mechanism should be observed in PE-treated cells even in the absence of light. To analyze the ability of PE to induce direct cytotoxic effect in PC-3 cells, three separate experiments were performed in this study: 1) cell viability assay, 2) scratch-wound assay, and 3) colony formation assay. Furthermore, membrane fusion activity and the ability of direct cytotoxicity induction were analyzed after irradiating the laser light to PE particles.

3.1 Materials and Methods

3.1.1 Cell line and culture

FBS and 100 units/mL penicillin-streptomycin were added to D-MEM to create complete D-MEM as mentioned in *Section 2.1.1*. Androgen-independent human prostate cancer cell line PC-3 was cultured in complete D-MEM at 37°C with humidity in 5% CO_2 atmosphere. For cell seeding, cells were harvested after reaching 80% confluence. All studies were conducted using stable lines.

3.1.2 Photosensitizers

Preparation of PE was done as follows: First, 5 mM PpIX lipid was diluted with D-PBS to 10.5 μM solution. HVJ-E was then prepared as previously reported and was separated to 2500 HAU each [11], [12]. This HVJ-E was suspended in 10.5 μM PpIX lipid solution with a final volume of 1 mL [12]. Then, PE was prepared by inserting PpIX lipid into HVJ-E via centrifugation (20,000 × g, 4°C, 10 min) [11]. Finally, the supernatant was removed after centrifugation and the pellet of PE was suspended in 835 μL of complete D-MEM. The ratio of PpIX lipid to HVJ-E in PE was 3.5 pmol/HAU.

In addition, 5-aminolevulinic acid hydrochloride (5-ALA, A7793, Sigma-Aldrich, USA) was dissolved in complete D-MEM to create 1 mM 5-ALA solution and 5 mM PpIX lipid was diluted with complete D-MEM to 10.5 μM. Suspensions of HVJ-E were prepared at concentrations of 1000 HAU/500 μL and 150 HAU/50 μL by suspending it in complete D-MEM. 5-ALA was stored at –20°C and an aqueous solution of 5 mM PpIX lipid was stored at 4°C [13]. All reagents were prepared prior to each experiment.

3.1.3 Direct cytotoxic effect of PE

Experiments were performed to address the ability of PE to induce direct cytotoxicity in PC-3 cells 1) with or 2) without light irradiation. For both experiments, PC-3 cells were seeded on a black 96-well cell culture plate with a clear bottom at a density of 5.0×10^3 cells/well and incubated for 24 h at 37 °C in 5% CO_2. For the first experiment, 50 μL of complete D-MEM, 5-ALA solution, PpIX lipid solution, HVJ-E suspension, or PE suspension were added to each well and were exposed to 10 min, 30 min, 1 h, 2 h, 3 h, 4 h, or 5 h, respectively. Cells were then washed once with D-PBS and incubated for 24 h at 37°C in 5% CO_2 condition in 100 μL of complete D-MEM. The cell survival rate after

respective treatment was determined by changing the medium of each well to a mixture of 90 μL of complete D-MEM and 10 μL of a cell counting reagent (07553- 44, Nacalai Tesque, Japan) that contains water-soluble tetrazolium salt (WST-8). An absorbance microplate reader (VersaMAX, Molecular Devices, USA) and light of 450 nm wavelength was measured using a to determine the optical density of each well. The cell survival rate for each sample was calculated as a percentage of the control (cells treated with complete D-MEM). Microscopic images of PC-3 cells were obtained using an inverted laboratory microscope (Leica DMIL, Leica Microsystems, Germany) for samples treated with complete D-MEM, PpIX lipid solution, HVJ-E suspension, or PE suspension for 10 min–5 h. For the second experiment, the ability of PE to induce direct cytotoxicity after being exposed to laser light of 405 nm was analyzed. Complete D-MEM and porphyrus envelope was exposed to 6 J/cm^2 light of 405 nm and were administered at 150 HAU/ 50 μL to PC-3 seeded 96 well plates. The plate was left for 24 h and the cell survival rate was evaluated as described above. Microscopic images were also obtained using an inverted laboratory microscope.

3.1.4 Wound healing ability of PE

A black 96-well cell culture plate with a clear bottom was used to seed PC-3 cells at a density of 5.0×10^3 cells/well. Seeded cells were incubated for 24 h at 37°C in 5% CO_2 condition. After 24 h incubation, cells were treated in complete D-MEM, 5-ALA solution, PpIX lipid solution, HVJ-E suspension (150 HAU/50 μL), or PE suspension (150 HAU/50 μL) for 10 min, 30 min, 1 h, 3 h, or 5 h. Right after respective immersion time, each well bottom was scratched using a sterile pipette tip (Neptune® Barrier Tips BT100, Biotix, USA) to create a “wound”. Cells were then washed twice with D-PBS and 100 μL of complete D-MEM was administered to each well. Microscopic images were obtained at 0 h and 24 h time points using an inverted laboratory microscope (Eclipse Ts2, Nikon, Japan). Image processing software ImageJ (National Institutes of Health, USA) was used to measure the wounded area.

3.1.5 Colony forming ability of PE

Colony forming ability of PC-3 cells were assesed by CytoSelect 96-Well Cell Transformation Assay (CBA-130, Cell Biolabs, USA). Experiment was performed following manufacturer’s instructions. In this experiment, PC-3 cells were seeded in soft

agar at a density of 7.0×10^3 cells/well in the presence of complete D-MEM, PpIX lipid solution, HVJ-E suspension, or PE suspension for 10 min, 1 h, 3 h, and 5 h. Respective reagents were removed after each immersion time and the cells were further incubated at 37°C in 5% CO_2 for 7 days in complete D-MEM. The medium was changed every two days until the clear formation of colonies were observed. Formed colonies were observed under an inverted laboratory microscope (Leica DMIL, Leica Microsystems, Germany). In addition, soft agar was sobulized and cells were lysed to stain with CyQUANT GR Dye (CBA-130, Cell Biolabs, USA) for quantitative analysis.

Fluorescence intensity was measured immediately after the immersion time using a fluorescence microplate reader (SpectraMAX Gemini, Molecular Devices, USA) at an excitation wavelength of 485 nm and an emission wavelength of 520 nm.

3.1.6 Statistical analysis

All results are expressed as the means ± SD for three canses ($n = 3$) or six cases ($n = 6$). A two-tailed unpaired Student's *t*-test was performed between two sample groups, and a probability value of $*P < 0.01$ was considered statistically significant.

3.2 Experimental results

3.2.1 Level of PE-induced direct cytotoxic effect in PC-3 cells

The direct cytotoxic effect of respective reagents used in this study was analyzed by determining the cell survival rate of cells treated with these drugs. As depicted by Figure 3-2, cells treated with complete D-MEM, 5-ALA solution, or PpIX lipid solution exhibited high cell survival rate independent of immersion time. On the other hand, cells treated with either HVJ-E suspension or PE suspension underwent evident cell death. In fact, cell survival rate dropped to approximately 60–65% after treatment with these drugs for 10 min–1 h. Further incubation with HVJ-E suspension or PE suspension resulted in lower cell survival rate.

In addition, when the cell morphology was analyzed under the microscope, cell-to-cell fusion was observed in cells treated with HVJ-E suspension or PE suspension (Figure 3-3). This change in cell morphology became evident after 3 h incubation; however, no such change was confirmed in cells treated with PpIX lipid solution. The cell shape was consistent with that of complete D-MEM-treated cells for all course of treatment period in PpIX lipid-treated cells (Figure 3-3).

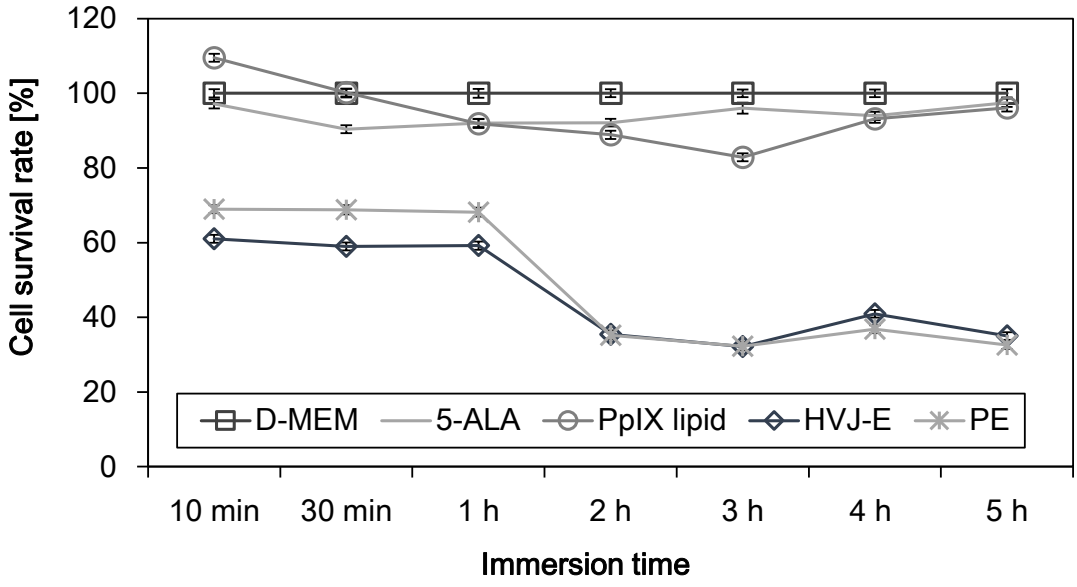

Figure 3-2 Direct cytotoxic effect induced in PC-3 cells

The cell survival rate of PC-3 cells incubated with complete D-MEM, 5-ALA solution, PpIX lipid solution, HVJ-E suspension, or PE suspension. Cells treated with complete D-MEM, 5-ALA solution, or PpIX lipid solution exhibited high cell survival rate, yet the ones treated with HVJ-E suspension or PE suspension resulted in the reduction of cell survival rate (n = 6).

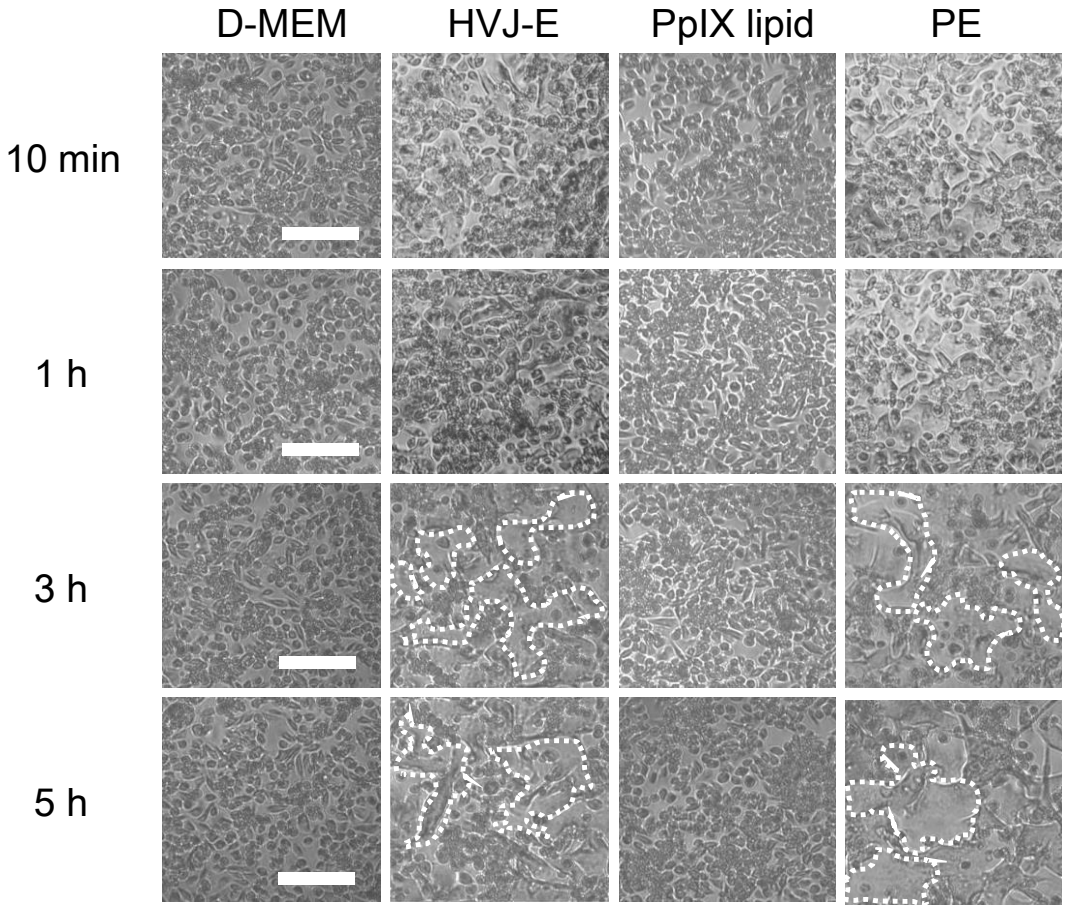

Figure 3-3 Morphological change in PC-3 cells after treatment

Microscopic images of PC-3 cells after incubation with complete D-MEM, HVJ-E suspension, PpIX lipid solution, or PE suspension. Treatment with HVJ-E or PE resulted in remarkable morphological alteration. Enlarged multinucleated cells were observed, confirming cell-to-cell fusion (dotted-lines). However, morphological changes were not observed in complete D-MEM- or PpIX lipid-treated cells. Scale bar indicates 200 μm.

3.2.2 Level of PE-induced direct cytotoxic effect in PC-3 cells after laser irradiation

PE has been shown to exhibit high cytotoxicity in absence of light. To evaluate if direct cytotoxic effect of PE is still conserved after PDT, PE particles were irradiated with laser at the same condition of PDT before administration and their level of cytotoxicity towards PC-3 cells was measured. The results indicate that fusion activity of PE is maintained even after light irradiation, exhibiting the formation of multinucleated syncytia (Figure 3-4). Moreover, the result shown in Figure 3-5 exhibits how high cytotoxicity of PE is maintained even after being exposed to light. This suggests how porphyrus envelope can induce direct cytotoxicity even after irradiation with light.

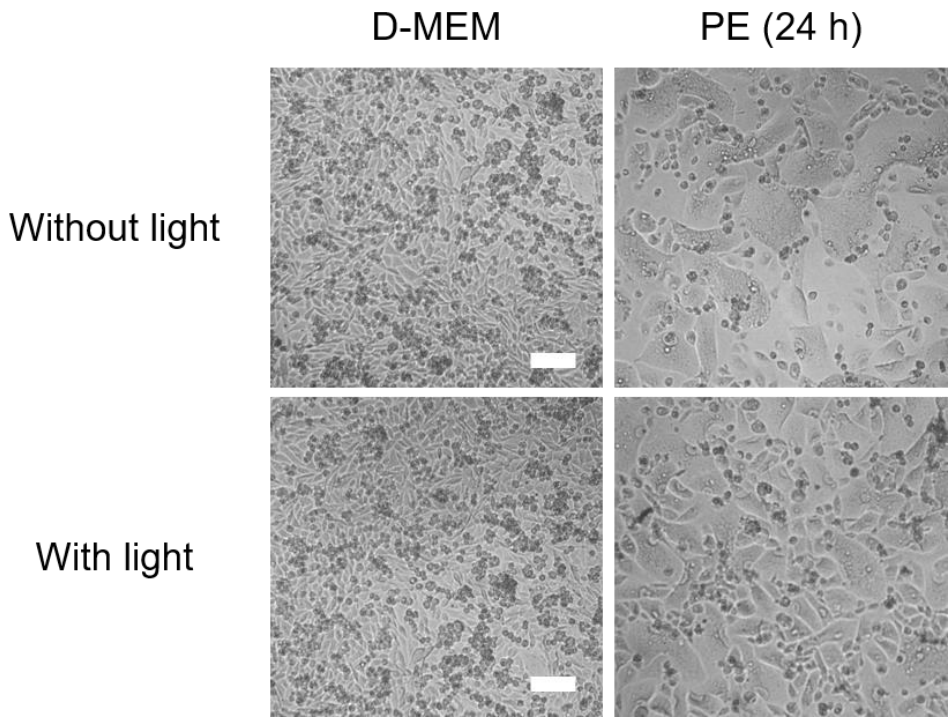

Figure 3-4 Morphological change in PC-3 cells treated with light exposed PE

PC-3 cells were imaged after incubation in complete D-MEM or PE suspension with or without laser irradiation to investigate the fusion ability of PE after performing PDT. PC-3 cells treated with irradiated and non-irradiated PE both exhibited the formation of multinucleated syncytia, confirming the ability of PE to induce membrane fusion after light exposure. On the other hand, treatment with irradiated or non-irradiated complete D-MEM did not cause any morphological change in PC-3 cells. Scale bars indicate 200 μm.

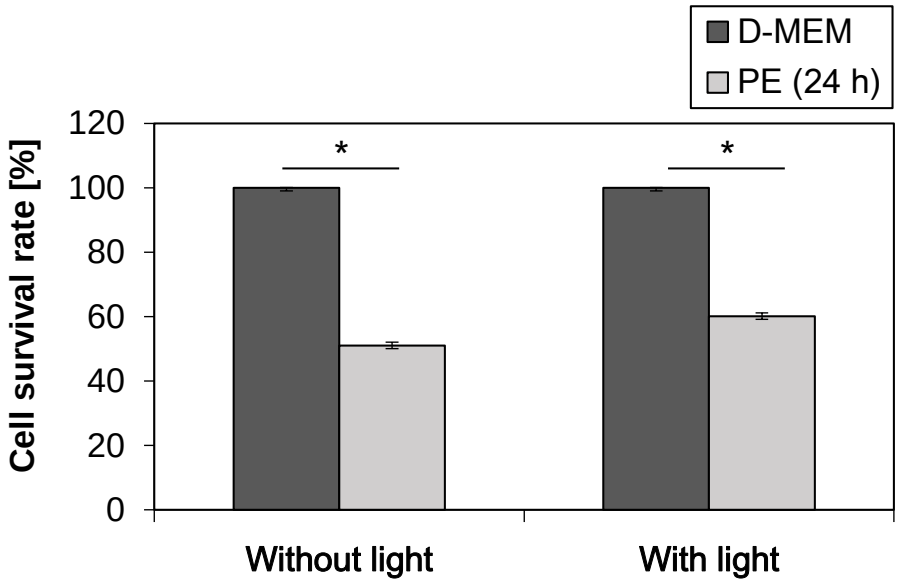

Figure 3-5 Cell survival rate after treating PC-3 cells with light irradiated PE

Cell survival rates of PC-3 cells incubated with complete D-MEM or PE that had been subjected to light irradiation at the dose used for PDT, i.e., 6 J/cm^2 at a laser wavelength of 405 nm, were calculated from optical density data. As indicated by dark gray bars, cytotoxicity was not confirmed in PC-3 cells treated with light irradiated or non-irradiated complete D-MEM. However, treatment with both light irradiated and non-irradiated PE resulted in significant reduction of cell survival rate. In addition, significant difference between the cell survival rate observed in light irradiated and non-irradiated PE was not confirmed. Thus, ability of PE to induce direct cytotoxic effect is maintained even after PE was exposed to laser light (n = 6; *P < 0.01).

3.2.3 Inhibition of wound healing activity in PC-3 cells

Inhibition of wound healing by PE was analyzed by performing scratch-wound assay (Figure 3-6 and Figure 3-7) [14]. 10 min incubation in either complete D-MEM, 5-ALA solution, or PpIX lipid resulted in clear reduction in wound area. In fact, treatment with complete D-MEM or 5-ALA solution prior to scratching resulted in > 20-fold reduction in wound surface area after 24 h incubation. Wound closure level was slightly inhibited in cells treated with PpIX lipid solution, however, approximately 5.5-fold reduction in wound area was confirmed after 24 h. As for the samples treated with HVJ-E suspension or PE suspension for 10 min, evident inhibition of wound closure was observed. Difference in wound area after 24 h incubation was approximately < 1.5-fold and < 1.3-fold for HVJ-E suspension and PE suspension, respectively.

A similar trend was observed in cells treated with respective reagents for longer time span. For instance, 5 h treatment with complete D-MEM or 5-ALA solution induced wound closure by < 15-fold, while incubation with PpIX lipid solution resulted in > 3.3-fold difference. Furthermore, incubation in HVJ-E suspension or PE suspension for same period led to significant inhibition of the wound healing ability, with < 1.36-fold difference in wound area after 24 h incubation. Inhibitory activity of cell migration and proliferation was most evident in samples treated with PE for 5 h.

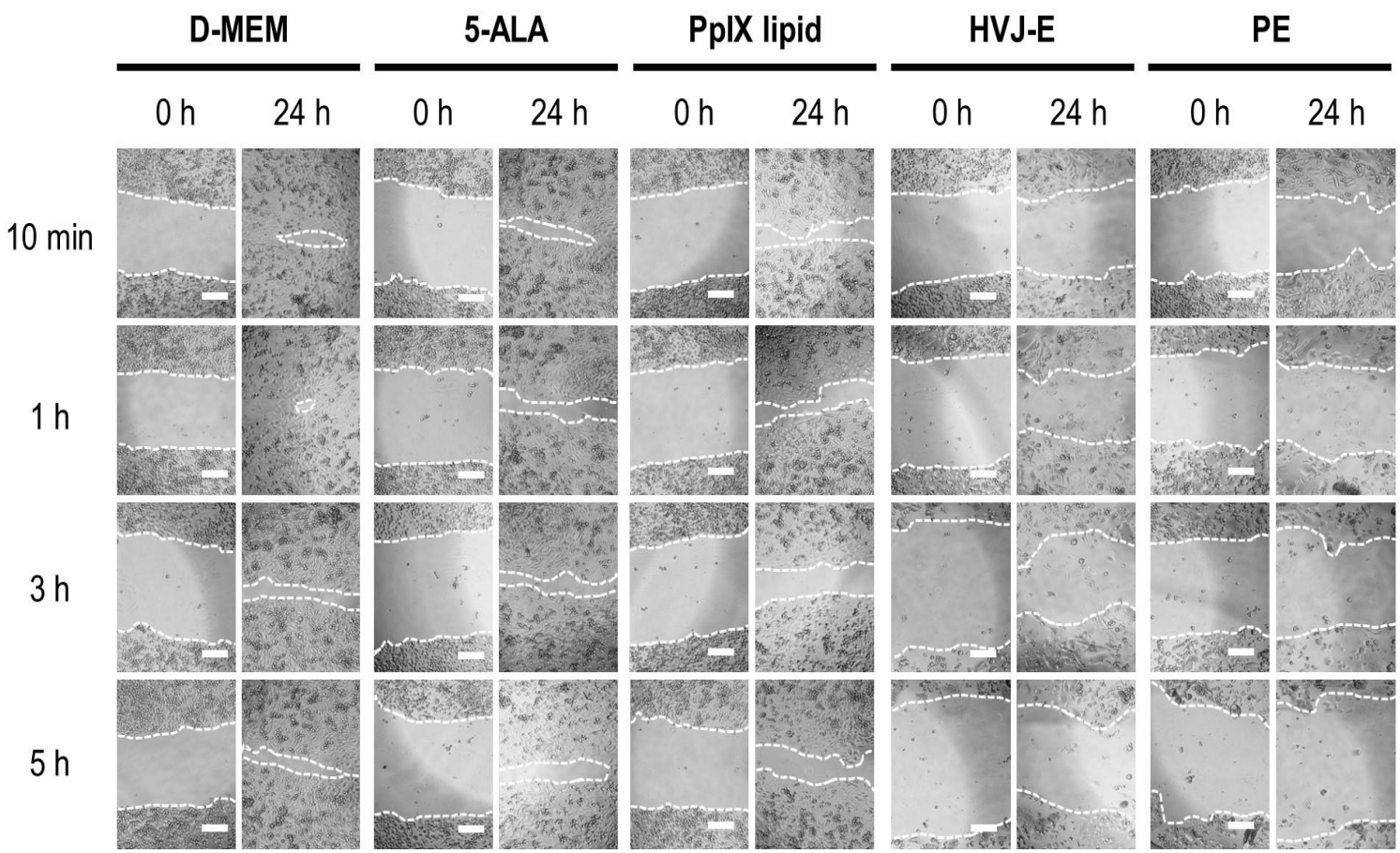

Figure 3-6 Wound healing ability of treated PC-3 cells

Microscopic images of PC-3 cells 0 h and 24 h after scratch-wound assay. Treatment with complete D-MEM, 5-ALA solution, and PpIX lipid solution resulted in remarkable wound closure. Incubation with HVJ-E suspension and PE suspension inhibited wound healing ability of the cells. Scale bar indicates 200 μm.

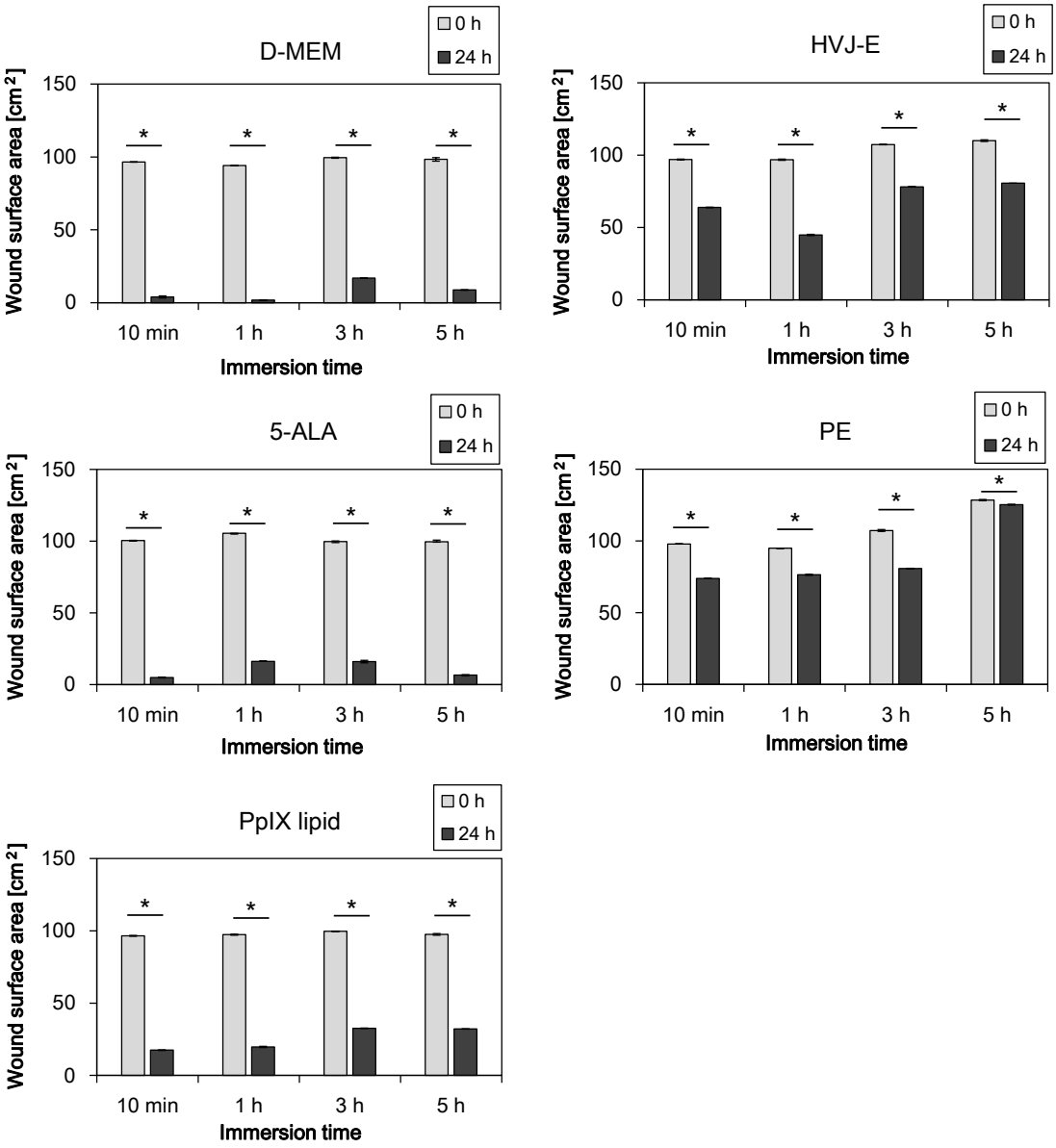

Figure 3-7 Wound surface area of PC-3 cells after PDT treatment

Wound surface area of PC-3 cells measured from the microscopic images shown in Figure 3-6. Treatment with complete D-MEM, 5-ALA solution, and PpIX lipid solution resulted in significant wound closure. On the other hand, incubation with HVJ-E suspension or PE suspension greatly inhibited the wound healing ability of PC-3 cells. Inhibition of wound healing was most evident in samples treated with PE for 5 h prior to scratching ($n = 3$; $^*P < 0.01$).

3.2.4 Inhibition of colony forming activity in PC-3 cells

Long-term proliferative potential of PC-3 cells was analyzed via colony formation assay (Figure 3-8 and Figure 3-9) [14]. Colony forming ability was evident in cells treated with complete D-MEM or PpIX lipid solution for 10 min, 1 h, 3 h, and 5 h. Relative fluorescence units (RFU) were all above > 0.8 in all conditions. On the other hand, suppression in colony formation was observed in cells treated with HVJ-E suspension or PE suspension. In fact, RFU observed were below < 0.3, resulting in significantly reduced oncological property.

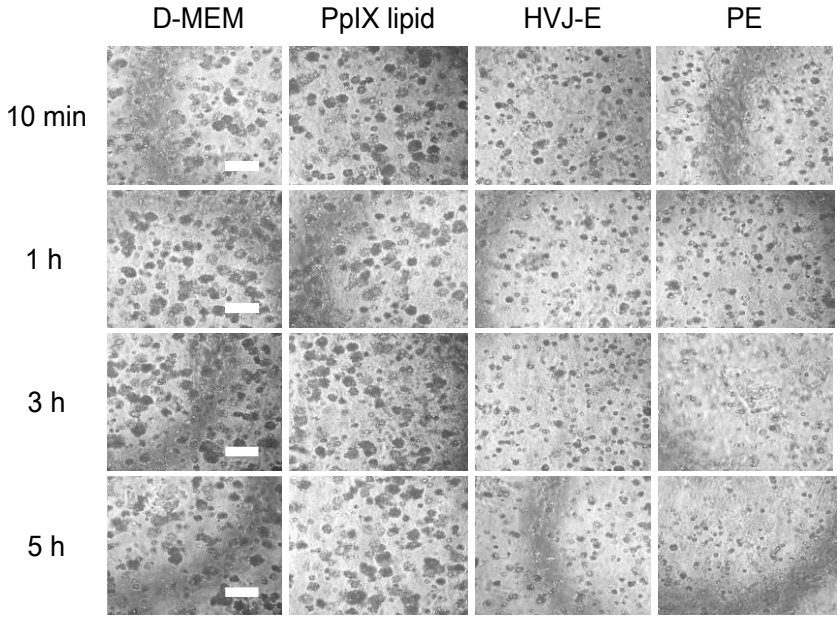

Figure 3-8 Colony formation in PC-3 cells after treatment

Microscopic images were obtained after treating the cells with complete D-MEM, PpIX lipid solution, HVJ-E suspension, or PE suspension. Formation of colonies were confirmed after the treatment with complete D-MEM or 5-ALA solution; however, HVJ-E- or PE-treatment resulted in remarkable inhibition of this activity. Scale bar indicates 200 μm.

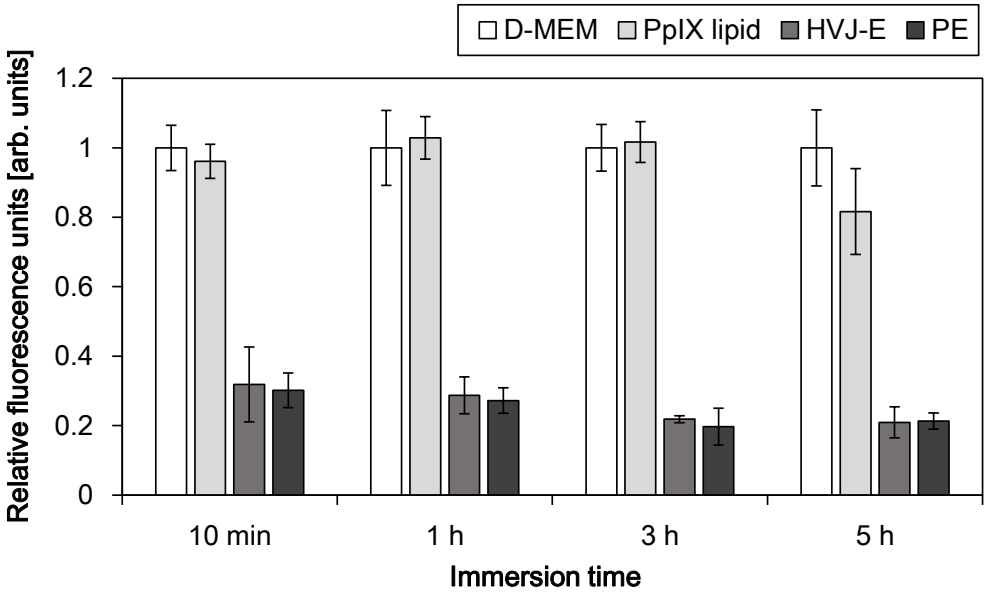

Figure 3-9 Relative fluorescence units of colony forming PC-3 cells

Relative fluorescence units (RFU) at 520 nm were determined for cells treated with respective reagents for 10 min, 1 h, 3 h, or 5 h. Measured fluorescence unit for each sample was divided by the units obtained for cells treated with D-MEM. RFU were well above 0.8 in cells treated with complete D-MEM or 5-ALA solution. Treatment with HVJ-E suspension or PE suspension greatly suppressed the colony forming phenotype of PC-3 cells in all immersion time (n = 3).

3.3 Discussion

As shown in Figure 3-2, the level of direct cytotoxicity induced via PE was similar to that observed in HVJ-E-treated cells. When PC-3 cells were observed under the microscope after each treatment (Figure 3-3), multinucleated cells resulting from cell-to-cell fusion were confirmed. The previous study performed by Gao *et al.* has shown how HVJ-E can inhibit tumor progression independent of T cell-dependent cytotoxicity *in vivo* [15]. In fact, fragmented RNA introduction in PC-3 cells via HVJ-E upregulates the activity of anti-viral reaction mediated through RIG-I/MAVS and MAPK signaling pathway [15]–[18]. Thus, similar pathways should have contributed in PE-mediated cytotoxicity that resulted in the reduction of the number of surviving PC-3 cells. Furthermore, previous research has shown how enhancement in cytoplasmic Ca^{2+} level is observed just before HVJ-E fusion [19][20]. Necroptosis induction via Ca^{2+} increase has been confirmed; therefore, necroptotic pathway may also play a key role in PE-induced direct cytotoxicity [20]. In addition, fusion activity and effect of direct cytotoxicity induced via PE was still intact after light exposure. Microscopic images of PC-3 cells shown in Figure 3-4 revealed how PE can induce fusion activity even after the light irradiation. Since RNA induction is required to induce direct cytotoxicity via apoptosis, this ensures that HVJ-E-mediated cell death can be carried out after PDT. Furthermore, when the cell survival rate of cells treated with PE with or without light irradiation was determined (Figure 3-5), significant reduction in cell survival rate was observed between D-MEM- and PE-treated cells. These results suggest that HVJ-E-induced direct cytotoxicity can be exhibited even after exposing the particles to laser light. Since this effect may act synergistically with PDT, therapeutic synergy was further analyzed in Chapter 4. Moreover, the marked wound area and reduced colony forming ability were confirmed after scratch-wound assay and colony formation assay, respectively (Figure 3-6; Figure 3-7; Figure 3-8; Figure 3-9). The apparent reduction in cancer cell activity shows that PE is a potent suppresser of cell migration and proliferation.

Moreover, as depicted in Figure 3-3, treatment with PE in scratch-wound assay resulted in cell-to-cell fusion. The previous study has confirmed how formation of the multinucleated cells alone can cause the cessation of cell proliferation process, while upregulating the genes involved in fusion activity that increases both the occurrence rate

of cell-to-cell fusion and oncolytic activity [21]–[23]. Thus, activation of RIG-I/MAVS pathway via fragmented RNA, induction of necroptotic cell death, and induction of cell-to-cell fusion in PC-3 cells may all have contributed to the cell killing effect observed after PE-treatment. This cancer-killing characteristic of PE was confirmed in the absence of light; therefore, PE should allow the induction of various cell death pathways. Highly efficient and effective treatment may be achieved by PE-mediated PDT.

3.4 Summary

Efficient cancer killing and remarkable suppression in cancer phenotype was confirmed in cells treated with PE. PE administration can cause the induction of fragmented RNA upon membrane fusion and can induce the formation of multinucleated cells. Thus, these activities may have acted to halt proliferative and migratory activities in cancer cells. Furthermore, both RIG-I/MAVS pathway and multinucleated cell formation can result in the upregulation of cancer killing effect, even in absence of light. Moreover, since the unique characteristics of HVJ-E are maintained even after light irradiation, it is highly likely that cell death are induced via multiple pathways even after PDT.

References

[1] Y. Kaneda, T. Nakajima, T. Nishikawa, S. Yamamoto, H. Ikegami, N. Suzuki, H. Nakamura, R. Morishita, and H. Kotani, "Hemagglutinating Virus of Japan (HVJ) Envelope Vector as a Versatile Gene Delivery System," *Mol. Ther.*, vol. 6, no. 2, pp. 219–226, 2002.

[2] Y. Kaneda, "Update on non-viral delivery methods for cancer therapy: possibilities of a drug delivery system with anticancer activities beyond delivery as a new therapeutic tool," vol. 7, no. 9, pp. 1079–1093, 2010.

[3] C. Loney, G. Mottet-Osman, L. Roux, and D. Bhella, "Paramyxovirus Ultrastructure and Genome Packaging: Cryo-Electron Tomography of Sendai Virus," *J. Virol.*, vol. 83, no. 16, pp. 8191–8197, 2009.

[4] E. S. Antonarakis, C. Lu, H. Wang, B. Luber, M. Nakazawa, J. C. Roeser, Y. Chen, T. A. Mohammad, Y. Chen, H. L. Fedor, T. L. Lotan, Q. Zheng, A. M. De Marzo, J. T. Isaacs, W. B. Isaacs, R. Nadal, C. J. Paller, S. R. Denmeade, M. A. Carducci, M. A. Eisenberger, and J. Luo, "AR-V7 and Resistance to Enzalutamide and Abiraterone in Prostate Cancer," *N. Engl. J. Med.*, vol. 371, no. 11, pp. 1028–1038, 2014.

[5] "NNCN guidelines for patients: prostate cancer," *National Comprehensive Cancer*, 2016. [Online]. Available: https://www.nccn.org/patients/guidelines/prostate/files/assets/basic-html/page-1.html#. [Accessed: 13-Nov-2017].

[6] T. Karantanos, C. P. Evans, B. Tombal, T. C. Thompson, R. Montironi, and W. B. Isaacs, "Understanding the mechanisms of androgen deprivation resistance in prostate cancer at the molecular level," *Eur. Urol.*, vol. 67, no. 3, pp. 470–479, 2015.

[7] K. J. Pienta and D. Bradley, "Mechanisms underlying the development of androgen-independent prostate cancer," *Clinical Cancer Research*, vol. 12, no. 6. pp. 1665–1671, 2006.

[8] R. B. Montgomery, E. A. Mostaghel, R. Vessella, D. L. Hess, T. F. Kalhorn, C. S. Higano, L. D. True, and P. S. Nelson, "Maintenance of intratumoral androgens in metastatic prostate cancer: A mechanism for castration-resistant tumor growth," *Cancer Res.*, vol. 68, no. 11, pp. 4447–4454, 2008.

[9] L. Graham and M. T. Schweizer, "Targeting persistent androgen receptor signaling in castration-resistant prostate cancer," *Medical Oncology*, vol. 33, no. 5. 2016.

[10] J. Holzbeierlein, P. Lal, E. LaTulippe, A. Smith, J. Satagopan, L. Zhang, C. Ryan, S. Smith, H. Scher, P. Scardino, V. Reuter, and W. L. Gerald, "Gene Expression Analysis of Human Prostate Carcinoma during Hormonal Therapy Identifies Androgen-Responsive Genes and Mechanisms of Therapy Resistance," *Am. J. Pathol.*, vol. 164, no. 1, pp. 217–227, 2004.

[11] M. Yamauchi, N. Honda, H. Hazama, S. Tachikawa, H. Nakamura, Y. Kaneda, and K. Awazu, "A novel photodynamic therapy for drug-resistant prostate cancer cells using porphyrus envelope as a novel photosensitizer," *Photodiagnosis Photodyn. Ther.*, vol. 11, no. 1, pp. 48–54, 2014.

[12] M. Inai, N. Honda, H. Hazama, S. Akter, S. Fuse, H. Nakamura, T. Nishikawa, Y. Kaneda, and K. Awazu, "Photodynamic therapy using a cytotoxic

photosensitizer porphyrus envelope that targets the cell membrane," *Photodiagnosis Photodyn. Ther.*, vol. 20, pp. 238–245, 2017.

[13] S. Tachikawa, M. E. El-Zaria, R. Inomata, S. Sato, and H. Nakamura, "Synthesis of protoporphyrin-lipids and biological evaluation of micelles and liposomes," *Bioorganic Med. Chem.*, vol. 22, no. 17, pp. 4745–4751, 2014.

[14] X. Wang, J. Hu, P. Wang, S. Zhang, Y. Liu, W. Xiong, and Q. Liu, "Analysis of the in vivo and in vitro effects of photodynamic therapy on breast cancer by using a sensitizer, Sinoporphyrin sodium," *Theranostics*, vol. 5, no. 7, pp. 772–786, 2015.

[15] H. Gao, X. C. Gong, Z. D. Chen, X. S. Xu, Q. Zhang, and X. M. Xu, "Induction of apoptosis in hormone-resistant human prostate cancer PC3 cells by inactivated Sendai virus.," *Biomed. Environ. Sci.*, vol. 27, no. 7, pp. 506–514, 2014.

[16] K. Saga and Y. Kaneda, "Oncolytic Sendai virus-based virotherapy for cancer: recent advances," *Oncolytic Virotherapy*, vol. 4, pp. 141–147, 2015.

[17] S. Li, T. Nishikawa, and Y. Kaneda, "Inactivated Sendai virus particle upregulates cancer cell expression of intercellular adhesion molecule-1 and enhances natural killer cell sensitivity on cancer cells," *Cancer Sci.*, vol. 108, no. 12, pp. 2333–2341, 2017.

[18] L.-W. Liu, T. Nishikawa, and Y. Kaneda, "An RNA Molecule Derived From Sendai Virus DI Particles Induces Antitumor Immunity and Cancer Cell-selective Apoptosis," *Mol. Ther.*, vol. 24, no. 1, pp. 135–145, 2016.

[19] M. B. Hallett, P. Fuchst, and A. K. Campbell, "Sendai virus causes a rise in intracellular free Ca2+ before cell fusion," *Biochem. J*, vol. 206, pp. 671–674, 1982.

[20] M. Nomura, A. Ueno, K. Saga, M. Fukuzawa, and Y. Kaneda, "Accumulation of cytosolic calcium induces necroptotic cell death in human neuroblastoma," *Cancer Res.*, vol. 74, no. 4, pp. 1056–1066, 2014.

[21] O. V. Matveeva, G. V. Kochneva, S. V. Netesov, S. B. Onikienko, and P. M. Chumakov, "Mechanisms of oncolysis by paramyxovirus Sendai," *Acta Naturae*, vol. 7, no. 2. pp. 6–16, 2015.

[22] O. Ebert, K. Shinozaki, C. Kournioti, M. S. Park, A. García-Sastre, and S. L. C. Woo, "Syncytia Induction Enhances the Oncolytic Potential of Vesicular Stomatitis Virus in Virotherapy for Cancer," *Cancer Res.*, vol. 64, no. 9, pp. 3265–3270, 2004.

[23] A. Bateman, F. Bullough, S. Murphy, L. Emiliusen, D. Lavillette, F. L. Cosset, R. Cattaneo, S. J. Russell, and R. G. Vile, "Fusogenic membrane glycoproteins as a novel class of genes for the local and immune-mediated control of tumor growth," *Cancer Res.*, vol. 60, no. 6, pp. 1492–1497, 2000.

4. Therapeutic efficacy of PE-mediated PDT

Studies performed in Chapter 2 have confirmed how PE-inserted PpIX lipid was delivered to the plasma membrane of PC-3 cells at relatively short immersion time. In Chapter 3, PE was confirmed to exhibit cytotoxicity towards cancer cells even without laser irradiation. This effect was conserved in PE particles exposed to light; therefore, direct cyototoxic effect induced by PE should further reduce the cell survival rate even after PDT. Thus, this chapter will consider the effect of PE-mediated PDT towards PC-3 cells and analyze the potential synergism observed after combining photodynamic activity and PE-mediated direct cytotoxicity.

PDT-related damage is dependent upon ROS production and PS localization [1], [2]. Since almost all cancer cells are susceptible to exogenous ROS, high level of ROS production is often desired to initiate both necrotic and apoptotic pathways in cells [3]. The initial site of photochemical reaction is the major factor determining the type of cell death with cell type playing an important role regulating the fate of cancer cells [4]. In this study, the level of ROS produced in PC-3 cells after PE-mediated PDT was assessed through fluorescence analysis to determine its therapeutic efficacy. As well, the induced cell death pathway after light irradiation was analyzed using confocal laser scanning microscope to uncover the mechanism and the rate of cell death.

Therapeutic efficacy of PE-mediated PDT can be addressed through the experiments described above; however, therapeutic benefit of PE-mediated PDT cannot be determined without considering the direct cytotoxicity induced via PE-mediated membrane fusion. Thus, combined therapeutic scheme of cell death resulting from the treatment with PE alone and PE-mediated PDT will be addressed in this chapter. Since combined therapy is often utilized to enhance the therapeutic outcome of resistant tumor in cancer management, potential ability of PE-mediated PDT to induce various cell death pathway may lead to effective regression of malignant cells [5], [6].

In combined therapy, synergistic therapeutic effect is often desired to enhance the therapeutic response in cancer, as synergism can lead to the reduction in the drug concentration and unwanted side effects [5]–[8]. The combination index (CI) method introduced in 1984 by Chou and Talalay is one of the most famous synergy assessment

used today [5], [7], [9], [10]. The CI values represent the combination effects of different drugs by quantitatively analyzing synergism (CI < 1), additive effect (CI = 1), or antagonism (CI > 1) using the median-effect principle of the mass-action law [5]–[8], [11], [12].

Calculation of CI values can be done by following three major steps: 1) determining effective cytotoxic dose 50% (EC_{50}), 2) plotting dose-response curve of combination, and 3) calculating the CI values. Cell survival rates of cancer cells after the exposure to different doses of cytotoxic treatment are first determined in this experiment. Then, a two-parameter logistic function is fit to dose-response curve based on the following equation:

$$f_{\mathrm{a}} = \frac{1}{[1 + \frac{1}{\left(\frac{D_n}{\mathrm{EC}_{50}}\right)^m}]}$$

where D_n is the dose of each treatment, EC_{50} is the dose of the treatment required to reduce the cell survival rate to 50%, f_a is the fraction of dead cells, and m is the estimation of the sigmoidicity of dose-response curve. This equation is called median-effect equation and can be rewritten as:

$$\frac{f_{\mathrm{a}}}{(1 - f_{\mathrm{a}})} = (\frac{D_n}{\mathrm{EC}_{50}})^m$$

to determine EC_{50} and m of the specific treatment condition. In this formula, $(1–f_a)$ is used to show the fraction of live cells. However, since the response variables obtained from this equation exhibit nonlinear relationship, logarithmic transformation is further applied to obtain the following equation:

$$\log\left(\frac{f_{\mathrm{a}}}{(1 - f_{\mathrm{a}})}\right) = m\log(D_n) - m\log(\mathrm{EC}_{50})$$

From this formula, m can be determined from the slope of linear regression, and EC_{50} can be estimated from the intercept of dose-response plot, $\log(EC_{50})$. Furthermore, precision of the experiment can easily be verified using the squared correlation coefficient R^2. The dose-response curves obtained for individual drugs and their combination can be utilized to identify the type of drug interaction (synergism, additive effect, or antagonism) via CI values using the following formula:

$$CI = \frac{D_{1,\mathrm{EC}_{50}}}{\mathrm{EC}_{50,1}} + \frac{D_{2,\mathrm{EC}_{50}}}{\mathrm{EC}_{50,2}}$$

where $D_{1,EC50}$ and $D_{2,\ EC50}$ are the dose required for D_1 and D_2 in combination to achieve EC_{50}. $EC_{50,1}$ and $EC_{50,2}$ are the dose required for each drug to achieve the same toxicity. In this study, all the calculations were done using CompuSyn software version 1.0 (ComboSyn, USA).

4.1 Materials and Methods

4.1.1 Cell line and culture

FBS and 100 units/mL penicillin-streptomycin were added to D-MEM to create complete D-MEM as mentioned in *Section 2.1.1*. Androgen-independent human prostate cancer cell line PC-3 was cultured in complete D-MEM at 37°C with humidity in 5% CO_2 atmosphere. For cell seeding, cells were harvested after reaching 80% confluence. All studies were conducted using stable lines.

4.1.2 Photosensitizers

Preparation of PE was done as follows. First, 5 mM PpIX lipid was diluted with D-PBS to 10.5 μM solution. HVJ-E was then prepared as previously reported and was separated to 2500 HAU each [13], [14]. This HVJ-E was suspended in 10.5 μM PpIX lipid solution with a final volume of 1 mL [14]. Then, PE was prepared by inserting PpIX lipid into HVJ-E via centrifugation (20,000 × g, 4°C, 10 min) [13]. Finally, the supernatant was removed after centrifugation and the pellet of PE was suspended in 835 μL of complete D-MEM. The ratio of PpIX lipid to HVJ-E in PE was 3.5 pmol/HAU.

In addition, 5 mM PpIX lipid was diluted with complete D-MEM to 10.5 μM. Suspensions of HVJ-E was prepared at concentrations of 1000 HAU/500 μL and 150 HAU/50 μL by suspending it in complete D-MEM. 5-ALA was stored at –20°C and an aqueous solution of 5 mM PpIX lipid was stored at 4°C [15]. All reagents were prepared prior to each experiment.

4.1.3 ROS production

Intracellular ROS/Superoxide generation in cells treated with respective reagents were addressed using ROS-ID® Total ROS/Superoxide Detection Kit (ENZ-51010, Enzo Life Sciences, USA). Experimental procedures were performed as written in instruction manual.

Microscopic imaging

A black 96-well cell culture plate with a clear bottom was used in this assay, and PC-3 cells were seeded at a density of 5.0×10^3 cells/well. The plate wasd left for 24 h at 37°C in 5% CO^2. After 24 h incubation, cells were treated with complete D-MEM, PpIX lipid solution, HVJ-E suspension, or PE suspension for 10 min, 1 h, or 5 h. Then, PC-3 cells

were washed with 1× wash buffer (ENZ-51010, Enzo Life Sciences, USA). ROS/Superoxide Detection Solution (ENZ-51010, Enzo Life Sciences, USA) was added in each well, and cells were simultaneously treated with PDT as described in *Section 4.1.5*. The plate was imaged under an inverted laboratory microscope (Eclipse Ts2, Nikon, Japan) to detect ROS/Superoxide.

Fluorescence microplate assay

PC-3 cells were seeded on a black 96-well cell culture plate with a clear bottom at a density of 5.0×10^3 cells/well and left for 24 h at 37°C in 5% CO^2 to let the cells adhere to the well bottom. After 24 h incubation, cells were treated with complete D-MEM, PpIX lipid solution, HVJ-E suspension, or PE suspension for 10 min, 1 h, or 5 h. Then, PC-3 cells were washed with 1× wash buffer (ENZ-51010, Enzo Life Sciences, USA). ROS/Superoxide Detection Solution (ENZ-51010, Enzo Life Sciences, USA) was added in each well, and cells were simultaneously treated with PDT as described in *Section 4.1.5*. Measurements of ROS and superoxide were performed using a fluorescence microplate reader (SpectraMAX Gemini, Molecular Devices, USA) and standard fluorescein (Ex: 488 nm, Em: 520 nm) and rhodamine (Ex: 550 nm, Em: 610 nm) filter.

4.1.4 Cell death pathway

Cell death pathway induced after the treatment was analyzed by using Apoptotic/Necrotic/Healthy Cells Detection Kit (PK-CA707-30018, PromoKine, Germany). Experimental procedures were performed as indicated in instruction manual. Briefly, PC-3 cells were seeded on a Nunc™ MicroWell™ 96-well Optical-Bottom Plates with Coverglass Base (160376, Thermo Fisher Scientific, USA) at a density of 5.0×10^3 cells/well and left for 48 h at 37c in 5% CO^2 condition. After 48 h incubation, cells were treated with complete D-MEM, PpIX lipid solution, HVJ-E suspension, or PE suspension for 10 min, 1 h, 3 h, or 5 h. PDT was performed as described in *Section 4.1.5*, and cells were washed twice with 1× binding buffer (160376, Thermo Fisher Scientific, USA). Then, cells were stained with a staining solution containing FITC-Annexin V, Ethidium Homodimer III, and Hoechst® 33342 for 15 min at room temperature and were imaged under confocal laser scanning microscope (EclipseTi equipped with A1R/A1, Nikon, Japan). The excitation wavelengths were set to 403 nm for Hoechst® 33342, 488 nm for FITC-Annexin V, and 562 nm for Ethidium Homodimer III. Detection wavelength ranges

were 425–475 nm for Hoechst® 33342, 500–550 nm for FITC-Annexin V, and 570–620 nm for Ethidium Homodimer III. The laser power was adjusted to exclude the autofluorescence obtained from the cells.

4.1.5 PDT experiment

Optical setup

Since the effect of light absorption and scattering can be ignored in 2D culture system, laser diode with a wavelength of 405 nm (VLM-500, Sumitomo Electric Industries, Ltd., Japan) was utilized in this study. PpIX lipid exhibits highest absoprtion peak at 405 nm region; therefore, efficiency of PE-mediated PDT should be enhanced. The optical setup was prepared as shown in Figure 4-1. The laser light was delivered via optical fiber (M22L02, Thorlabs Inc., USA), and the emitted light was passed thorough aspheric lens (ACL1210-A, Thorlabs Inc., USA) to correct abberation. Furthermore, laser was adjusted to desired power by adjusting variable neutral density filter (NDHN-50, SIGMA KOKI, Japan). An aperture was utilized to set the laser diameter to 6 mm and laser was irradiated through the bottom of 96 well plates. The laser diode used in this experiment has a flat profile and allows even irradiation.

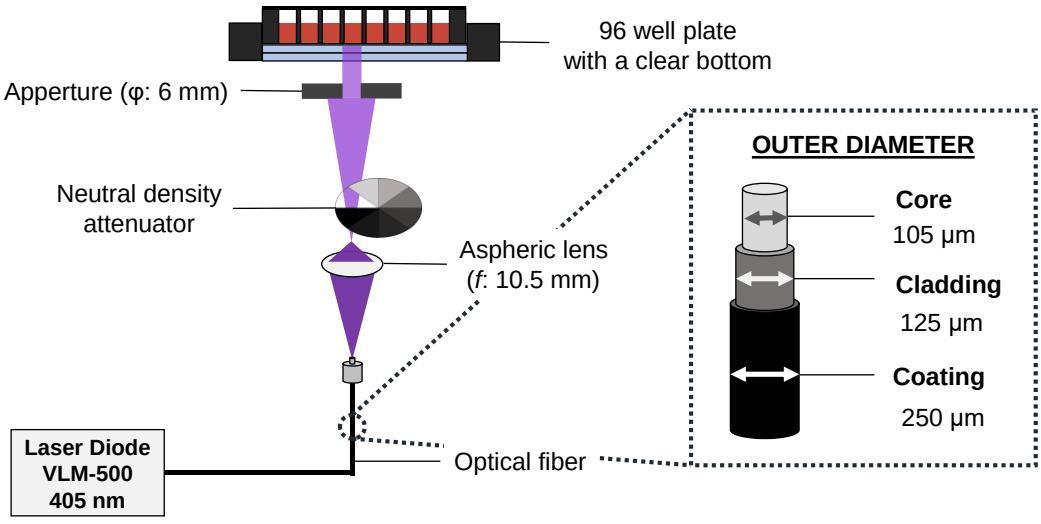

Figure 4-1 Optical setup of the laser diode used in this experiment
Laser diode of 405 nm was used in this experiment. The beam diameter was adjusted to 6 mm by aperture to evenly irradiate the bottom of 96 well plate. Laser diode used in this study has a flat profile.

PDT experiment

PC-3 cells were seeded on a black 96-well cell culture plate with a clear bottom at a density of 5.0×10^3 cells/well and the plate was placed in 5% CO^2 condition at 37°C for 24 h. On the following day, 50 μL of PpIX lipid solution, HVJ-E suspension (150 HAU), or PE suspension (150 HAU) was added for treatment of 10 min, 1 h, 3 h, or 5 h. Then, respective reagents were exchanged with 100 μL of complete D-MEM before performing laser irradiation. For PDT, the plate was placed on a plate warmer (KM-1, Kitazato Science, Japan) to maintain the temperature at 37°C and the wells were irradiated with a 405 nm laser diode with power density of 100 mW/cm^2 for 60 s each. The position of the plate and the time of irradiation was controlled by a two-axis motorized linear stage (SGSP26-150(XY), SIGMAKOKI, Japan). After laser irradiation, cells were further incubated for 24 h in 100 μL of complete D-MEM or in the reagent used for treatment before laser irradiation. The cell survival rate after respective treatment was determined by changing the medium of each well to a mixture of 90 μL of complete D-MEM and 10 μL of a cell counting reagent that contains WST-8. An absorbance microplate reader with wavelength set to 450 nm was used to determine the optical density of each well. The cell survival rate for each sample was calculated as a percentage of control (cells treated with complete D-MEM).

4.1.6 Synergistic effect

The type of interaction (synergism, additive effect, or antagonism) observed in the combination of PE-induced direct cytotoxicity and PE-mediated PDT was evaluated using CompuSyn software version 1.0 (ComboSyn, USA). For this experiment, survival rate of cells after the treatment with varying doses of PE and PE-mediated PDT was utilized to calculate CI values through Chou-Talalay equation [25,26]:

$CI=D_{1,EC50}/EC_{50,1} + D_{2,EC50}/EC_{50,2}$, where $D_{1,EC50}$ and $D_{2,EC50}$ are the doses required for D_1 and D_2 in combination to achieve EC_{50}. CI < 1, CI = 1, and CI > 1 indicate synergistic effect, additive effect, and antagonistic effect, respectively. Here, PC-3 cells were treated with PE and PE-mediated PDT, either alone or in combination to calculate CI values. The dose of PE was changed by setting the HAU to 4.7, 9.4, 19, 38, 75, 150, or 300 HAU, and PE-mediated PDT was changed by setting the laser irradiation time to 60, 120, 180, or 240 s at the same power density of 100 mW/cm^2. Logarithmic median effect plot, logarithmic combination index (CI) plot, CI and EC_{50} were generated through CompuSyn software. CI values generated were analyzed using Table 4-1.

Table 4-1 Synergy assignment criteria for CI values

CI	Description
< 0.1	Very strong synergism
0.1–0.3	Strong synergism
0.3–0.7	Synergism
0.7–0.85	Moderate synergism
0.85–0.9	Slight synergism
0.9–1.1	Nearly additive
1.1–1.2	Slight antagonism

4.1.7 Statistical analysis

All results are expressed as the means ± SD for six cases ($n = 6$). A two-tailed unpaired Student's *t*-test was performed between two sample groups, and a probability value of $*P < 0.01$ was considered statistically significant.

4.2 Experimental results

4.2.1 Intracellular ROS/Superoxide generation in PC-3 cells

PC-3 cells were subjected to PDT to analyze the intracellular ROS and superoxide generation (Figure 4-2 and Figure 4-3). Strong fluorescence for ROS or superoxide was not confirmed in cells treated with complete D-MEM, PpIX lipid solution, or HVJ-E suspension, and the fluorescence intensity remained constant in all conditions. Fluorescence imaging of superoxide production in PE-treated cells exhibited slightly brighter red fluorescence in 5 h sample, yet significant difference was not confirmed between other conditions. On the other hand, time dependent increase in ROS production was observed with significant difference. Discrepancy in the measured fluorescence intensity between PE-treated cells and others was smallest in 10 min sample with approximately 2-fold difference. The difference increased to < 10-fold in cells treated for 1 h and 5 h. PC-3 cells treated for 5 h with PE exhibited the highest ROS fluorescence intensity.

Furthermore, morphological differences were verified amongst the cells treated with different reagents (Figure 4-2). Treatment with complete D-MEM or PpIX lipid solution did not result in evident change in morphology; however, both HVJ-E- and PE-treatment caused the formation of multinucleated cells, syncytia. In adadition, cytoplasmic swelling was confirmed in cells subjected to PE-treatment.

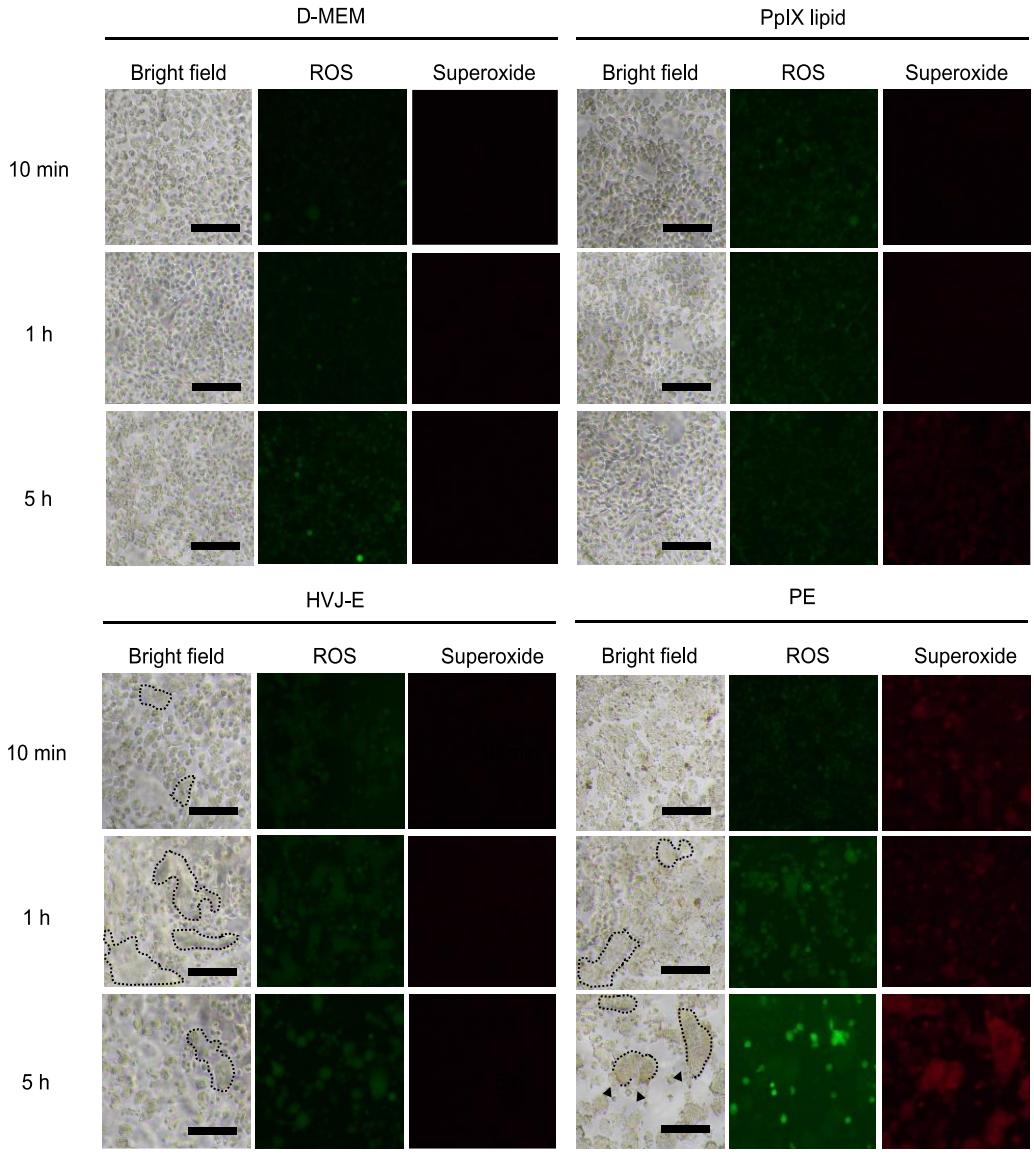

Figure 4-2 Profile of ROS/superoxide in PC-3 cells after treatment

Cells were subjected to PDT after 10 min–5 h treatment with respective reagents and microscopic images were obtained to observe cellular morphology and ROS/superoxide fluorescence. Bright green fluorescence for ROS was observed in cells treated with PE for 5 h. In addition, cell-to-cell fusion was confirmed after treating with HVJ-E and PE as indicated by black doted-lines. Cytoplasmic swelling was confirmed after PE-mediated PDT (black arrowheads).

ROS

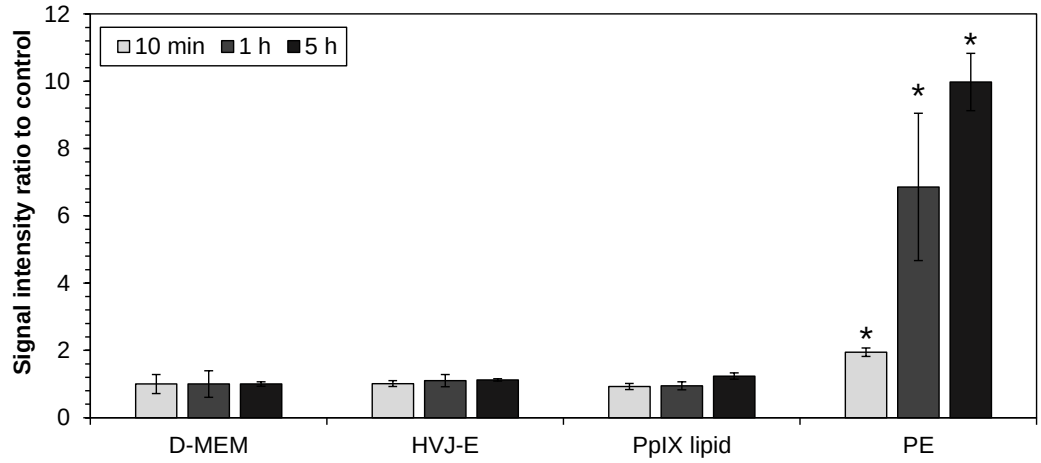

Superoxide

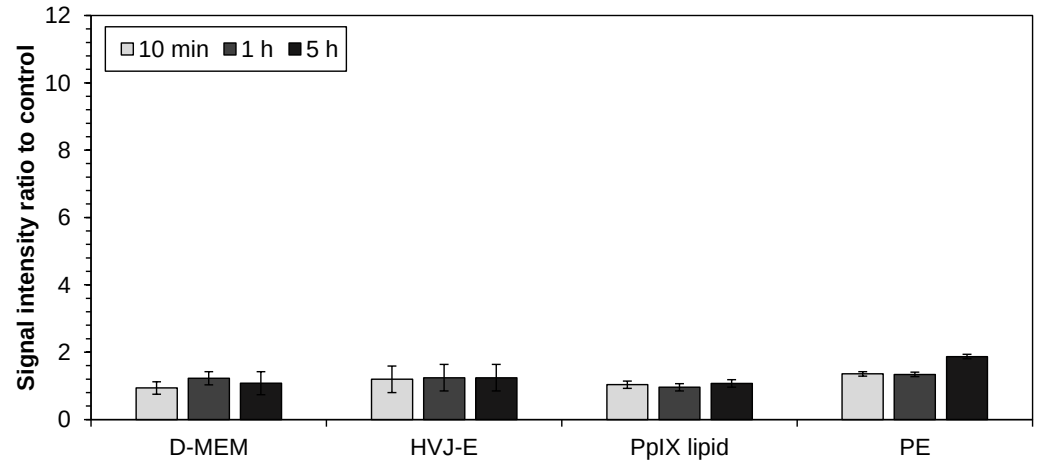

Figure 4-3 ROS/superoxide signal intensity in PC-3 cells

Level of ROS and superoxide generation in PC-3 cells were measured as fluorescence intensity right after the PDT treatment. Complete D-MEM, HVJ-E suspension, or PpIX lipid solution did not induce high ROS or superoxide production. PE suspension was not a strong superoxide inducer neither; however, time dependent increase in ROS production was confirmed. Significant difference was confirmed when compared with cells treated with complete D-MEM ($n = 6$; $^*P < 0.01$).

4.2.2 Mode of cell death induced in PC-3 cells

PC-3 cells were incubated with complete D-MEM, PpIX lipid solution, HVJ-E suspension, or PE suspension for 10 min–5 h and the type of cell death induced before and after PDT was assessed. Figure 4-4 shows the images obtained using confocal laser scanning microscope. In this assay, healthy cells are stained by Hoechst®33342 (blue) only, not by FITC-Annexin V (green) or ethidium homodimer III (red). On the other hand, apoptotic cells are stained both green and blue, while necrotic cells appear red and blue. Dead cells exhibit triple staining of blue, green, and red.

Treatment with complete D-MEM did not cause any type of cell death regardless of light irradiation. PpIX lipid-treatment exhibited few dead cells 24 h after PDT; however, majority of the cells remained alive. Cells that were treated with HVJ-E for 3–5 h prior to PDT underwent apoptosis right after the light irradiation. Presence of both apoptotic and dead cells were confirmed after 24 h, yet some cells exhibited only blue fluorescence. In the case of PE-treated cells, cells incubated for 10 min prior to PDT exhibited similar result to that of cells treated with HVJ-E for same duration. However, unlike the cells incubated with HVJ-E suspension, cells treated with PE for 1 h resulted in apoptosis right after PDT. In addition, induction of necrosis was confirmed in cells treated for 3 h with almost all the cells dead in 5 h sample. When cells treated for 1–5 h with PE before light irradiation was observed 24 h after PDT, all the cells exhibited triple staining, confirming high cell killing effect of PE-mediated PDT.

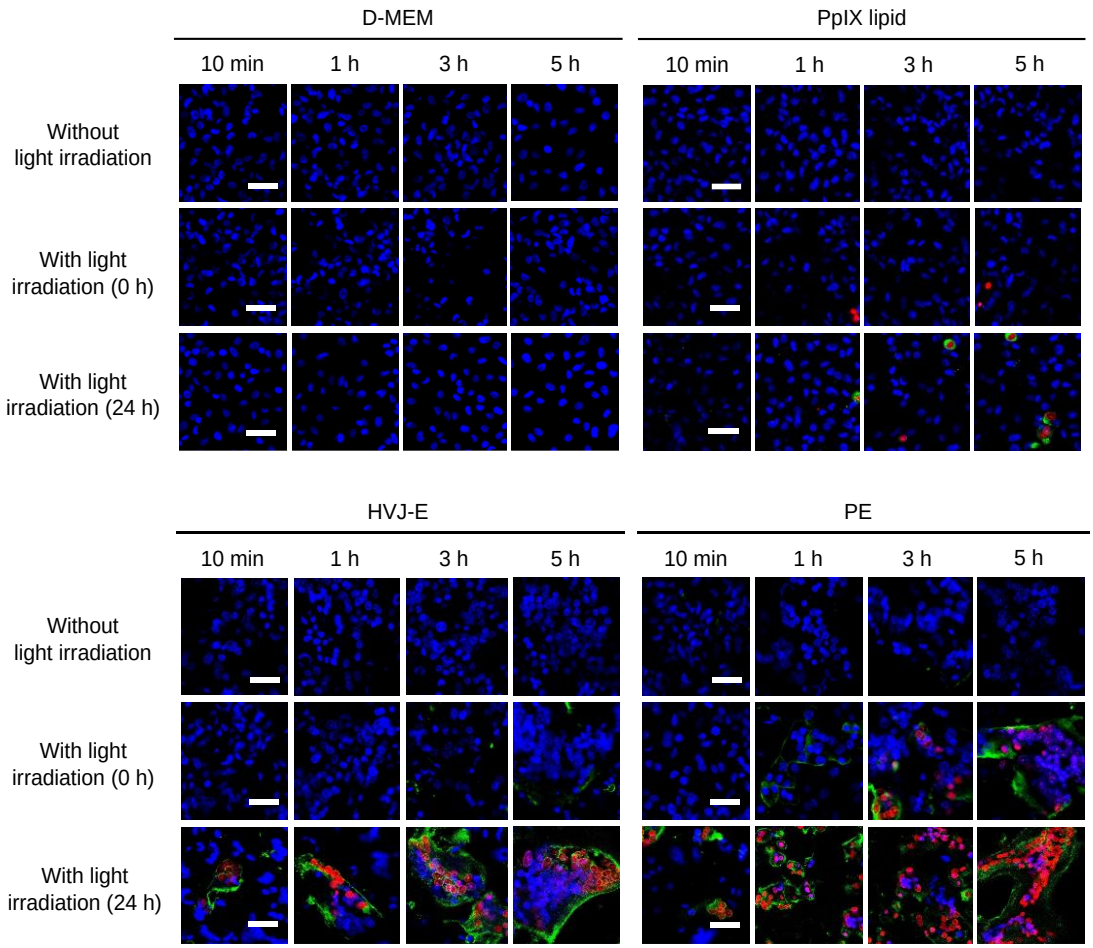

Figure 4-4 Mode of cell death induced in PC-3 cells before and after PDT

PC-3 cells were treated with complete D-MEM, PpIX lipid solution, HVJ-E suspension, or PE suspension for 10 min–5 h and were imaged under confocal laser scanning microscope before and after PDT. Live cells are stained blue with Hoechst®33342, nuclei of necrotic or dead cells are shown in red by ethidium homodimer III, and phosphatidylserine of apoptotic or dead cells are stained green by FITC-Annexin V. Treatment with complete D-MEM or PpIX lipid did not induce strong cytotoxic effect. HVJ-E exposed to light induced apoptosis right after light irradiation, and caused cell death in some cells 24 h after PDT. PE-mediated PDT induced both apoptosis and necrosis and could effectively kill all the cells in samples treated with PE for 1–5 h prior to PDT. Scale bar indicates 50 μm.

4.2.3 Therapeutic efficacy of PE-mediated PDT

PC-3 cells were subjected to PDT and the survival rate of remaining cells was calculated in this study (Figure 4-5). Cells were incubated in either PpIX lipid solution, HVJ-E suspension, or PE suspension prior to PDT, and after irradiation the medium was replaced with either complete D-MEM or the same solution or suspension that had been used prior.

High treatment efficacy was not observed in cells treated with PpIX lipid alone, with the cell survival rate of above 90% in all conditions. 1.2-fold increase in cell survival rate was confirmed by further incubating the cells with PpIX lipid solution after PDT. In contrast, treatment with HVJ-E suspension or PE suspension successfully reduced the cell survival rate in time dependent manner. In fact, further incubation with HVJ-E after PDT led to a 1.5–3-fold decrease in the cell survival rate. A similar trend was observed in cells treated with PE. Specifically, when cells were incubated with PE for 10 min prior to PDT, further incubation with PE subsequent to PDT led to a roughly 2-fold reduction in survival rate compared with cells incubated in complete D-MEM after PDT. Moreover, cell survival rate for samples treated with PE-mediated PDT were 1–3-fold lower than that of samples treated with HVJ-E only.

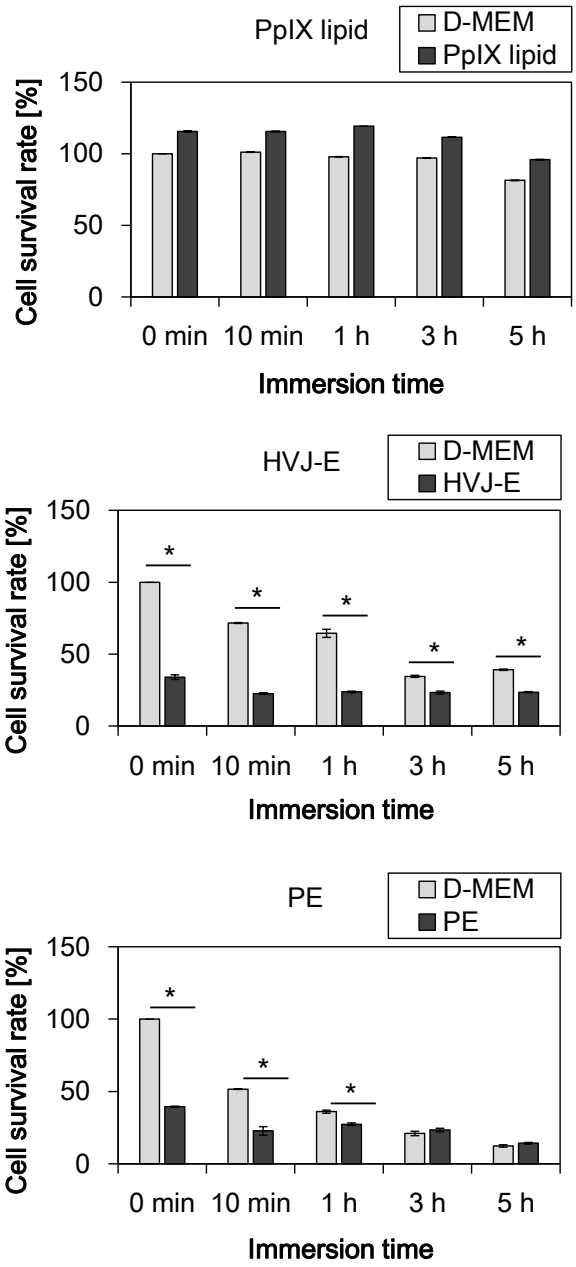

Figure 4-5 Therapeutic efficacy of PE-mediated PDT

PC-3 cells were subjected to PpIX lipid solution, HVJ-E suspension, or PE suspension for 0 min–5 h before PDT. After the light irradiation, the medium was changed to either complete D-MEM, or the solution or suspension used for incubation prior to PDT. Exposure to PpIX lipid exhibited > 90% cell survival rate in all conditions. However, HVJ-E or PE treatment resulted in the reduction of cell survival. Further incubation in HVJ-E or PE after PDT could induce < 3-fold decrease in cell survival rate. (n = 3; *P < 0.01).

4.2.4 Synergy quantification of PE-mediated PDT

In this assay, PC-3 cells were incubated with PE suspension for 10 min–5 h and the growth inhibition rate was determined before and after PDT. Then, CI theorem of Chou-Talalay was utilized to analyze the drug interaction relationship of PE and light irradiation [5], [7], [8].

Figure 4-6 shows the logarithmic median effect plots obtained from the dose-response curve. EC_{50} values, which estimate the dose required to kill 50% of the cells were determined from this graph and each value is listed in Table 4-2. Since the correlation coefficients (r) obtained from logarithmic median effect plots exhibited good linear correlation of $r > 0.95$, the calculated values in this study were confirmed to be eligible [5]. As shown in Table 4-2, marked reduction in the dose of PE and PDT, which is required to reduce the cell survival rate to 50%, was observed when PE and PDT were performed simultaneously. When in combination, the required amount of PE and PDT for 10 min immersion time was reduced 4.4-fold and 5.5-fold, respectively. Highest dose reduction for PE was achieved in 5 h condition with 7.4-fold difference, while 1 h immersion time dropped PDT dose to 3 J/cm^2 with 6.3-fold difference.

Effect of HVJ-E-derived direct cytotoxicity and PDT effect in combination were studied using CompuSyn software to identify the type of interaction taking place: synergistic, additive, or antagonistic. Value of CI identified in this study corresponds to quantitative definition for synergism (CI < 1), additive effect (CI = 1), and antagonism (CI > 1) [5], [7], [8]. The results shown in Figure 4-7 and Table 4-3 revealed that the combination of PE and PE-mediated PDT result in antagonistic or synergistic effect, depending on the condition. Slight antagonistic activity was confirmed when cells were simultaneously treated with lower dose of PE and PE-PDT for 5 h. However, all the other conditions shown synergistic activity with higher dose of PE and PE-PDT in 5 h sample exhibiting very strong synergistic activity.

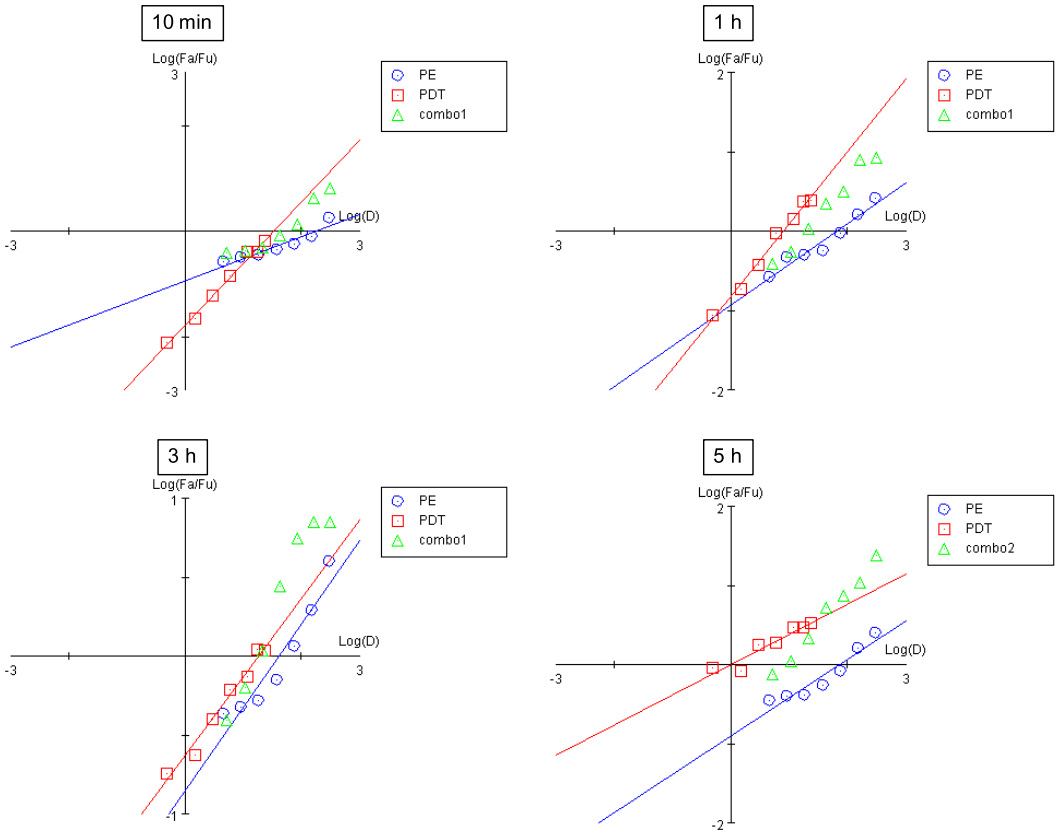

Figure 4-6 Logarithmic median effect plots for PC-3 cells

Linear function was obtained from dose-effect curve by CompuSyn software to calculate the estimated values of effective cytotoxic dose 50% (EC_{50}) and slope. In this graph, x indicates log(dose of each treatment) and y shows log(fraction of dead cells/fraction of live cells). Precision of this calculation was testified by determining correlation coefficient *r*. Lineal correlation was observed in samples treated with PE and PDT alone.

Table 4-2 Parameters for cytotoxicity induced in PC-3 cells

Table 2 (a) and (b) show effective cytotoxic dose 50% (EC_{50}), slope of logarithmic median effect plots, and correlation coefficient (*r*) for respective immersion time. Table 2 (c) indicates EC_{50} values for both PE and PE-PDT at different immersion time. Remarkable reduction in PE and PE-PDT dose was observed when they were used as combination.

(a)

PE (HAU/well)	Immersion time			
	10 min	1 h	3 h	5 h
EC_{50}	166	63	41	70
slope	0.42	0.52	0.53	0.49
r	0.95	0.98	0.95	0.95

(b)

PE-PDT (J/cm^2)	Immersion time			
	10 min	1 h	3 h	5 h
EC_{50}	33	19	7.8	0.94
slope	1.2	0.92	0.5	0.38
r	0.99	0.99	0.99	0.95

(c)

EC_{50} for Combo	Immersion time			
	10 min	1 h	3 h	5 h
PE (HAU/well)	38	19	19	9.4
PE-PDT (J/cm^2)	6	3	3	1.5

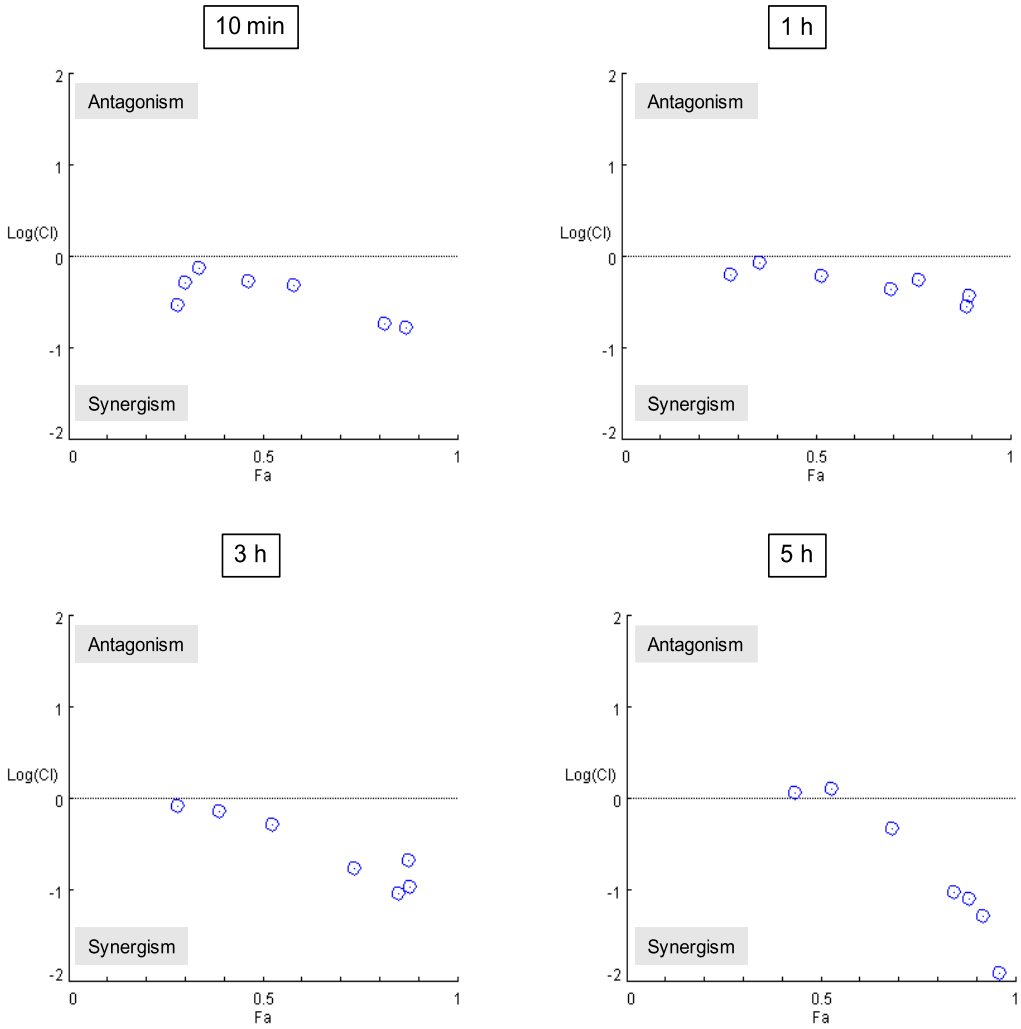

Figure 4-7 Logarithmic combination index plot for PC-3 cells

Circles that fall below the line is synergistic and the ones go over the line is antagonistic. Circles that are on the line is additive. Combined treatment with PE and PE-PDT for 5 h using lower dose exhibited slight antagonistic activity. However, all the other conditions were confirmed to show strong synergistic activity.

Table 4-3 CI values of PE and PE-PDT in combination

Combination index (CI) summary of cells treated with PE and PE-PDT in combination. CI values of < 1 indicates synergism, =1 show additive effect, and > 1 demonstrates antagonism. Combined therapy with PE and PE-PDT in 5 h sample treated with low dose PE and PE-PDT resulted in the values of > 1, indicating slight antagonism; however, all the other values were < 1.

HVJ-E	PE-PDT	CI			
(HAU/well)	(J/cm^2)	10 min	1 h	3 h	5 h
4.7	0.5	0.29	0.24	0.84	1.2
9.4	1.5	0.52	0.19	0.73	1.2
18.8	3	0.75	0.21	0.52	0.5
37.6	6	0.53	0.19	0.17	0.14
75.2	12	0.49	0.31	0.092	0.029
150	18	0.18	0.16	0.11	0.035
300	24	0.17	0.13	0.21	0.034

4.3 Discussion

Since the effect of PDT can be determined by ROS production in cells, level of ROS induced after PE-mediated PDT was determined in this study [1]. As shown in Figure 4-2 and Figure 4-3, time-dependent increase in ROS was confirmed in PE-treated cells. The ROS detection kit used in this study measured the production of hydrogen peroxide (H_2O_2) and hydroxyl radical (·OH); therefore, killing effect of PE-mediated PDT should result from the combination of at least $^1O_2$, H_2O_2, and ·OH. H_2O_2, and ·OH can move freely through the membrane and cause the loss of membrane integrity through lipid peroxidation [16]. Thus, it is highly likely that rapid cell death is induced via PE-mediated PDT through necrosis. In fact, increase in ROS level seemed to have an effect in reducing the cell survival rate at relatively early stage of treatment scheme (Figure 4-4 and Figure 4-5).

Increased susceptibility to cell death was also confirmed in cells treated with PE for more than 3 h prior to PDT – PC-3 cell death was observed right after the light irradiation – whereas cell death in HVJ-E-treated cells was not confirmed till 24 h after PDT treatment (Figure 4-4). These results suggest that PDT effect increased the therapeutic efficacy and the rate of cell death. In previous study, HVJ-E has been confirmed to induce necroptosis in cells through Ca^{2+} upregulation [17]–[19]. This enhancement of Ca^{2+} level confirmed in caspase-8-deficient neuroblastoma resulted from the membrane fusion induced by HVJ-E [18], [19]. Since PDT treatment alone is a necroptosis inducer, light exposure after PE treatment may have intensified the activity of necroptotic pathway [20]–[23]. In PDT using membrane-targeting PS, cytosolic upregulation of Ca^{2+} level is induced via 1) activation of calcium channel and 2) secondary damage to endoplasmic reticulum [20], [24], [25]. Thus, these pathways may have contibuted in upregulating the necroptotic pathway induced in treated cancer cells. Furthermore, upregulation of death receptor-ligand system (such as Fas ligand (FasL) and TRAIL) can also result in necroptosis in Ca^{2+}-independet manner [26].

Necroptosis may play an important role in inducing cytotoxicity towards PC-3 cells, as their expression level of caspase-8 is low; however, the effect of apoptosis cannot be ignored in PE-mediated PDT [27]. As has been discussed earlier, fusion of HVJ-E results in the transduction of RIG-I/MAVS pathway that results in apoptotic cell death [17], [28].

In prostate cancer cells, upregulation of RIG-I/MAVS pathway is observed through the activation of TRAIL and Noxa [29]. Thus, apoptotic pathway should also be carried out in PE-mediated PDT. Further, death via apoptosis can be exhibited in PDT via membrane-targeting PS via upregulation of death receptor-ligand system (such as FasL and TRAIL) in cells that express caspase-8 [2]. In this system, increase in cytosolic Ca^{2+} results in the instability of mitochondrial membrane, releasing the apoptotic inducer, cytochrme c [30]–[32]. Thus, necrosis, apoptosis, and necroptosis should all play part in PE-mediated PDT (Figure 4-8).

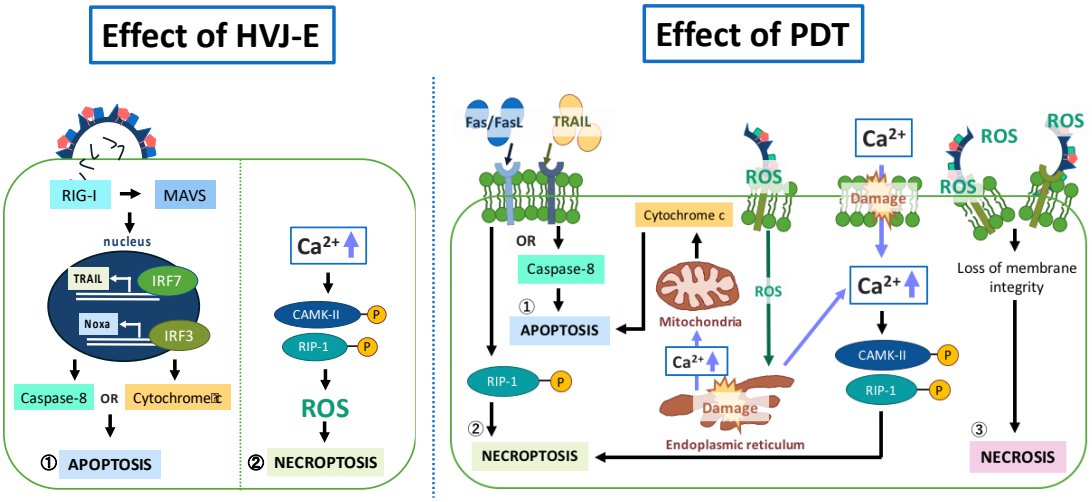

Figure 4-8 Cytotoxic pathway induced via HVJ-E and PE-mediated PDT

Various types of cell death can be induced through treatment with HVJ-E and PE-mediated PDT. In HVJ-E-treated cells, induction of membrane fusion will activate both apoptotic and necroptotic cell death. PE-mediated PDT can also allow multimodal treatment. Treatment of prostate cancer cells using membrane-targeting PS will result in the rupture of cell membrane via necrosis. Also, the increase in cytoplasmic Ca^{2+} level via 1) calcium channel activation and 2) damage to endoplasmic reticulum membrane by ROS will upregulate necroptosis. Necroptotic death can also be activated by death receptor-ligand system when caspase-8 level is low. Expression of caspase-8 in cytosol will induce apoptosis through death receptor-ligand system.

As discussed in *Section 3.2.2*, direct cytotoxic effect of PE was preserved even after exposing the particles to laser light. Therefore, cell death should be induced and enhance therapeutic outcome even after PDT. To further address the effect of combining PE-mediated direct cytotoxicity and photodynamic reaction, therapeutic synergy was

addressed by calculating CI values using CompuSyn software. The results shown in Figure 4-6 and Table 4-2 revealed that combination of PE and PDT could induce higher therapeutic efficacy at lower dose. Moreover, as depicted by Figure 4-7 and Table 4-3, resulting CI values for almost all conditions were below 1, confirming synergy. Study performed by Budman *et al.* has shown that strong synergism of CI < 0.1–0.3 was revealed in only one combination of docetaxel and other chemotherapeutic drug [33]. In the case of PE-mediated PDT, although slight antagonism was confirmed in 5 h samples, all the other conditions exhibited strong or very strong synergism in PE-mediated PDT. As was indicated in Figure 2-2, PE readily delivers PpIX lipid to cell membrane at all immersion time. Thus, photodynamic reaction resulting from PE-mediated PDT causes acute disruption of membrane structure and result in necrosis. Necrotic cell death induced via PE-mediated PDT can be initiated right after the light irradiation, when the cells were exposed to PE for more than 3 h prior to light irradiation (Figure 4-4). Furthermore, PE-mediated PDT achieved lowest cell survival at all immersion time when compared to HVJ-E or PpIX lipid alone (Figure 4-5). Although more research needs to be performed, it is highly likely that PE-mediated PDT allows multimodal treatment by inducing necrosis, apoptosis, and necroptosis. Since treatment with HVJ-E and PDT both induce factors related to apoptosis and necroptosis, these pathway should be upregulated when these two modalities are combined. Moreover, enhancement in drug delivering efficacy and its ability to induce various cell death pathways should support the idea that combination of HVJ-E and PDT is effective in eradiating the castration-resistant prostate cancer due to their highly efficient synergistic activity.

4.4 Summary

Time-dependent increase in ROS production was confirmed after PE-mediated PDT. This has contributed in enhancing the cell sensitivity to cell death cascades, with PC-3 cells exhibiting cell death when treated with PE for more than 3 h prior to light irradiation. Since treatment with HVJ-E alone has been confirmed to induce various pathways, such as apoptosis via RIG-I/MAVS pathway and necroptosis through Ca^{2+} upregulation, PE-mediated PDT should also induce variety of death cascade. For instance, activities of direct cytotoxicity induced by PE and photodynamic reaction caused by PE-mediated PDT have been confirmed to work in synergy. Since synergistic antitumor effect is necessary to improve therapeutic outcome in androgen-insensitive prostate cancer, PE-mediated PDT should possess favorable characteristics to be used for prostate cancer management.

References

[1] H. Kolarova, R. Bajgar, K. Tomankova, P. Nevrelova, and J. Mosinger, "Comparison of sensitizers by detecting reactive oxygen species after photodynamic reaction in vitro," *Toxicol. Vitr.*, vol. 21, pp. 1287–1291, 2007.

[2] P. Mroz, A. Yaroslavsky, G. B. Kharkwal, and M. R. Hamblin, "Cell death pathways in photodynamic therapy of cancer," *Cancers*. pp. 2516–2539, 2011.

[3] Z. Zhou, J. Song, L. Nie, and X. Chen, "Reactive oxygen species generating systems meeting challenges of photodynamic cancer therapy," *Chem. Soc. Rev.*, vol. 45, pp. 6597–6626, 2016.

[4] L. Wyld, M. Reed, and N. Brown, "Differential cell death response to photodynamic therapy is dependent on dose and cell type," *Br. J. Cancer*, vol. 84, no. 10, pp. 1384–1386, 2001.

[5] N. Zhang, J. N. Fu, and T. C. Chou, "Synergistic combination of microtubule targeting anticancer fludelone with cytoprotective panaxytriol derived from panax ginseng against MX-1 cells in vitro: Experimental design and data analysis using the combination index method," *Am. J. Cancer Res.*, vol. 68, no. 3, pp. 621–681, 2016.

[6] T. Lombardo, L. Anaya, L. Kornblihtt, and G. Blanco, *Median Effect Dose and Combination Index Analysis of Cytotoxic Drugs Using Flow Cytometry*, vol. 20. 2012.

[7] C. Le, "Experiment designs for the assessment of drug combination synergism," *Austin Biometrics Biostat.*, vol. 1, no. 2, pp. 1–6, 2014.

[8] T. C. Chou, "Drug combination studies and their synergy quantification using the chou-talalay method," *Cancer Research*, vol. 70, no. 2. pp. 440–446, 2010.

[9] T. C. Chou and P. Talalay, "Quantitative analysis of dose-effect relationships: the combined effects of multiple drugs or enzyme inhibitors," *Adv. Enzyme Regul.*, vol. 22, no. C, pp. 27–55, 1984.

[10] T.-C. Chou, "Theoretical Basis, Experimental Design, and Computerized Simulation of Synergism and Antagonism in Drug Combination Studies," *Pharmacol. Rev.*, vol. 58, no. 3, pp. 621–681, 2006.

[11] J. Foucquier and M. Guedj, "Analysis of drug combinations: current methodological landscape," *Pharmacol. Res. Perspect.*, vol. 3, no. 3, pp. 1–11, 2015.

[12] L. Zhao, J. L-S Au, and M. Guillaume Wientjes, "Comparison of methods for evaluating drug-drug interaction," *Front. Biosci.*, vol. 2, pp. 241–249, 2010.

[13] M. Yamauchi, N. Honda, H. Hazama, S. Tachikawa, H. Nakamura, Y. Kaneda, and K. Awazu, "A novel photodynamic therapy for drug-resistant prostate cancer cells using porphyrus envelope as a novel photosensitizer," *Photodiagnosis Photodyn. Ther.*, vol. 11, no. 1, pp. 48–54, 2014.

[14] M. Inai, N. Honda, H. Hazama, S. Akter, S. Fuse, H. Nakamura, T. Nishikawa, Y. Kaneda, and K. Awazu, "Photodynamic therapy using a cytotoxic photosensitizer porphyrus envelope that targets the cell membrane," *Photodiagnosis Photodyn. Ther.*, vol. 20, pp. 238–245, 2017.

[15] S. Tachikawa, M. E. El-Zaria, R. Inomata, S. Sato, and H. Nakamura, "Synthesis of protoporphyrin-lipids and biological evaluation of micelles and liposomes," *Bioorganic Med. Chem.*, vol. 22, no. 17, pp. 4745–4751, 2014.

[16] M. Repetto, J. Semprine, and A. Boveris, “World's largest Science , Technology & Medicine Open Access book publisher Lipid Peroxidation : Chemical Mechanism , Biological Implications and Analytical Determination,” in *INTECH*, 2012, pp. 1–30.
[17] K. Saga and Y. Kaneda, “Oncolytic Sendai virus-based virotherapy for cancer: recent advances,” *Oncolytic Virotherapy*, vol. 4, pp. 141–147, 2015.
[18] M. Nomura, A. Ueno, K. Saga, M. Fukuzawa, and Y. Kaneda, “Accumulation of cytosolic calcium induces necroptotic cell death in human neuroblastoma,” *Cancer Res.*, vol. 74, no. 4, pp. 1056–1066, 2014.
[19] S. Fulda, “Therapeutic exploitation of necroptosis for cancer therapy,” *Seminars in Cell and Developmental Biology*. pp. 51–56, 2014.
[20] M. Neginskaya, E. Berezhnaya, A. B. Uzdensky, and A. Y. Abramov, “Reactive Oxygen Species Produced by a Photodynamic Effect Induced Calcium Signal in Neurons and Astrocytes,” *Mol. Neurobiol.*, pp. 1–7, 2017.
[21] A. P. Castano, T. N. Demidova, and M. R. Hamblin, “Mechanisms in photodynamic therapy: part two—cellular signaling, cell metabolism and modes of cell death,” *Photodiagnosis Photodyn Ther*, vol. 2, no. 1, pp. 1–23, 2005.
[22] T. Kushibiki, T. Hirasawa, S. Okawa, and M. Ishihara, “Responses of Cancer Cells Induced by Photodynamic Therapy,” *J. Healthc. Eng.*, vol. 4, no. 1, pp. 87–108, 2013.
[23] Z. Su, Z. Yang, L. Xie, J. P. Dewitt, and Y. Chen, “Cancer therapy in the necroptosis era,” *Cell Death and Differentiation*. pp. 748–756, 2016.
[24] P. Agostinis, K. Berg, K. A. Cengel, T. H. Foster, A. W. Girotti, S. O. Gollnick, S. M. Hahn, M. R. Hamblin, A. Juzeniene, D. Kessel, M. Korbelik, J. Moan, P. Mroz, D. Nowis, J. Piette, B. C. Wilson, and J. Golab, “Photodynamic therapy of cancer: An update,” *CA. Cancer J. Clin.*, vol. 61, no. 4, pp. 250–281, 2011.
[25] A. Görlach, K. Bertram, S. Hudecova, and O. Krizanova, “Calcium and ROS: A mutual interplay,” *Redox Biol.*, vol. 6, pp. 260–271, 2015.
[26] K. Jeon, “Effective therapeutic strategies for PDT,” in *International Review of Cell and Molecular Biology*, 2012, pp. 160–163.
[27] D. G. Stupack, “Caspase-8 as a Therapeutic Target in Cancer,” *Cancer Lett.*, vol. 332, no. 2, pp. 133–140, 2013.
[28] K. Saga and Y. Kaneda, “Virosome presents multimodel cancer therapy without viral replication,” *Biomed Res. Int.*, vol. 2013, 2013.
[29] T. Matsushima-Miyagi, K. Hatano, M. Nomura, L. Li-Wen, T. Nishikawa, K. Saga, T. Shimbo, and Y. Kaneda, “TRAIL and Noxa are selectively upregulated in prostate cancer cells downstream of the RIG-I/MAVS signaling pathway by nonreplicating Sendai virus particles,” *Clin. Cancer Res.*, vol. 18, no. 22, pp. 6271–6283, 2012.
[30] a Andreyev and G. Fiskum, “Calcium induced release of mitochondrial cytochrome c by different mechanisms selective for brain versus liver.,” *Cell Death Differ.*, vol. 6, no. 9, pp. 825–32, 1999.
[31] D. J. Granville, H. Jiang, B. M. McManus, and D. W. C. Hunt, “Fas ligand and TRAIL augment the effect of photodynamic therapy on the induction of apoptosis in JURKAT cells,” *Int. Immunopharmacol.*, vol. 1, no. 9–10, pp. 1831–1840, 2001.
[32] D. Gewirtz, S. Holt, and S. Grant, “PDT-induced apoptosis,” in *Apoptosis,*

Senescence and Cancer, 2007, pp. 562–564.
[33] D. R. Budman, A. Calabro, and W. Kreis, “Synergistic and antagonistic combinations of drugs in human prostate cancer cell lines in vitro,” *Anticancer. Drugs*, vol. 13, pp. 1011–1016, 2002.

5. Efficacy of PE-mediated PDT towards different cell lines

Studies performed through Chapters 2 to 4 have utilized PC-3 cells to analyze the therapeutic efficacy of PE-mediated PDT. However, prostate cancer is considered multifocal and its heterogeneous characteristic attributes to a different sensitivity towards therapeutic modalities [1]–[3]. Thus, to investigate how broadly PE-mediated PDT can be applied in prostate cancer management, studies were performed using normal prostate epithelia PNT2 and castration-resistant prostate cancer cell line DU145.

Kawaguchi *et al.* have confirmed the differential organization of gangliosides in castration-resistant prostate cancer cell lines and normal prostate epithelia [4]. Gangliosides, such as GD1a and SPG, act as HVJ-E receptors and expression of these sialic acids are approximately 2–3-fold higher in castration-resistant prostate cancer cells [4], [5]. Therefore, HVJ-E exhibits higher affinity towards malignant cells. Moreover, previous studies have shown how HVJ-E can act as an efficient inhibitor of tumor cell growth in both PC-3 cells and DU145 cells [4], [6], [7]. Matsushima-Miyagi *et al.* revealed that HVJ-E-induced apoptosis is only observed in PC-3 cells even under the mixed culture condition of PNT2 cells and PC-3 cells [7]. In addition, upregulation of effector molecules for HVJ-E, TRAIL and Noxa, were observed in PC-3 cells and DU145 cells but not in PNT2 cells [7]. These characteristics of HVJ-E together suggest that PE-mediated PDT can be performed in cancer-selective manner.

In this chapter, 1) cellular uptake of PE-PpIX lipid, 2) level of direct cytotoxicity, and 3) efficacy of PE-mediated PDT were addressed using DU145 cells and PNT2 cells.

5.1 Materials and Methods

5.1.1 Cell line and culture

FBS and 100 units/mL penicillin-streptomycin were added to D-MEM to create complete D-MEM as mentioned in *Section 2.1.1*. Normal prostate epithelia PNT2 was cultured in complete D-MEM at 37°C with humidity in 5% CO_2 atmosphere. In addition, castration-resistant human prostate cancer cell line DU145 was cultured in RPMI 1640 (30264-56, Nacalai Tesque, Japan) supplemented with 10% FBS and 100 units/mL penicillin–streptomycin, referred to as complete RPMI. For cell seeding, cells were harvested after reaching 80% confluence. All studies were conducted using stable lines.

5.1.2 Photosensitizers

Preparation of PE was done as follows. First, 5 mM PpIX lipid was diluted with D-PBS to 10.5 μM solution. HVJ-E was then prepared as previously reported and was separated to 2500 HAU each [8], [11]. This HVJ-E was suspended in 10.5 μM PpIX lipid solution with a final volume of 1 mL [11]. Then, PE was prepared by inserting PpIX lipid into HVJ-E via centrifugation (20,000 × g, 4°C, 10 min) [8]. Finally, the supernatant was removed after centrifugation and the pellet of PE was suspended in 835 μL of complete D-MEM. The ratio of PpIX lipid to HVJ-E in PE was 3.5 pmol/HAU.

In addition, 5 mM PpIX lipid was diluted with complete D-MEM to 10.5 μM. Suspensions of HVJ-E were prepared at concentrations of 1000 HAU/500 μL and 150 HAU/50 μL by suspending it in complete D-MEM. 5-ALA was stored at –20°C and an aqueous solution of 5 mM PpIX lipid was stored at 4°C [10]. All reagents were prepared prior to each experiment.

5.1.3 Fluorescence assay for uptake of PpIX

Relative cellular uptake of PpIX lipid delivered by PE was measured using a cell-based fluorescent assay. A black 96-well cell culture plate with a clear bottom was used in this experiment. PNT2 cells and DU145 cells with a density of 5.0×10^3 cells/well were incubated at 37°C in 5% CO^2 condition for 24 h. The following day, cells were exposed to 50 μL of complete D-MEM, complete RPMI, 5-ALA solution, PpIX lipid solution, HVJ-E suspension, or PE suspension for 10 min, 30 min, 1 h, 2h, 3 h, 4 h or 5 h. To observe the cellular uptake of photosensitive agents in cells, cells were washed with

D-PBS once, and were lysed in D-PBS containing 0.1% sodium dodecyl sulphate. Fluorescence intensity of PpIX was measured right after this process using a fluorescence microplate reader at an excitation wavelength of 401 nm and an emission wavelength of 625 nm.

5.1.4 Direct cytotoxic effect of PE

PNT2 cells and DU145 cells were seeded on a 96-well cell culture plate with a clear bottom at a density of 5.0×10^3 cells/well and were incubated for 24 h at 37°C in 5% CO_2 condition. Cells were then incubated with 50 μL of complete D-MEM, PpIX lipid solution, HVJ-E suspension, or PE suspension for 10 min, 1 h, 3 h, or 5 h. Following this step, cells were washed once with D-PBS and incubated in 100 μL of complete D-MEM for 24 h at 37°C in 5% CO_2. To evaluate the cell survival rate, a mixture that contains 90 μL of complete D-MEM or complete RPMI and 10 μL of a cell counting reagent containing WST-8 was administered. An absorbance microplate reader with the light of 405 nm wavelength was used to determine the optical density of each well. The cell survival rate for each sample was calculated as a percentage of control. Microscopic images of PNT2 cells and DU145 cells were obtained using an inverted laboratory microscope.

5.1.5 PDT experiment

PNT2 cells and DU145 cells were seeded on a 96-well cell culture plate with a clear bottom at a density of 5.0×10^3 cells/well and the plate was placed in 5% CO^2 condition at 37°C for 24 h. The following day, 50 μL of PpIX lipid solution, HVJ-E suspension (150 HAU), or PE suspension (150 HAU) was added for treatment of 10 min, 1 h, 3 h, or 5 h. Then, respective reagents were exchanged with 100 μL of complete D-MEM or complete RPMI before performing laser irradiation. To perform PDT, the plate was placed on a plate warmer to maintain the temperature at 37°C and a laser diode of 405 nm with power density of 100 mW/cm^2 was irradiated to each well for 60 s. The position of the plate and the time of irradiation was controlled by a two-axis motorized linear stage. After laser irradiation, cells were further incubated for 24 h in 100 μL of complete D-MEM or complete RPMI. The cell survival rate after respective treatment was determined by changing the medium of each well to a mixture of 90 μL of complete D-MEM or complete RPMI and 10 μL of a cell counting reagent that contains WST-8. An absorbance microplate reader with a light of 450 nm wavelength was used to determine the optical

density of each well. The cell survival rate for each sample was calculated as a percentage of control (cells treated with complete D-MEM or complete RPMI).

5.1.6 Statistical analysis

All results are expressed as the means ± SD for six cases ($n = 6$). A two-tailed unpaired Student's *t*-test was performed between two sample groups, and a probability value of $*P < 0.01$ was considered statistically significant.

5.2 Experimental results

5.2.1 Cellular uptake of PpIX lipid in different cell lines

Cancer specificity of PE was analyzed by first measuring the cellular uptake of PE-delivered PpIX lipid in PNT2 cells and DU145 cells. As shown in Figure 5-1, neither cell lines exhibited PpIX lipid fluorescence at any point of the treatment period when exposed to cell media or HVJ-E. Uptake of PpIX lipid was confirmed in both cell lines only when they were exposed to PpIX lipid solution or PE suspension.

In the case of PNT2 cells, PpIX lipid-treated cells exhibited significantly higher fluorescence intensity than that of PE-treated cells with the difference of approximately 1.4–2-fold. On the other hand, PE appeared to be 1.4–3-fold more efficient in delivering PpIX lipid in DU145 cells. In addition, fluorescence intensities for PNT2 obtained after PE treatment were approximately 2–6-fold lower than those observed in DU145. Thus, together with the results presented in *Section 2.2.2*, PE has been revealed to achieve cancer-selective delivery.

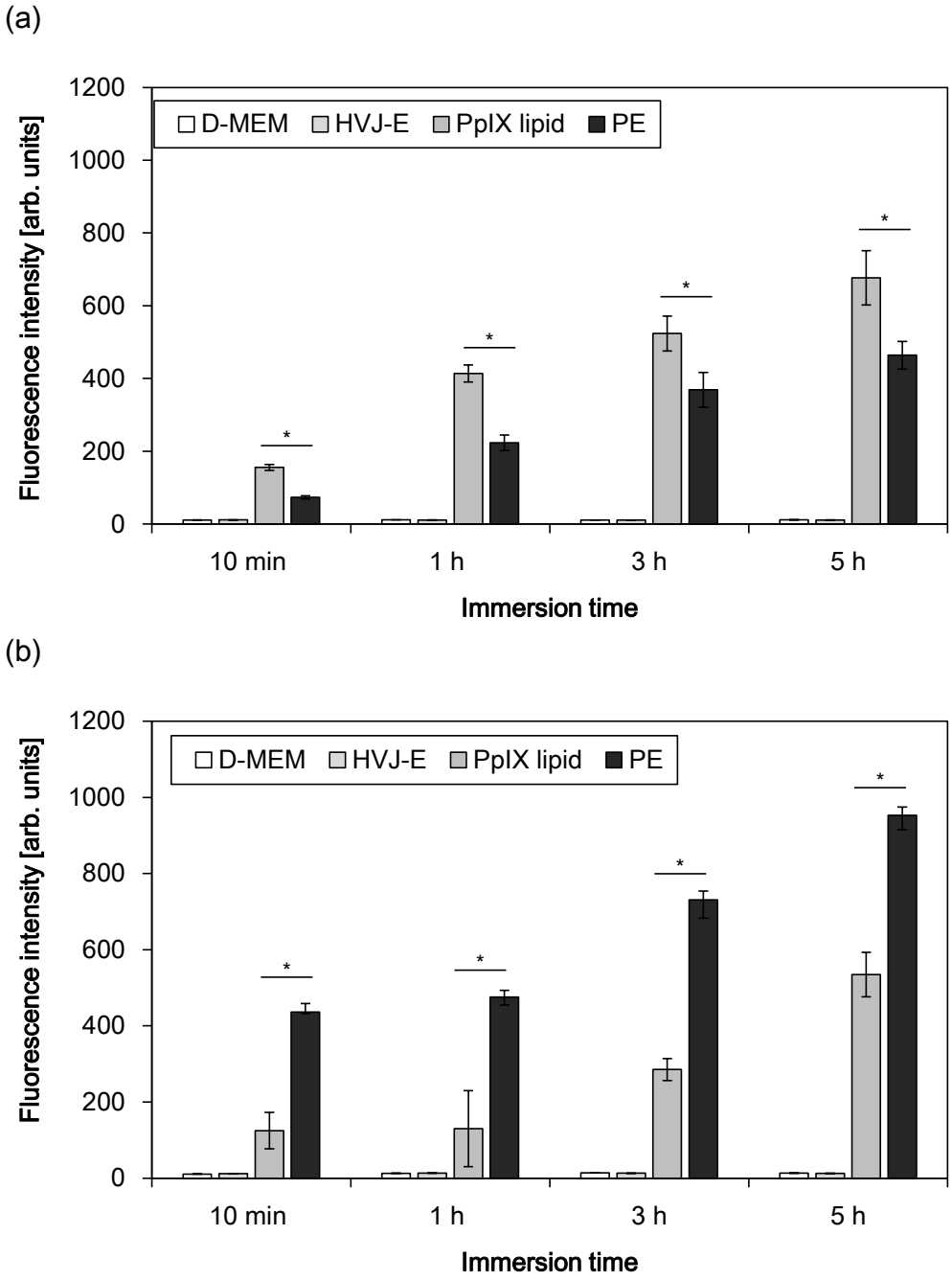

Figure 5-1 Cancer selective uptake of PpIX lipid via PE

(a) PNT2 cells and (b) DU145 cells were treated with cell media, PpIX lipid solution, HVJ-E suspension, or PE suspension. Although both cell lines exhibited uptake of photosensitizer when treated with PpIX lipid solution or PE suspension, PE was 2–6-fold more potent in delivering PpIX lipid in cancer cells ($n = 3$; $^*P < 0.01$).

5.2.2 Effect of PE-induced direct cytotoxicity in different cell lines

Cells were incubated with cell media, PpIX lipid solution, HVJ-E suspension or PE suspension to see the cancer selectivity of direct cytotoxicity induced by PE. In both cell lines, treatment by cell media or PpIX lipid solution resulted in the survival rate of ≥ 100%. Slight reduction in cell survival rate was confirmed for PNT2 cells after the treatment with HVJ-E or PE, however, cell survival rate remained above 77% in all conditions (Figure 5-2(a)). On the other hand, DU145 exhibited time dependent decrease in cell survival rate after being exposed to PE for 10 min–5 h (Figure 5-2(b)). Treatment with PE for 5 h resulted in the lowest cell survival rate of approximately 48%. In fact, PE-induced cytotoxicity observed towards DU145 cells was > 1.2–1.6-fold higher than PNT2 cells.

Morphological changes in PNT2 cells and DU145 cells were addressed after treating the cells with respective reagents for 10 min–5 h (Figure 5-3). Evident change in cell morphology was not confirmed in PNT2 cells at all conditions; however, treatment with HVJ-E or PE led to the change in DU145 cell structure. This change became evident after 3 h incubation with HVJ-E or PE. The bubble-like structures started to appear after 3 h incubation and covered the well bottom after 5 h.

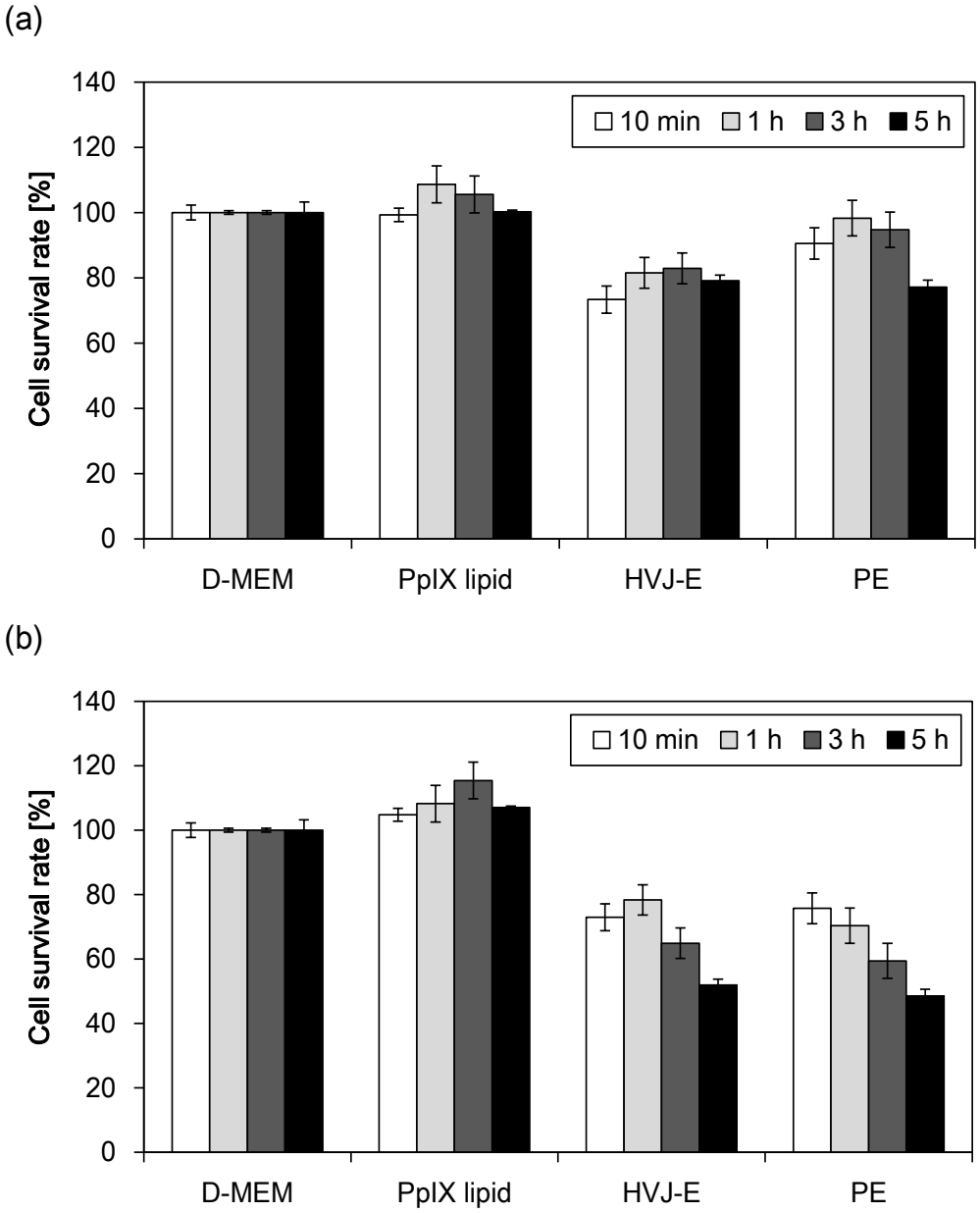

Figure 5-2 Direct cytotoxic effect in PNT2 cells and DU145 cells
Direct cytotoxicity induced after immersing the cells in cell media, PpIX lipid solution, HVJ-E suspension, or PE suspension was observed. The resulting cell survival rate for (a) PNT2 was maintained above 77% even after PE treatment. On the other hand, cell survival rate after PE treatment decreased in time dependent manner in (b) DU145 cells. Direct cytotoxic effect of PE was > 1.2–1.6-fold higher in DU145 cells (n = 3).

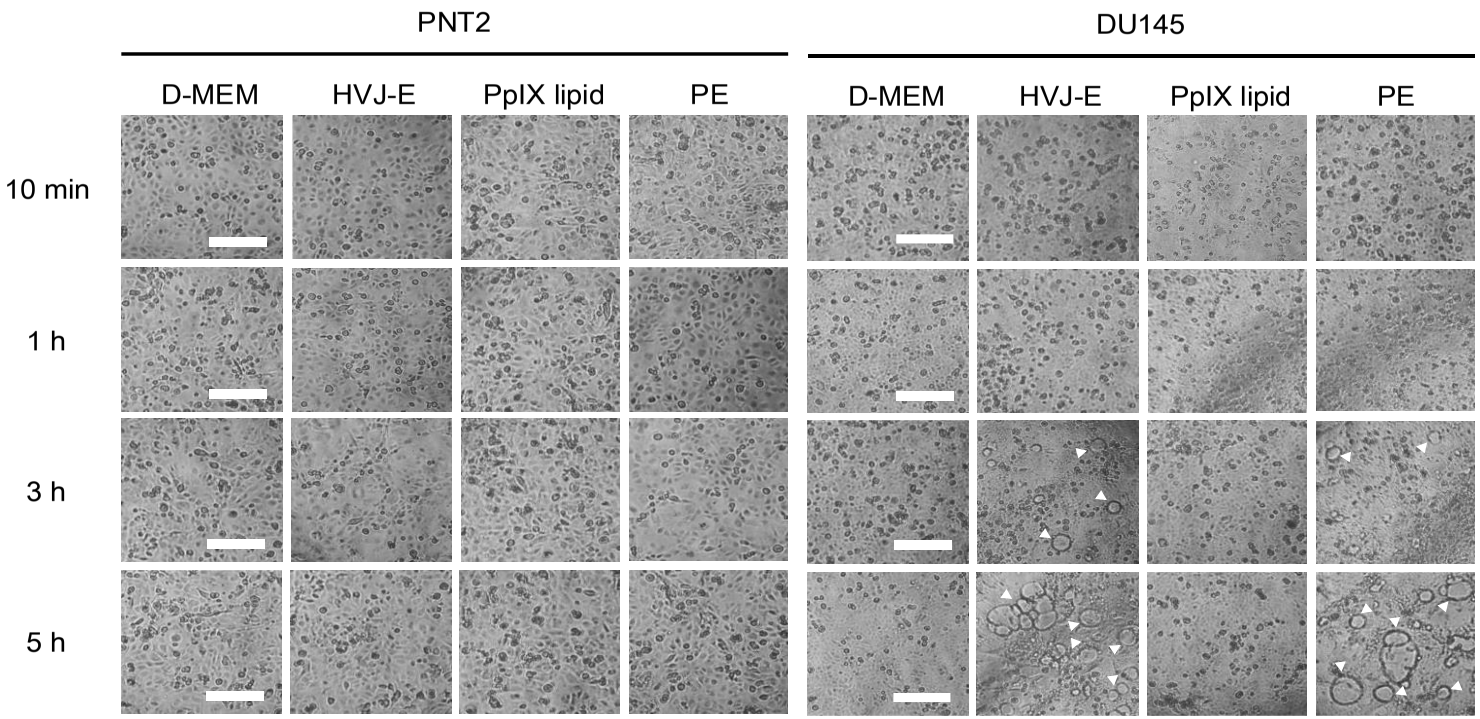

Figure 5-3 Morphological change in cells after PE treatment

PNT2 cells and DU145 cells were exposed to respective reagents to observe their effect on cell morphology. No evident difference was confirmed in PNT2 cells; however, 3–5 h treatment with HVJ-E or PE resulted in structural change in DU145 cells (white arrowheads). Scale bar indicates 200 μm.

5.2.3 Effect of PE-mediated PDT in different cell lines

Cells were incubated with cell media, PpIX lipid solution, HVJ-E suspension or PE suspension for 10 min–5 h before light irradiation to see the cancer selectivity of PE-mediated PDT. As shown in Figure 5-4, PDT after treatment with cell media or PpIX lipid did not result in strong cytotoxicity in both cell lines. HVJ-E-treatment for PNT 2 cells resulted in the slight reduction in cell survival rate. In addition, PE-mediated PDT caused the cell survival rate to drop to > 58% when incubated with PE for 5 h prior to light irradiation. However, both HVJ-E and PE exhibited higher cytotoxicity towards DU145 cells (Figure 5-4). In fact, treatment with HVJ-E for more than 1 h resulted in sudden reduction of cell survival rate to < 52%. In addition, PE-treatment prior to PDT showed time dependent decrease in overall cell survival rate against cancer cells. The minimal cell survival rate of approximately 23% was achieved in DU145 cells with PE treatment of 5 h before PDT.

The overall PDT efficacy was approximately 1.4–2.5-fold higher in DU145 cells, confirming the cancer selective activity of PE-mediated PDT.

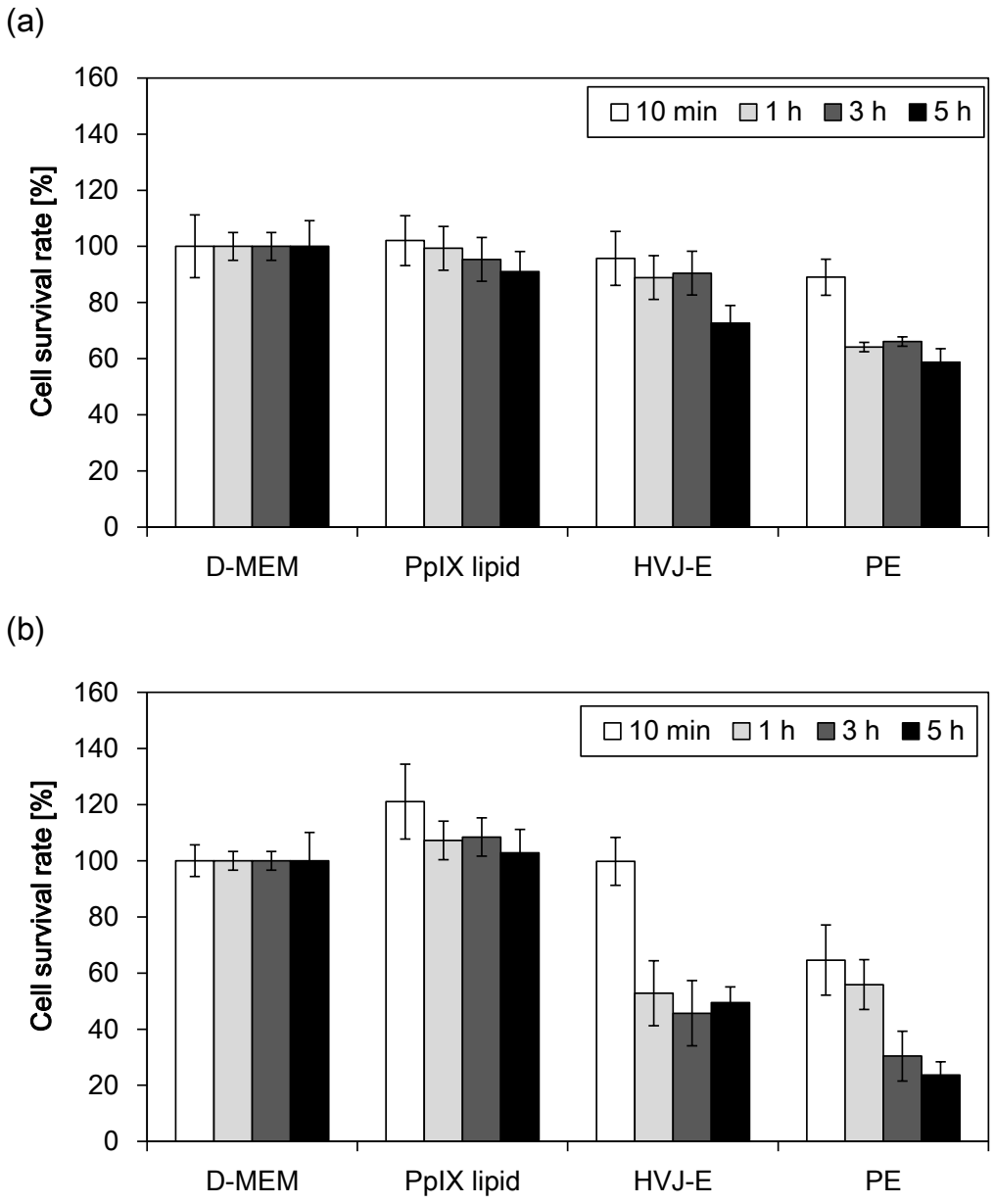

Figure 5-4 Effect of PE-mediated PDT in PNT2 cells and DU145 cells
Cells were incubated in cell media, PpIX lipid solution, HVJ-E suspension, or PE suspension for 10 min–5 h before light irradiation. Cell survival rate after PDT was compared between (a) PNT2 cells and (b) DU145 cells to confirm the cancer selective activity of PE-mediated PDT. PE-mediated PDT reduced survival rate of PNT2 cells to 58% after 5 h, yet the rate was 2.5-fold lower in DU145 cells with 23%. Overall, PDT efficacy was 1.4 – 2.5-fold higher in cancer cells, confirming cancer selectivity (n = 3).

5.3 Discussion

As discussed in the introduction of this chapter, HN proteins distributed on the bilayer of HVJ-E has been noted to exhibit affinity towards glycosphingolipids that contain sialic acids, named GD1a and SPG [4], [5]. Since the number of these receptors differ between PNT2 cells and DU145 cells by approximately 2-fold, cancer-selective delivery of PS can be achieved by HVJ-E [4]. Thus, difference in the number of HN proteins on respective cell lines should have contributed in the 2–6-fold difference in PpIX lipid uptake confirmed between PE-treated DU145 cells and PNT2 cells (Figure 5-1). Furthermore, preferential induction of anti-tumor activity resulting from the induction of apoptotic RIG-I/MAVS pathway or Ca^{2+}-dependent necroptosis was still intact in PE. The results shown in Figure 5-2 and Figure 5-3 revealed that PE-mediated membrane fusion caused the formation of multinucleated syncytia in DU145 cells after 1 h exposure, and reduced the cell survival rate of DU145 cells to < 50%. Since 1.2–1.6-fold difference in cell survival rate was confirmed in PE-treated DU145 cells and PNT2 cells, the cancer-selective characteristic of PE was indicated in this study. Likewise, therapeutic activity of PE-mediated PDT was confirmed to be cancer-selective. As depicted by Figure 5-4, cell survival rate obtained after 10 min–5 h incubation with PE was 1.4–2.5-fold higher in PNT2 cells. Since abundance ratio of HN receptors on DU145 cells and PNT2 cells differ by approximately 2-fold, cancer-selective treatment via PE-mediated PDT should attribute to this difference in receptor ratio. Cancer selectivity with at least 2-fold difference should be confirmed in PE-mediated PDT by carefully selecting the treatment condition.

Moreover, PE-mediated PDT in DU145 cells reduced the cell survival rate by 1.5–2-fold compared to HVJ-E-mediated PDT (Figure 5-4). As indicated in *section 4.2.4*, PE-mediated PDT induced synergistic interaction between PE-induced direct cytotoxicity and photodynamic reaction in PC-3 cells. Thus, similar mechanism should have contributed in further reducing the cell survival rate in DU145 cells.

5.4 Summary

PE exhibited cancer-selective advantage with high treatment efficacy. For instance, cancer preferetive uptake of PE-inserted PpIX lipid and cell death was observed in this study. Since HN receptors for HVJ-E located on castration-resistance cancer cells and normal prostate epithelia differ in nature, PE should allow selective PS uptake and treatment efficacy in prostate cancer.

References

[1] L. H. Higgins *et al.*, "Hypoxia and the metabolic phenotype of prostate cancer cells," *Biochim. Biophsica Acta*, vol. 1787, pp. 1433–1443, 2009.

[2] V. Nwosu, J. Carpten, J. M. Trent, and R. Sheridan, "Heterogeneity of genetic alterations in prostate cancer: evidence of the complex nature of the disease PROSTATE CANCER SUSCEPTIBILITY LOCI: RARE WITH HIGH PENETRANCE," *Hum. Mol. Genet.*, vol. 10, no. 20, pp. 2313–2318, 2001.

[3] S. Marchiani *et al.*, "Androgen-responsive and -unresponsive prostate cancer cell lines respond differently to stimuli inducing neuroendocrine differentiation," *Int. J. Androl.*, vol. 33, pp. 784–793, 2010.

[4] Y. Kawaguchi, Y. Miyamoto, T. Inoue, and Y. Kaneda, "Efficient eradication of hormone-resistant human prostate cancers by inactivated Sendai virus particle," *Int. J. Cancer*, vol. 124, pp. 2478–2487, 2009.

[5] T. Nakajima, T. Itai, H. Wada, T. Yamauchi, E. Kiyohara, and Y. Kaneda, "A Novel Therapy for Melanoma and Prostate Cancer Using a Non-Replicating Sendai Virus Particle (HVJ-E)," in *INTECH*, 2013.

[6] K. Fujita *et al.*, "Phase I/II clinical trial to assess safety and efficacy of intratumoral and subcutaneous injection of HVJ-E in castration-resistant prostate cancer patients," *Cancer Gene Ther.*, vol. 24, pp. 277–281, 2017.

[7] T. Matsushima-Miyagi *et al.*, "TRAIL and Noxa are selectively upregulated in prostate cancer cells downstream of the RIG-I/MAVS signaling pathway by nonreplicating Sendai virus particles," *Clin. Cancer Res.*, vol. 18, no. 22, pp. 6271–6283, 2012.

[8] M. Yamauchi *et al.*, "A novel photodynamic therapy for drug-resistant prostate cancer cells using porphyrus envelope as a novel photosensitizer," *Photodiagnosis Photodyn. Ther.*, vol. 11, no. 1, pp. 48–54, 2014.

[9] M. Inai *et al.*, "Photodynamic therapy using a cytotoxic photosensitizer porphyrus envelope that targets the cell membrane," *Photodiagnosis Photodyn. Ther.*, vol. 20, pp. 238–245, 2017.

[10] S. Tachikawa, M. E. El-Zaria, R. Inomata, S. Sato, and H. Nakamura, "Synthesis of protoporphyrin-lipids and biological evaluation of micelles and liposomes," *Bioorganic Med. Chem.*, vol. 22, no. 17, pp. 4745–4751, 2014.

6. Efficacy of PE-mediated PDT in 3D tumor spheroid model

Studies reviewed in previous chapters have confirmed the possibility of cancer-selective and highly efficient treatment using PE. However, all the experiments were done in 2D model which do not integrate mechanical and chemical signals exerted *in vivo* [1]. In 2D condition, cells are evenly exposed to the cell media and have full access to nutrients and oxygen required for cell growth [1]. On the contrary, tumor physiology is often far more complex in real-life situation, so analysis in 2D model can sometimes lead to the overestimation of therapeutic outcome [1], [2]. Unlike homogenous cell population observed in 2D systems, tumors *in vivo* exhibit three different zones: 1) zone of proliferation, 2) zone of quiescent, and 3) hypoxic necrotic core [1], [3]. Since both normoxic and hypoxic areas are present in natural cancer environment, a single cancer consists of cells of different stages that exhibit different level of sensitivity towards cancer treatment [4]–[6].

As to simulate the functional and physiological properties of human cancer, while preventing the ethical dilemmas of *in vivo* study, multicellular spheroid cultures were developed by Sutherland [2], [7], [8]. Three-dimensional (3D) *in vitro* cancer spheroid models provide tissue-like morphology and phenotype, including cell-cell interactions, mass transport limitation, and nutrients/oxygen gradient, while overcoming the simplicity of 2D culture system [1], [2], [6]. Recently 3D models have been integrated in PDT studies as a treatment response platform, as different response rate was confirmed between 2D and 3D model, with 2D culture exhibiting 2-fold higher sensitivity towards PDT regimen [1], [4], [6]. On the other hand, PDT moiety has been proven to be effective towards chemoresistant cells in 3D model [4], [9]. Since most of the chemotherapeutic agents target proliferative cancer cells, possibility of PDT targeting cancer initiating cells (CICs) that are quiescent and slow-growing have gathered much interest in the medical field [6].

The following sections will review the efficacy of PE-mediated PDT using 3D spheroid model. Analysis of cellular uptake of PE-inserted PpIX lipid, effect of PE-

induced direct cytotoxicity, and therapeutic efficacy of PE-mediated PDT was performed to determine the combined efficacy of newly established therapeutic modality in *in vivo*-mimickning model.

6.1 Materials and Methods

6.1.1 Cell line and culture

FBS and 100 units/mL penicillin-streptomycin were added to D-MEM to create complete D-MEM as mentioned in *Section 2.1.1*. Androgen-independent human prostate cancer cell line PC-3 was cultured in complete D-MEM at 37°C with humidity in 5% CO_2 atmosphere. For cell seeding, cells were harvested after reaching 80% confluence. All studies were conducted using stable lines.

6.1.2 Photosensitizers

Preparation of PE was done as follows. First, 5 mM PpIX lipid was diluted with D-PBS to 10.5 μM solution. HVJ-E was then prepared as previously reported and was separated to 2500 HAU each [10], [11]. This HVJ-E was suspended in 10.5 μM PpIX lipid solution with a final volume of 1 mL [11]. Then, PE was prepared by inserting PpIX lipid into HVJ-E via centrifugation (20,000 × g, 4°C, 10 min) [10]. Finally, the supernatant was removed after centrifugation and the pellet of PE was suspended in 835 μL of complete D-MEM. The ratio of PpIX lipid to HVJ-E in PE was 3.5 pmol/HAU.

In addition, 5 mM PpIX lipid was diluted with complete D-MEM to 10.5 μM. Suspensions of HVJ-E were prepared at concentrations of 1000 HAU/500 μL and 150 HAU/50 μL by suspending it in complete D-MEM. 5-ALA was stored at –20°C and an aqueous solution of 5 mM PpIX lipid was stored at 4°C [12]. All reagents were prepared prior to each experiment.

6.1.3 Number of PC-3 cells in spheroid system

To obtain a cell calibration curve, PC-3 cells were seeded on a black 96-well cell culture plate with a clear bottom at a density of 0.0–5.0 × 10^4 cells/well and left for 24 h at 37°C in 5% CO^2 in a mixture of 90 μL of complete D-MEM and 10 μL of a cell counting reagent containing WST-8. A wavelength of 450 nm was measured using an absorbance microplate reader to determine the optical density of each well.. Furthermore, PC-3 cells were seeded on a 96-well cell culture plate with steep shaped bottom (PrimeSurface® 96M plate (MS-9096M), Sumito Bakelite, Japan) at a density of 1.0–5.0 × 10^3 cells/well and incubated for 3 days at 37°C in 5% CO_2 to form spheroids. Absorbance in each well was measured as described above, and the number of PC-3 cells after 3 days incubation was

calculated from the calibration curve.

6.1.4 Fluorescence assay for uptake of PpIX

Relative cellular uptake of PpIX lipid delivered by PE was measured using a cell-based fluorescent assay. Cells were seeded into a 96-well cell culture plate with steep shaped bottom at a density of 1.0×10^3 cells/well and were incubated for 3 days at 37°C in 5% CO_2 to form spheroids. Cells were then incubated in complete D-MEM, PpIX lipid solution, HVJ-E suspension, or PE suspension for 10 min, 1 h, 3 h, or 5 h, and were lysed in D-PBS containing 0.1% sodium dodecyl sulphate. Fluorescence intensity of PpIX was measured right after lysing the cells using a fluorescence microplate reader at an excitation wavelength of 401 nm and an emission wavelength of 625 nm.

6.1.5 Direct cytotoxic effect of PE

PC-3 cells were seeded on a 96-well cell culture plate with steep shaped bottom at a density of 1.0×10^3 cells/well and were incubated for 3 days at 37°C in 5% CO_2 to form spheroids. Cells were incubated with 50 μL of complete D-MEM, PpIX lipid solution, HVJ-E suspension, or PE suspension for 10 min, 1 h, 3 h, or 5 h. Cells were then washed once with D-PBS and incubated in 100 μL of complete D-MEM for 24 h at 37°C in 5% CO_2. To evaluate the cell survival rate, cells were trypsynized before medium in each well was replaced with a mixture of 90 μL of complete D-MEM and 10 μL of a cell counting reagent that contains WST-8. An absorbance microplate reader with a light of 450 nm wavelength was used to obtain the optical density of each well. The cell survival rate for each sample was calculated as a percentage of control (spheroids treated with complete D-MEM). Microscopic images of PC-3 spheroids were obtained using an inverted laboratory microscope.

6.1.6 PDT experiment

PC-3 cells were seeded on a 96-well cell culture plate with steep shaped bottom at a density of 1.0×10^3 cells/well and the plate was placed in 5% CO^2 condition at 37°C for 24 h. Following day, 50 μL of PpIX lipid solution, HVJ-E suspension (150 HAU), or PE suspension (150 HAU) was added for treatment of 10 min, 1 h, 3 h, or 5 h. Then, respective reagents were exchanged with 100 μL of complete D-MEM before performing laser irradiation. To perform PDT, the plate was placed on a plate warmer to maintain the temperature at 37°C and wells were irradiated with 405 nm laser diode with power density

of 100 mW/cm^2 for 60 s each. The position of the plate and the time of irradiation was controlled by a two-axis motorized linear stage. After laser irradiation, cells were further incubated for 24 h in 100 μL of complete D-MEM. Cells were then trypsynized and the cell survival rate after respective treatment was determined by changing the medium of each well to a mixture of 90 μL of complete D-MEM and 10 μL of a cell counting reagent that contains WST-8. An absorption microplate reader with a light of 450 nm wavelength was used to determine the optical density of each well. The cell survival rate for each sample was calculated as a percentage of control (cells treated with complete D-MEM).

6.1.7 Statistical analysis

All results are expressed as the means ± SD for six cases ($n = 6$). A two-tailed unpaired Student's *t*-test was performed between two sample groups, and a probability value of $*P < 0.01$ was considered statistically significant.

6.2 Experimental results

6.2.1 Comparison of PC-3 cell numbers in 2D and 3D spheroid model

Number of PC-3 cells in spheroids were calculated using the calibration curve as shown in Figure 6-1. The initial cell number was set to 1.0×10^3 cells/well, 2.0×10^3 cells/well, and 5.0×10^3 cells/well, respectively. For each condition, 8-fold, 5-fold, and 2-fold increase in cell number was confirmed, yielding 8.2×10^3 cells/well, 9.2×10^3 cells/well, and 1.2×10^4 cells/well each. The highest growth rate was obtained when initial cell number was set to 1.0×10^3 cells/well; therefore, seeding density was set to this rate for all the 3D experiments. Since the cells were seeded at a density of 5.0×10^3 cells/well in 2D culture, final cell number was 1.6-fold higher in 3D system.

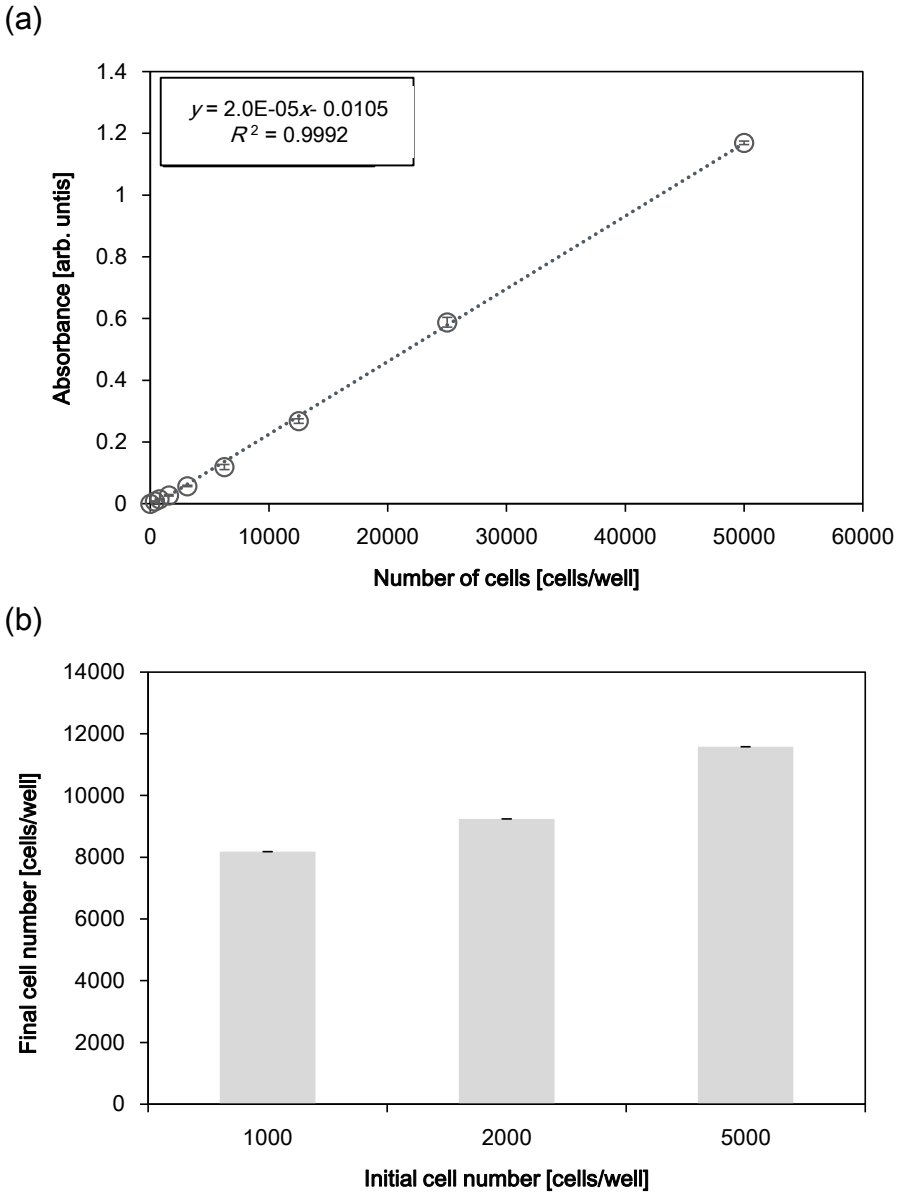

Figure 6-1 Number of PC-3 cells in spheroid system

The (a) calibration curve was used to calculate the (b) number of PC-3 cells in each spheroid (n = 4). The R^2 value obtained in this experiment was between 0.999–1; therefore, credibility of the experiments was shown. The number of PC-3 cells in each spheroid at respective initial cell number (1.0×10^3 cells/well, 2.0×10^3 cells/well, and 5.0×10^3 cells/well) was revealed to be 8.2×10^3 cells/well, 9.2×10^3 cells/well, and 1.2×10^4 cells/well, respectively. The intensity of cell proliferation has decreased as the initial cell number increased.

6.2.2 Uptake of PE-inserted PpIX lipid in PC-3 spheroids

Cellular uptake of PpIX lipid delivered by PE was compared with the amount of intracellular PpIX lipid after administration of exogenous PpIX lipid (Figure 6-2). Fluorescence intensity observed in cells treated with either complete D-MEM or HVJ-E suspension was low; however, cells treated with exogenous PpIX lipid and PE exhibited high fluorescence intensity.

As observed in *Section 2.2.2*, stronger PpIX lipid fluorescence was confirmed in spheroids treated with PE with significant difference. Approximate 1.3–2-fold difference was observed in fluorescence when PE was utilized as carrier; thus, PE should be a potent photosensitizer carrier *in vivo*.

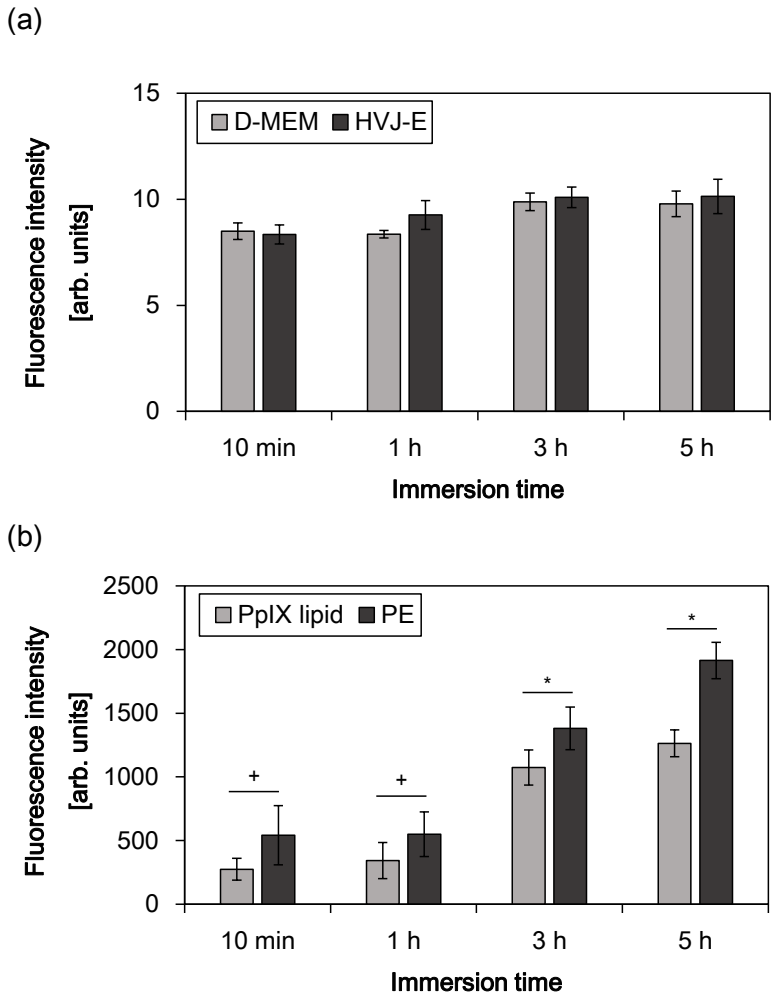

Figure 6-2 Uptake of PpIX lipid in PC-3 spheroids

PpIX lipid fluorescence intensity was compared amongst the spheroids treated with (a) complete D-MEM or HVJ-E suspension, and (b) PpIX lipid solution or PE suspension (n = 6; $+P < 0.05$; $*P < 0.01$). The treatment with neither complete D-MEM nor HVJ-E suspension resulted in high fluorescence intensity. However, fluorescence intensity has increased with the treatment with PpIX lipid or PE. Significant difference was confirmed between PpIX lipid- and PE-treated spheroids. PE induced 1.3–2-fold enhancement in fluorescence intensity.

6.2.3 Effect of PE-induced direct cytotoxicity towards PC-3 spheroids

PC-3 spheroids were subjected to the treatment with either complete D-MEM, PpIX lipid solution, HVJ-E suspension, or PE suspension to analyze the effect of direct cytotoxicity. Morphological changes after respective treatment are shown in Figure 6-3. Evident change in spheroid morphology was not confirmed in samples treated with complete D-MEM or PpIX lipid solution. On the other hand, exposure to HVJ-E suspension or PE suspension resulted in the shrinkage of formed spheroids after 1 h immersion time. In addition, bud-like structure confirmed 1–5 h after HVJ-E- or PE-treatment, causing the enlargement of treated PC-3 spheroids.

Quantification of cell survival rate after each treatment was performed as indicated by Figure 6-4 to compare the resulting cytotoxic effect. No change in survival rate was observed in cells treated with complete D-MEM, whereas slight increase in overall survival was confirmed in cells that underwent PpIX lipid treatment. 10 min–1 h treatment with HVJ-E and PE did not induce marked cell killing effect. However, cytotoxic effect confirmed in spheroids exposed to HVJ-E suspension or PE suspension for 3–5 h was significantly higher than in those treated with complete D-MEM. Approximately 2–3.7-fold reduction in cell survival rate was achieved by exposing the spheroids to PE for 3–5 h.

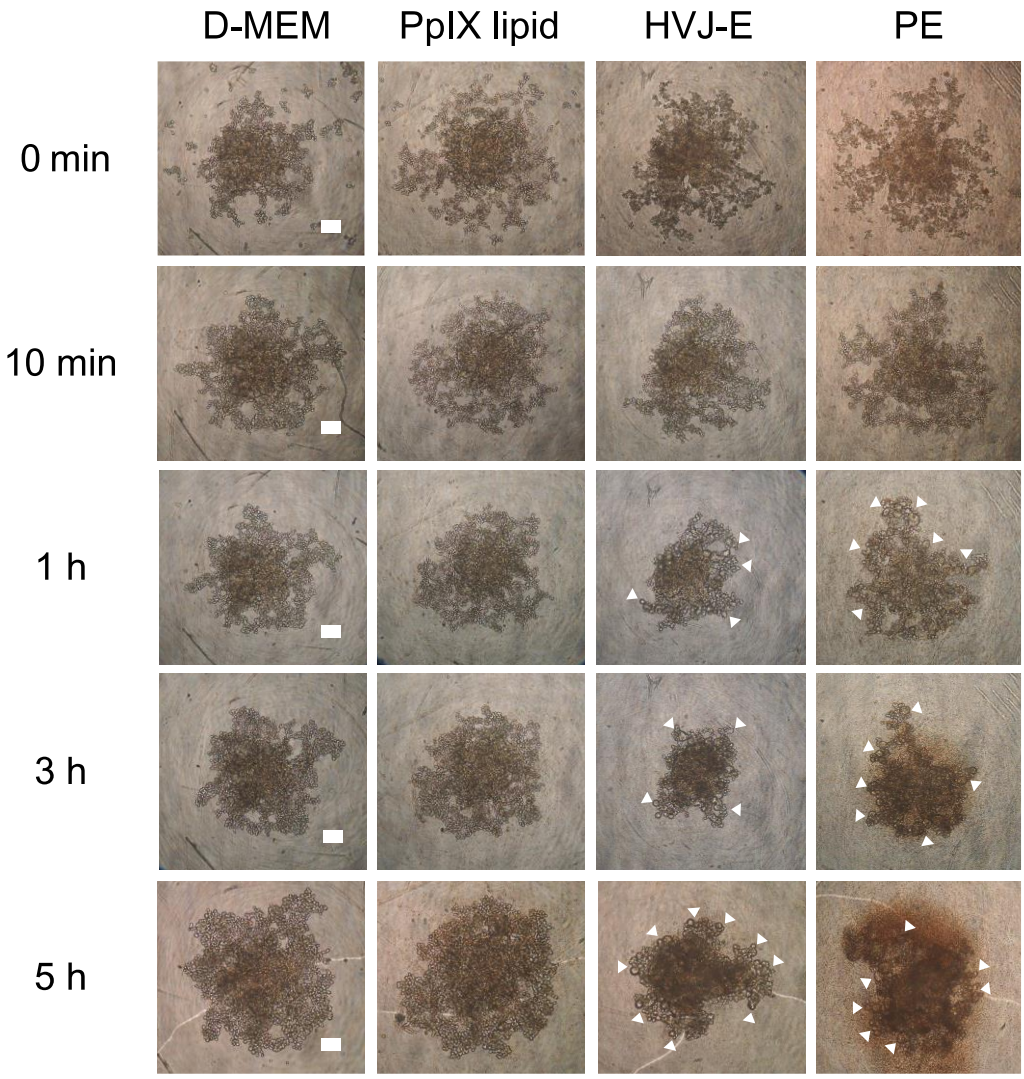

Figure 6-3 Morphological changes in PC-3 spheroids after treatment

Morphological changes after 0 min–5 h treatment with complete D-MEM, PpIX lipid solution, HVJ-E suspension, or PE suspension were observed under microscope. Evident change in morphology was not observed in spheroids after complete D-MEM or PpIX lipid solution administration. However, exposure to HVJ-E and PE both resulted in the formation of bud-like structure, confirming the enlargement of treated spheroids (arrowheads). Shrinkage of PC-3 spheroids were also confirmed in 1 h and 3 h samples that were treated with HVJ-E or PE. Scale bars indicate 200 μm.

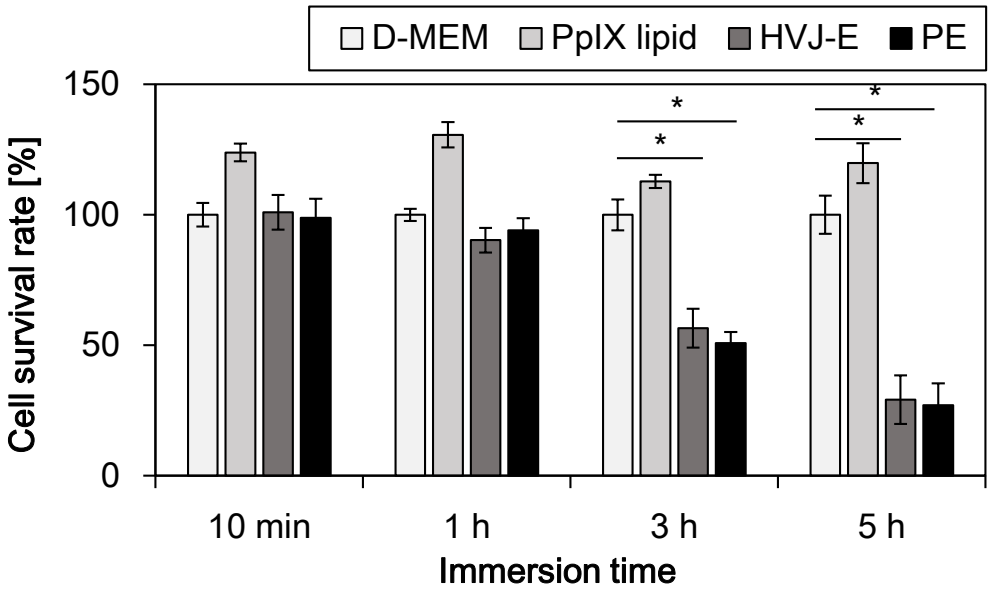

Figure 6-4 Effect of direct cytotoxicity in PC-3 spheroids

The cell survival rate of PC-3 cells treated with complete D-MEM, PpIX lipid solution, HVJ-E suspension, or PE suspension was analyzed. The cell survival rates of spheroids treated with complete D-MEM or PpIX lipid solution were ≥ 100% in all conditions. Exposure to HVJ-E or PE for 3–5 h resulted in significant reduction in cell survival rate ($n = 6$; $^*P < 0.01$).

6.2.4 Effect of PE-mediated PDT towards PC-3 spheroids

PC-3 spheroids were subjected to PDT after treatment with either complete D-MEM, PpIX lipid solution, HVJ-E suspension, or PE suspension for 10 min–5 h to observe the efficacy of PE-mediated PDT in tumor spheroid model (Figure 6-5). As was shown in *Section 4.2.1*, high treatment efficacy was not confirmed in spheroids treated with PpIX lipid alone. In contrast, time dependent decrease in overall survival was confirmed in HVJ-E- or PE-treated spheroids. Significant reduction in cell survival rate was confirmed between D-MEM- and HVJ-E- or PE-treated cells that underwent 1–5 h exposure to respective agents prior to PDT. Approximately 1.3-fold decrease in cell survival rate was confirmed when compared to the rate calculated for spheroids treated with complete D-MEM. The level of cell killing effect for HVJ-E and PE were about the same, with no significant difference.

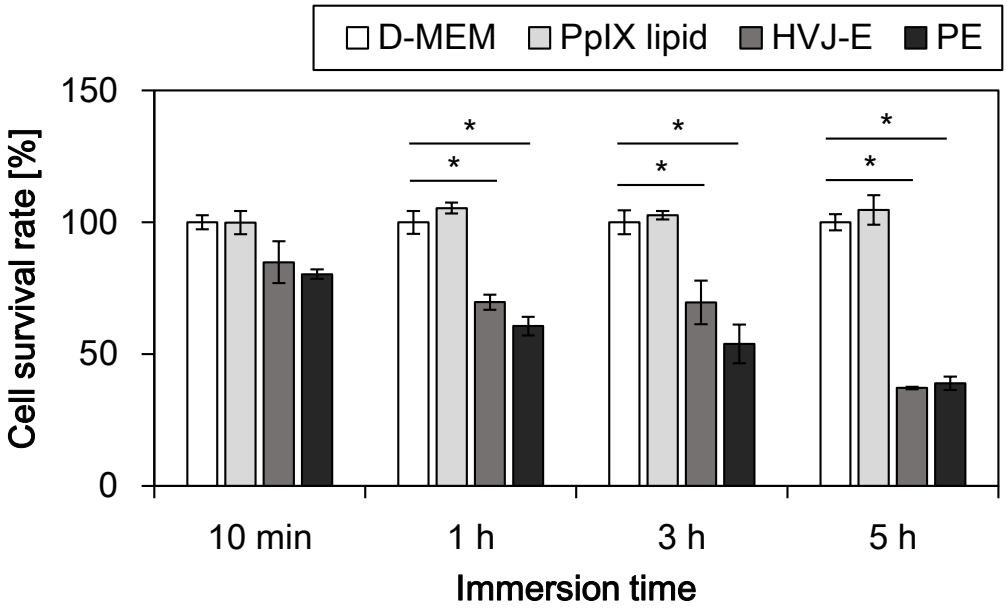

Figure 6-5 Therapeutic efficacy of PDT in PC-3 spheroids

PC-3 spheroids were treated with complete D-MEM, PpIX lipid solution, HVJ-E suspension, or PE suspension for 10 min–5 h and were subjected to PDT. The cell survival rates obtained for spheroids treated with complete D-MEM or PpIX lipid solution were ≥ 100% in all conditions. However, reduction in cell survival rate was confirmed after treatment with HV-E suspension or PE suspension. No significant difference was confirmed between the survival rates obtained for HVJ-E- or PE-treated spheroids ($n = 3$; $^*P < 0.01$).

6.3 Discussion

In order to simulate the effect of PE-mediated PDT in *in vivo* tumor system, PC-3 spheroid system was utilized in this study. As depicted by Figure 6-1, number of PC-3 cells were 1.6-fold higher in 3D model when compared to 2D system. The results obtained in Figure 6-2 show that incorporation of PE-inserted PpIX lipid was 1.3–2-fold higher than exogenous PpIX lipid alone. Similar tendency was observed in 2D system as described in *Section 2.2.2*; however, unlike in the 2D model, significant PpIX lipid uptake was not confirmed between spheroids treated with PE for 10 min and 1 h. Furthermore, when the cellular uptake of PE-inserted PpIX lipid in 2D and 3D system was compared in a single cell level, level of PpIX lipid uptake was approximately the same (Table 6-1). Since the number of PC-3 cells was higher in 3D model, it is suggested that the efficacy of PpIX lipid delivery is suppressed in a *in vivo*-like system. PE particles should delvier PS to the outer lining of PC-3 spheroids after respective immersion time, yet with the limitation of mass transport, PS delivery to the inner core may be difficult to achieve [1], [2].

Table 6-1 PpIX lipid fluorescence in a single cell

Fluorescence intensities of PE-inserted PpIX lipid obtained from 2D and 3D system was compared at a single cell level. Time-dependent increase in PpIX lipid uptake was confirmed in 2D model; however, fluorescence level remained the same in 10 min and 1 h sample for 3D model. Longer immersion time was required for increased PpIX lipid uptake in PC-3 spheroids.

	2D culture	3D spheroid
10 min	0.062	0.066
1 h	0.11	0.067
3 h	0.16	0.17
5 h	0.18	0.23

In addition, when the cell survival rate was observed after exposing PC-3 spheroids to complete D-MEM, PpIX lipid solution, HVJ-E suspension, or PE suspension, strong induction of PE-mediated direct cytotoxicity was not confirmed in spheroids after 10 min or 1 h treatment (Figure 6-4). As indicated in Table 6-2, 1.4–1.6-fold reduction in the

efficacy of PE-mediated direct cytotoxicity was confirmed in spheroid system to that of 2D culture system. Although the precise mechanism is not clear, strong cell-cell contact observed in 3D system may have contributed in upregulating the pro-survival signal, causing the reduction in treatment efficacy [6]. At the same time, however, it should be noted that 3D conformation makes it hard for PE particles to reach the core of spheroid. It can be suggested that low occurrence rate of PE-mediated membrane fusion have affected the therapeutic outcome. In fact, cell survival rate of spheroids exposed to PE for more than 3 h resulted in sudden reduction of cell survival rate, with strongest cytotoxicity confirmed after 5 h exposure. PE-mediated direct cytotoxicity requires PE particles to fuse with the target cancer cells; therefore, longer immersion times may be necessary to induce effective level of fusion activities that exert necessary reactions in cells. Furthermore, since several studies have revealed the precence of CICs in spheroid system, it is probable that PE-mediated direct cytotoxicity exhibit strong therapeutic efficacy towards undifferenciated cancer cells with high tumorigenic activity after several hours of immersion time [13]–[15].

Table 6-2 Cell death induced by PE-mediated direct cytotoxic effect

Cell survival rate of PE-treated PC-3 cells in 2D and 3D system was compared. Time-dependent decrease in cell survival rate was confirmed in spheroids; however, cell survival rate was 1.4–1.6-fold higher when compared to 2D culture system.

	2D culture	3D spheroid
10 min	69%	98%
1 h	68%	94%
3 h	32%	51%
5 h	37%	27%

Although time-dependent decrease in cell survival rate was confirmed in both system, cell survival after PE-mediated PDT was 1.5–2.8-fold higher in spheroid model (Table 6-3). Since PC-3 exhibits mass-type spheroids as shown in Figure 6-3, robust cell-cell

adhesion should be confirmed in PC-3 spheroids [5]. Strong enhancement in the level of cellular communication is confirmed in spheroids that exhibit robust cell-cell adhesion; therefore, this may have caused PC-3 cells to escape the cytotoxic effect induced by PE-mediated PDT, together with the effect of PE particle graduation observed in PC-3 spheroids [5], [6]. Thickness of all PC-3 spheroid models used in this study was less than 1 mm; therefore, suppression in PDT efficacy should not have resulted from the limitation of light penetration depth [16]. Distribution of receptors for HVJ-E on PC-3 cells are heterogeneous in spheroid models; thus, this may have hindered PE particles to fuse with PC-3 cells located at the core of the spheroids, reducing the therapeutic outcome. Moreover, CICs that reside in PC-3 spheroids could have contributed in allowing the cells to escape the cytotoxcity induced by PE-mediated PDT. Previous research has revealed that CD44, one of the widely known CICs markers, is highly expressed in PC-3 cells [17]. Isoforms of CD44 variants can form a complex with the membrane-localizing xCT to act as ROS scavenger; therefore, accumulation of ROS produced via PE-mediated PDT may have been suppresed through this mechanism [18], [19]. Since PDT efficacy depends on the production of ROS, ROS scavenging activity of CICs may have inhibited the cytotoxic effect induced via PE-mediated PDT.

On the bright side, PE treatment resulted in the shrinkage of PC-3 spheroid (Figure 6-3). Previous study has confirmed that the shrinkage in spheroids cause synergistic sensitization of cancer cells to apoptotic signal; therefore, death rate may be enhanced by longer immersion time or upregulation of anti-tumor immune activity [4]. Further analysis is required to confirm this, however, longer treatment period with PE may be sufficient to expose quiescient layer to the surface, as PC-3 spheroids seemed somewhat vulnerable to external stimuli after 3 h immersion time (Figure 6-3). A fragile outer layer may permit PE particles to penetrate to the inner layer, treating the apoptosis-sensitive core.

Table 6-3 Cell death induced by PE-mediated PDT

Cell survival rate of PC-3 cells in 2D and 3D system after PE-mediated PDT was compared. Time-dependent decrease in cell survival rate was confirmed in both systems; however, cell survival rate observed for 3D system was 1.5–2.8-fold higher than that observed in 2D system.

	2D culture	3D spheroid
10 min	52%	80%
1 h	36%	61%
3 h	21%	54%
5 h	12%	34%

Moreover, since the presence of CICs has been confirmed in spheroid systems, reduction in cell survival rate observed after PE-mediated PDT suggests how this modality can effectively reduce the number of CICs in cancer systems [13]. Roulois *et al.* have reported that viral RNA can effectively eradicate CICs by activating anti-viral pathway. Thus, upregulation of RIG-I/MAVS pathway by HVJ-E might exhibit similar mechanism [20]. *In vivo* analysis needs to be performed to investigate the therapeutic efficacy of PE-mediated PDT when anti-tumor immunity is intact.

Although further research is needed to analyze the effective dose of PE-mediated PDT to enhance the PDT effect, 3D spheroid analysis has revealed how PE-mediated PDT may be effective towards highly metastatic prostate cancer.

6.4 Summary

Therapeutic efficacy of PE-mediated PDT was suppressed in PC-3 spheroid model. For instance, longer immersion time was required in 3D spheroid system to efficiently accumulate PE-inserted PpIX lipid and to induce cytotoxic response in PC-3 cells. Maximum of 2.8-fold reduction in cell survival rate was confirmed in spheroid model as opposed to 2D culture system, suggesting the induction of pro-survival signal is observed in PC-3 spheroids due to strong cell-cell communication. Moreover, gradient in PE particles throughout the spheroid system may have also contributed in the supression of therapuetic efficacy. Since exposure to PE for more than 3 h caused the spheroids to be more vulnerable, relatively longer immersion time may allow PE particles to penetrate deep inside the core. Efficacy towards CICs was also suggested, implicating its potency in *in vivo*.

References

[1] M. Alemany-Ribes, M. Garcia-Diaz, P. Acedo, M. Agut, S. Nonell, M. Sagrista, M. Mora, M. Canete, A. Villanueva, J. Stockert, and C. Semino, "Why not introducing the third dimension in photodynamic therapy research?," *J. Anal. Bioanal. Tech.*, vol. S1, pp. 1–6, 2013.

[2] D. Antoni, H. Burckel, E. Josset, and G. Noel, "Three-dimensional cell culture: A breakthrough in vivo," *International Journal of Molecular Sciences*, vol. 16, no. 3. pp. 5517–5527, 2015.

[3] I. Rizvi, A.-L. Bulin, E. Briars, S. Anbil, and T. Hasan, "Mind the Gap: 3D Models in Photodynamic Therapy," in *Photodynamic Medicine: From Bench to Clinic*, 2016, pp. 197–221.

[4] I. Rizvi, J. P. Celli, C. L. Evans, A. O. Abu-Yousif, A. Muzikansky, B. W. Pogue, D. Finkelstein, and T. Hasan, "Synergistic enhancement of carboplatin efficacy with photodynamic therapy in a three-dimensional model for micrometastatic ovarian cancer," *Cancer Res.*, vol. 70, no. 22, pp. 9319–9328, 2010.

[5] R. Edmondson, J. J. Broglie, A. F. Adcock, and L. Yang, "Three-Dimensional Cell Culture Systems and Their Applications in Drug Discovery and Cell-Based Biosensors," *Assay Drug Dev. Technol.*, vol. 12, no. 4, pp. 207–218, 2014.

[6] C. L. Evans, "Three-dimensional in vitro cancer spheroid models for photodynamic therapy: strengths and opportunities," *Front. Phys.*, vol. 3, 2015.

[7] Y. Fang and R. M. Eglen, "Three-Dimensional Cell Cultures in Drug Discovery and Development," *SLAS Discov. Adv. Life Sci. R&D*, vol. 22, no. 5, pp. 456–472, 2017.

[8] R. M. Sutherland, W. R. Inch, J. A. McCredie, and J. Kruuv, "A multi-component radiation survival curve using an in vitro tumour model," *International Journal of Radiation Biology*, vol. 18, no. 5. pp. 491–495, 1970.

[9] G. M. Cramer, D. P. Jones, H. El-Hamidi, and J. P. Celli, "ECM Composition and Rheology Regulate Growth, Motility, and Response to Photodynamic Therapy in 3D Models of Pancreatic Ductal Adenocarcinoma," *Mol. Cancer Res.*, vol. 15, no. 1, pp. 15–25, 2017.

[10] M. Yamauchi, N. Honda, H. Hazama, S. Tachikawa, H. Nakamura, Y. Kaneda, and K. Awazu, "A novel photodynamic therapy for drug-resistant prostate cancer cells using porphyrus envelope as a novel photosensitizer," *Photodiagnosis Photodyn. Ther.*, vol. 11, no. 1, pp. 48–54, 2014.

[11] M. Inai, N. Honda, H. Hazama, S. Akter, S. Fuse, H. Nakamura, T. Nishikawa, Y. Kaneda, and K. Awazu, "Photodynamic therapy using a cytotoxic photosensitizer porphyrus envelope that targets the cell membrane," *Photodiagnosis Photodyn. Ther.*, vol. 20, pp. 238–245, 2017.

[12] S. Tachikawa, M. E. El-Zaria, R. Inomata, S. Sato, and H. Nakamura, "Synthesis of protoporphyrin-lipids and biological evaluation of micelles and liposomes," *Bioorganic Med. Chem.*, vol. 22, no. 17, pp. 4745–4751, 2014.

[13] J. Liao, F. Qian, N. Tchabo, P. Mhawech-Fauceglia, A. Beck, Z. Qian, X. Wang, W. J. Huss, S. B. Lele, C. D. Morrison, and K. Odunsi, "Ovarian cancer spheroid cells with stem cell-like properties contribute to tumor generation, metastasis and chemotherapy resistance through hypoxia-resistant metabolism," *PLoS One*,

2014.
[14] Z. F. Bielecka, K. Maliszewska-Olejniczak, I. J. Safir, C. Szczylik, and A. M. Czarnecka, “Three-dimensional cell culture model utilization in cancer stem cell research,” *Biol. Rev.*, vol. 92, no. 3, pp. 1505–1520, 2017.
[15] L. B. Weiswald, D. Bellet, and V. Dangles-Marie, “Spherical Cancer Models in Tumor Biology,” *Neoplasia (United States)*, vol. 17, no. 1, pp. 1–15, 2015.
[16] E. Ruggiero, S. Alonso-de Castro, A. Habtemariam, and L. Salassa, “Upconverting nanoparticles for the near infrared photoactivation of transition metal complexes: new opportunities and challenges in medicinal inorganic photochemistry,” *Dalt. Trans.*, vol. 45, no. 33, pp. 13012–13020, 2016.
[17] B. L. Lokeshwar, V. B. Lokeshwar, and N. L. Block, “Expression of CD44 in prostate cancer cells: Association with cell proliferation and invasive potential,” *Anticancer Res.*, vol. 15, no. 4, pp. 1191–1198, 1995.
[18] G. J. Yoshida and H. Saya, “Clinical & Experimental Pharmacology The Novel Anti-tumor Therapy Targeting the " Functional " Cancer Stem Cell Markers,” *Clin Exp Pharmacol*, vol. 4, no. 2, pp. 2–5, 2014.
[19] G. J. Yoshida and H. Saya, “Therapeutic strategies targeting cancer stem cells,” *Cancer Sci.*, vol. 107, no. 1, pp. 5–11, 2016.
[20] D. Roulois, H. Loo Yau, R. Singhania, Y. Wang, A. Danesh, S. Y. Shen, H. Han, G. Liang, P. A. Jones, T. J. Pugh, C. O’Brien, and D. D. De Carvalho, “DNA-Demethylating Agents Target Colorectal Cancer Cells by Inducing Viral Mimicry by Endogenous Transcripts,” *Cell*, 2015.

7. Conclusion

The aim of this study was to develop a PDT regimen that induces multiple cell death pathways that allows efficient erradication of castration-resistant prostate cancer. In this dissertation, membrane-targeting delivering potential of novel photosensitzer PE and its therapeutic efficacy against recurrent prostate cancer were analyzed using normal prostate epithelia PNT2 and castration-resistant human prostate cancer cell line PC-3 and DU145.

In Chapter 2, subcellular fluorescence localization analysis has shown that PE could deliver PpIX lipid to cancer plasma membrane after the treatment period of 10 min–5 h. Since PS localization in plasma membrane is known to induce acute inflammation due to necrosis; PE may also act as a potent enhancer of anti-tumor immune response. In addition, significant uptake of PpIX lipid in PC-3 cells was observed 10 min after PE administration. Conventional photosensitizer 5-ALA requires more than 2 h to efficiently accumulate in PC-3 cells. Therefore, drug-light interval may be shorted by utilizing PE as a PS carrier.

Furthermore, remarkable cancer eradication efficacy of PE was revealed in Chapter 3. In the studies performed in this chapter, PC-3 cells were exposed to PE for 10 min–5 h and the resulting cell survival rate or alteration in oncologic phenotype was observed. HVJ-E alone is known to induce cancer cell death by upregulating the activity of RIG-I/MAVS pathway and increasing cytotoxic Ca^{2+}. Since PE underwent membrane fusion at host cell surface, which resulted in the formation of multinucleated syncytia, RIG-I activation and increase in cytotoxic Ca^{2+} should both be observed in cancer cells. In addition, the formation of multinucleated cells were observed after PE treatment. Syncytia act to halt proliferative and migratory activities in cancer cells; therefore, PE-induced cell-cell fusion may cause the supression of invasive characteristic of malignant cells. In all, PE was shown to exhibit cytotoxicity through various pathways even in absence of light.

In order to confirm the therapeutic efficacy of combined therapy using PE-induced cytotoxicity and photodynamic effect, therapeutic efficacy of PE-mediated PDT was analyzed in Chapter 4. As a result, time-dependent increase in ROS production and enhancement of cancer cell sensitivity towards cell death was confirmed after PE-

mediated PDT. In fact, PC-3 cells treated with PE for more than 3 h prior to light irradiation exhibited higher number of dead cancer cells than the cells treated with other reagents. Since treatment with HVJ-E alone has been confirmed to induce various pathways, such as apoptosis via RIG-I/MAVS pathway and necroptosis through Ca^{2+} upregulation, a variety of death cascade resulting from PE-mediated PDT are to be expected. Moreover, direct cytotoxicitc ability of PE and photodynamic reaction caused by PE-mediated PDT have been confirmed to work in synergy. Since synergistic anti-tumor effect is necessary to improve therapeutic outcome in androgen-insensitive prostate cancer, PE-mediated PDT should possess favorable characteristics to be used for prostate cancer management.

In Chapter 5, several studies were performed using normal prostate epithelia PNT2 and another castration-resistant prostate cancer cell line DU145 to analyze how broadly PE-mediated PDT can be applied in prostate cancer management. The results indicate that PE exhibited cancer-selective advantage with high treatment efficacy. For instance, cancer-selective uptake of PE-inserted PpIX lipid and cell death was observed in this study. Since HN receptors for HVJ-E located on castration-resistance cancer cells and normal prostate epithelia differ in nature, PE should allow selective PS uptake and treatment efficacy in prostate cancer. Prostate cancer exhibits multifocal characteristic; therefore, selective treatment that effectively eradicate different types of castration-resistant prostate cancer implies how treatment using PE-mediated PDT allows both highly efficient and effective prostate cancer treatment.

Finally, to obtain some insights into the efficacy of PE-mediated PDT *in vivo*, studies using PC-3 spheroid model were performed in Chapter 6. Therapeutic efficacy of PE-mediated PDT was suppressed in PC-3 spheroid model, with longer immersion time required to efficiently induce cytotoxic response in PC-3 cells. Strong cell-cell comunication between PC-3 cells and gradiation in PE paticles in spheroids may have contibuted in the maximum of 2.8-fold reduction in therapeutic efficacy. Moreover, ROS scavenging ability of CICs could have reduced the therapeutic outcome of PDT. However, it should be noted that the immersion time of 5 h exhibited strong direct cytotoxic effect and PDT efficacy. Therefore, PE-mediated PDT may exhibit high therapeutic outcome with longer exposure time to PE. In addition, since PE can also induce anti-tumor immunity response in cancer cells, this response may further enhance the therapeutic

efficacy of newly created modality. Although *in vivo* analysis is required to throughly examine the effect of PE-mediated PDT, multimodal function of this treamtment modality and its efficacy of CICs were revealed from these studies.

In all, PE has exhibited significant cytotoxicity towards advanced and reccurent prosate cancer. Due to its ability to induce various types of cell death pathways, it has a high potential as a novel photosensitizer that allows multimodal treatment. Since the induction of robust cell death in primary tumor can result in the upregulation of anti-tumor immune response, potent cytotoxicity observed after PE-mediated PDT may efficiently activate HVJ-E-mediated anti-tumor immune reaction. However, photosensitzer used in this system is yet to be approved for clinical application. Thus, a clinically approved photosensitizer, talaporfin sodium (Laserphyrin®, Meiji Seika Pharma Co., Japan), may be a potential drug that can be incorporated in HVJ-E. Since HVJ-E is now under clinical trial, the combination of these two drugs may facilitate the drug development and approval process.

Acknowledgement

First and foremost, I would like to express my sincerest gratitude to my supervisor, Prof. Kunio Awazu, who has supported me throughout my PhD study. His guidance, patience, and immense knowledge of the field have helped me at the various stages of my research work. I would never have been able to finish my dissertation without his guidance. My sincere thanks and appreciation also goes to my dissertation committee, Prof. Toru Nakano, Prof. Masaru Ishii, and Prof. Yasushi Inoue, for their insightful comments and encouragement. Their sharp critical eyes widened my perspectives and allowed me to clarify my research goal.

I convey my heartfelt and sincere thanks to Prof. Yasufumi Kaneda for his precious support and valuable input. His practical advice has largely improved the integrity of this work. Many thanks also go out to Prof. Hiroyuki Nakamura and Associate Prof. Fuse of Tokyo Institute of Technology for all their support and encouragement. I am truly grateful for their help in synthesizing PpIX lipid at short notice and their insights from chemists' point of view. Furthermore, I am grateful for Specially Appointed Lecturer Tomoyuki Nishikawa for all his time and technical tips.

I would like to express my special appreciation to Associate Prof. Hisanao Hazama, Assistant Prof. Katsunori Ishii, Assistant Prof. Yuichiro Manabe, and Specially Appointed Assistant Prof. Norihiro Honda for their support to make this thesis possible. I also acknowledge all the staff and students of Awazu laboratory and IPBS program for their support and encouragement whenever I was in need.

Last but not least, I thank my parents and my dearest sisters for their spiritual support throughout all my experimental work at Osaka University; I could not have done it without them.

List of Research Achievements

Articles

M. Inai, M. Yamauchi, N. Honda, H. Hazama, S. Tachikawa, H. Nakamura, T. Nishida, H. Yasuda, Y. Kaneda, K. Awazu: Photodynamic therapy using hemmaglutinating virus of Japan envelope (HVJ-E): a novel therapeutic approach for the treatment of hormone antagonistic prostate cancer, *Proceedings of SPIE*, 9308, 930814, doi:10.1117/12.2090692 (2015)

M. Inai, M. Yamauchi, N. Honda, H. Hazama, S. Tachikawa, H. Nakamura, T. Nishida, H. Yasuda, Y. Kaneda, K. Awazu: Hemmaglutinating virus of Japan envelope (HVJ-E) allows targeted and efficient delivery of photosensitizer for photodynamic therapy against advanced prostate cancer, *Proceedings of Optics in the Life Sciences, Optical Society of America 2015*, doi: 10.1364/OMP.2015.OM2D.3 (2015)

粟津邦男, 本多典広, 稲井瑞穂: 不活性化され複製能を欠損させたセンダイウイルス粒子による光線力学的治療法の効率化, 総説, *医学のあゆみ*, 258(11): 1063–1067 (2016)

稲井瑞穂,本多典広, 間久直, 中村浩之, 保田英洋, 西川智之, 金田安史, 粟津邦男: ホルモン拮抗ヒト前立腺がん細胞株(PC-3)における新規光感受性物質 porphyrus envelope 細胞内局在の検討, 第 35 回 日本レーザー医学会総会賞受賞論文, *日本レーザー医学会誌*, **37**(4): 415–420 (2017)

稲井瑞穂: レーザー医学この人 稲井瑞穂 大阪大学 大学院生命機能研究科, 総説, *日本レーザー医学会誌*, **38**(1): 46–47 (2017)

S. Saito, M. Inai, N. Honda, H. Hazama, Y. Kaneda, K. Awazu: Evaluation of a novel photosensitizing drug having antitumor effect for advanced prostate cancer, *Proceedings of European Conference on Biomedical Optics 2017*, doi: 10.1117/12.2286071 (2017)

M. Inai, N. Honda, H. Hazama, S. Akter, S. Fuse, H. Nakamura, T. Nishikawa, Y. Kaneda, K. Awazu: Photodynamic therapy using a cytotoxic photosensitizer *porphyrus envelope* that targets the cell membrane, journal article, *Photodiagnosis and Photodynamic Therapy*, **20**: 238–245 (2017)

Y. Hong, M. Inai, N. Honda, H. Hazama, M.A. Joshi, H. Nakamura, T. Nishikawa, Y. Kaneda, K. Awazu: Highly selective photodynamic therapy with a short drug-light interval using a cytotoxic photosensitizer porphyrus envelope for drug-resistant prostate cancer cells, *International Journal of Clinical Medicine*, **9**: 8–22 (2018)

Presentations

International Conference

M. Inai, M. Yamauchi, N. Honda, H. Hazama, S. Tachikawa, H. Nakamura, T. Nishida, H. Yasuda, Y. Kaneda, K. Awazu: Therapeutic effect of porphyrus envelope-mediated photodynamic therapy: a novel therapeutic approach for the treatment of hormone antagonistic prostate cancer. Photonics West BiOS 2015, (2015.2.7–12), The Moscone Center, San Francisco, CA, USA

M. Inai, M. Yamauchi, N. Honda, H. Hazama, S. Tachikawa, H. Nakamura, T. Nishida, H. Yasuda, Y. Kaneda, K. Awazu: Hemmaglutinating virus of Japan envelope (HVJ-E) allows targeted and efficient delivery of photosensitizer for photodynamic therapy against advanced prostate cancer. Bio-Optics: Design and Application (BODA) (2015.4.12–15), Pinnacle Vancouver Harbourfront Hotel, Vancouver, BC, Canada

M. Inai, N. Honda, H. Hazama, T. Nishikawa, H. Nakamura, H. Yasuda, Y. Kaneda, K. Awazu: Hemmaglutinating virus of Japan envelope as a versatile vector for photodynamic therapy against advanced and recurrent prostate cancer. Chemical Congress of Pacific Basin Societies (Pacifichem2015) (2015.12.15–20), The Royal Hawaiian Hotel, Honolulu, HI, USA

M. Inai, N. Honda, H. Hazama, T. Nishikawa, H. Nakamura, H. Yasuda, Y. Kaneda, K. Awazu: Hemmaglutinating virus of Japan envelope as a versatile vector for photodynamic therapy against prostate cancer. The 3rd International ALA and Porphyrin Symposium (IAPS3) (2015.12.17), University of Hawaii, Honolulu, HI, USA

N. Honda, M. Inai, T. Furuyama, Young Soon Hong, H. Hazama, H. Nakamura, H. Yasuda, T. Nishikawa, Y. Kaneda, K. Awazu: Usage of replication-deficient viral particle for photodynamic therapy against prostate cancer allows high cytotoxicity through different pathways. Photodynamic Therapy and Photodiagnosis update (2016.10.24–28), National School of Chemical Engineering, Nancy, France

S. Saito, M. Inai, N. Honda, H. Hazama, Y. Kaneda, K. Awazu: Development of photosensitizing drug using replication-deficient virus particles and talaporfin sodium for photodynamic therapy of prostate cancer. Research Institute of Electrical Communivation (RIEC) International Workshop on Biomedical Optics 2017 (2017.3.6), Toholu University, Sendai, Japan

S. Saito, M. Inai, N. Honda, H. Hazama, Y. Kaneda, K. Awazu: Evaluation of a Novel Photosensitizing Drug Having Antitumor Effect for Advanced Prostate Cancer. European Conference on Biomedical Optics 2017 (2017.6.25–29), Messe Munich, Munich, Germany

Domestic Conference

稲井瑞穂, 山内将哉, 本多典広, 間久直, 立川将士, 中村浩之, 西田倫希, 安田英洋, 西川智之, 金田安史, 粟津邦男: ホルモン拮抗ヒト前立腺がん細胞株(PC-3)における新規光感受性物質 porphyrus envelope 細胞内局在の検討. 第 35 回 日本レーザー医学会総会 (2014.11.29–30), 京王プラザホテル, 東京都新宿区

山内将哉, 稲井瑞穂, 本多典広, 間久直, 立川将士, 中村浩之,金田安史, 粟津邦男: 非ウイルスベクターを用いた薬剤耐性前立腺がんへのPDTにおける最適な薬剤調整条件の検討. 第35回 日本レーザー医学会総会 (2014.11.29–30), 京王プラザホテル, 東京都新宿区

稲井瑞穂,本多典広, 間久直, 中村浩之, 金田安史, 粟津邦男: 不活化ウイルスベクターを用いた新規光感受性薬剤の薬剤輸送過程と腫瘍選択性の検討. 第25回 日本光線力学学会 学術講演会 (2015.7.10–7.11), 京王プラザホテル, 東京都新宿区

稲井瑞穂,本多典広, 間久直, 中村浩之, 金田安史, 粟津邦男: 複製能を無くしたウイルス粒子を用いた新規光感受性薬剤の薬剤輸送過程と腫瘍選択性の評価. 第28回 日本レーザー医学会 関西地方会 (2015.7.25), TKPガーデンシティ京都, 京都府京都市

古山祐, 稲井瑞穂,本多典広, 間久直, 布施新一朗, 中村浩之, 金田安史, 粟津邦男: 複製能欠損ウイルス粒子とプロトポルフィリンIX脂質を利用したPDT過程のタイムラプス撮影による作用機序の検討. 第26回 日本光線力学学会 学術講演会 (2016.6.26–27), 横浜はまぎんホール ヴィアマーレ, 神奈川県横浜市

斎藤祥子, 稲井瑞穂, 本多典広, 間久直,金田安史, 粟津邦男: タラポルフィンナトリウムを封入した複製能欠損ウイルス粒子を用いた効果的なPDTの検討. 第26回 日本光線力学学会 学術講演会 (2016.6.26–27), 横浜はまぎんホール ヴィアマーレ, 神奈川県横浜市

洪暎淳, 稲井瑞穂, 本多典広, 間久直, 布施新一朗, 中村浩之, 金田安史, 粟津邦男: 迅速な薬剤輸送に向けた複製能欠損センダイウイルス粒子への光感受性物質の封入条件の検討. 第26回 日本光線力学学会学会 学術講演会 (2016.6.26–27), 横浜はまぎんホール ヴィアマーレ, 神奈川県横浜市

斎藤祥子, 稲井瑞穂, 本多典広, 間久直,金田安史, 粟津邦男: タラポルフィンナトリウムを封入した複製能欠損ウイルス粒子を用いた光線力学療法の検討. レーザー学会 第493回 研究会 (2016.8.5), 東北大学, 宮城県仙台市

洪暎淳, 稲井瑞穂, 古山祐,本多典広, 間久直, 布施新一朗, 中村浩之, 金田安史, 粟津邦男: 抗がん剤耐性前立腺がん細胞への迅速な薬剤輸送に向けた複製能欠損ウイルス粒子への光感受性物質の封入. 電気学会 光・量子デバイス研究会 バイオメディカルフォトニクス応用 (2016.9.26), 東北大学東京分室, 東京都千代田区

稲井瑞穂, 古山祐, 洪暎淳,本多典広, 間久直, 布施新一朗, 中村浩之, 金田安史, 粟津邦男: 複製能欠損ウイルス粒子を用いた光感受性薬剤の細胞内局在と腫瘍選択性の検討. 第37回 日本レーザー医学会総会 (2016.10.21–22), 旭川グランドホテル, 北海道旭川市

古山祐, 稲井瑞穂,本多典広, 間久直, 布施新一朗, 中村浩之, 金田安史, 粟津邦男: 複製能欠損ウイルス粒子をキャリアとした新規光感受性物質による光線力学治療の作用機序の検討. レーザー学会学術講演会 第37回次大会 (2017.1.7–9), 徳島大学 常三島キャンパス, 徳島県徳島市

稲井瑞穂, 斎藤祥子, 本多典広, 大崎智弘, 間久直, 岡本芳晴,金田安史, 粟津邦男: タラポルフィンナトリウム封入不活化センダイウイルス粒子を用いたPDTのin vivo抗腫瘍効果. 第27回 日本光線力学学会 学術講演会 (2017.7.14–15), 京都大学 芝蘭会館, 京都府京都市

洪暎淳, 稲井瑞穂, 本多典広, 間久直, 布施新一朗, 中村浩之, 金田安史, 粟津邦男: 複製能欠損ウイルス粒子とプロトポルフィリンIXを用いたPDTにおける腫瘍選択性向上のための治療条件の検討. 第27回 日本光線力学学会 学術講演会 (2017.7.14–15), 京都大学 芝蘭会館, 京都府京都市

S. Akter, S. Saito, M. Inai, N. Honda, H. Hazama, Y. Okamoto, Y. Kaneda, K. Awazu: Evaluation of therapeutic efficacy induced by a novel photosensitizer: tala porfin sodium-incorporated viral particle. レーザー学会 第507回研究会 (2017.8.), 北海道大学大学院 情報科学研究科棟, 北海道札幌市

稲井瑞穂, 斎藤祥子, 本多典広, 大崎智弘, 間久直, 岡本芳晴,金田安史, 粟津邦男: タラポルフィンナトリウム封入不活化センダイウイルスを用いたPDTのin vivoでの抗腫瘍効果. 第38回 日本レーザー医学会総会 (2017.11.10–11), 慶應義塾大学 日吉キャンパス, 神奈川県横浜市

Awards

第35回 日本レーザー医学会　総会賞 受賞 (2014.11)
生産技術振興協会 海外論文発表奨励賞 (平成27年度上期) 受賞 (2015.4)